Eötvös Loránd Research Network
Institute for Computer Science and Control
Systems and Control Laboratory
Budapest, Hungary

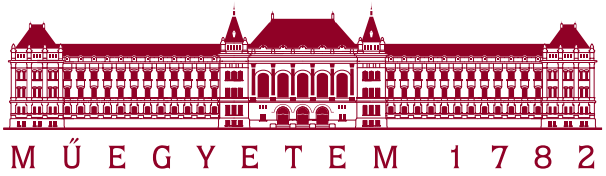

Budapest University of Technology and Economics
Faculty of Transportation Engineering and Vehicle Engineering
Department of Control for Transportation and Vehicle Systems
Budapest, Hungary

Analysis and Synthesis Methods for the Optimal Design of Control Systems in Automated Vehicles

Analízis és szintézis módszerek automatizált járművek irányítórendszereinek optimális tervezéséhez

Thesis by

BALÁZS NÉMETH

In Partial Fulfillment of the Requirements for the Degree of Doctor of Sciences

2022.

dc_1992_22

"Steward for the glory of God
using your talents from God."

Admonition from Count Ferenc Széchényi, 1817

dc_1992_22

ACKNOWLEDGEMENTS

During the last fifteen years SZTAKI Systems and Control Laboratory and BME Department of Control for Transportation and Vehicle Systems have provided excellent scientific and friendly atmosphere for growing in knowledge and experiences, which have helped me in my research activity and in the writing of the thesis. I am grateful to God for placing me here.

I am grateful to Prof. Péter Gáspár and to Prof. József Bokor, who have ensured their support during my research activity. I am also grateful to the Board of Trustees of János Bolyai Research Scholarship for supporting my research between 2014-2017 and 2018-2021.

I would like to thank my closest colleagues, Prof. Zoltán Szabó, Dr. Dániel Fényes, Tamás Hegedűs, Máté Fazekas for their cooperation and for all the help I received from them.

Last, but not least, special thanks for my parents and my family, who have supported me with their love during the whole period of my studies. My greatest gratitude goes for my wife Márta, who has been my helper meet for me, and for my children Simon András, Adél Anna and Ábel Balázs.

dc_1992_22

dc_1992_22

ABSTRACT

Automated vehicles pose various system analysis and control synthesis challenges on the levels of vehicles, vehicle interactions and transportation systems. Although the complexities and structures of these levels are different, methods with which stability and performance requirements through optimal control systems are guaranteed must be developed.

This thesis provides new robust control synthesis frameworks based on the Linear Parameter-Varying (LPV) theory, in which the designed robust controller is in cooperation with unconventional control elements, e.g., learning-based agents. The frameworks developed are used for providing energy-optimal controllers to various control problems. In the thesis the analysis and synthesis methods for the longitudinal control of individual automated vehicles, for the coordination of automated vehicles in intersection, and for the coordination of automated vehicles on the global transportation level are elaborated.

The contributions of the thesis on each level are formed. From the viewpoint of control theory, design frameworks for control systems with learning-based agents for different control structures have been formulated. On the level of automated vehicles control, a novel method for achieving energy-optimal motion profile has been provided and implemented, in which several road signals on the forthcoming road horizon have been incorporated. Moreover, the guaranteed frameworks and motion profile methods for handling safety critical interactions of automated vehicles have been transformed, i.e., the complex multi-vehicle coordinated control problem of cruising vehicles in intersections has been solved. Finally, the coordination of automated vehicles in macroscopic traffic context has been developed, i.e., simulation-based and polynomial analysis methods for exploring the impact of automated vehicles on the traffic flow have been elaborated. The results of the analysis in the control synthesis for improving macroscopic traffic performances have been incorporated.

The contributions of this thesis have been published in books, international journals and in conference papers.

Keywords: automated vehicles, optimal control design, learning-based methods, multi-vehicle scenarios, traffic-vehicle relationships

dc_1992_22

CONTENTS

1. INTRODUCTION AND MOTIVATION

1.1 Introduction and motivation

Due to the rapid development of automated control systems, the challenges in the control design of road vehicles and transportation systems have been transformed. It has induced the advent of novel research fields, i.e., the coordination of vehicle systems and transportation systems to achieve guaranteed performances on the local vehicle level and on the global transportation level. The coordination of the automated vehicle control and the intelligent transportation systems requires the consideration of traffic and infrastructural environments in the design of the coordination strategy. Consequently, the control design of individual vehicles results in the extension of models on the local level to ensure required local performances. Nevertheless, the designed local control significantly determines the performance level on the global level, e.g., the operation of the cruise control system has impact on the traffic flow if the ratio of automated vehicles in the traffic network is significant.

Relations and connections between autonomous vehicles and traffic environment in several recent papers have been examined. The traffic flow model, which is characterized by autonomous vehicles, is proposed in [84]. In the paper the dynamics of vehicles with intelligent cruise control is considered in a mesoscopic traffic-flow model, which is used to derive a macroscopic model for the traffic flow. An analysis on the mixed traffic flow with semi-automated and human-driver controlled is proposed in [22]. It is shown that fuel consumption and level of pollutants through the reduction of rapid acceleration maneuvers of semi-autonomous driving can be decreased. Furthermore, the semi-automated vehicles are able to smooth traffic flow by filtering response to the rapid motion of vehicles in the traffic. The impacts and benefits of the cooperative cruise control on the traffic flow are examined in [155], and the role of vehicle automation on the energy and emission is presented in [14]. The aspects of optimal control design for traffic flow in motorways in the presence of vehicle automation and communication are shown in [128].

The coordination of automated vehicles and transportation systems relies on the availability of a high number of measured signals, i.e., some information on automated vehicles can be transferred to the transportation level, and similarly, information on the traffic flow properties through automated vehicles can be achieved. From the side of the vehicle, a recent technology of the coordination is the predictive control, in which the forthcoming information on the road section (terrain characteristics, speed limitations, traffic flow, traffic light information etc.) for the reason of minimizing energy consumption and traveling time is considered to be available [Gáspár and Németh, 2019]. Several control design methods exist in this field, e.g., look-ahead control concept [56, 118, 55] or eco-cruise control methods [131]. The method on individual vehicles has also been extended for

platooning systems to achieve the benefits of the cooperation, as it has been proposed in [146, 127, 3, 153],[Németh and Gáspár, 2014].

In spite of extensive development in vehicle automation, the coordination of vehicle systems and transportation systems in a mixed traffic must be carried out. A huge challenge for the automated vehicle control design is the presence of human-driven vehicles in the traffic network, e.g., pedestrians, cyclists, vehicle drivers. Next to the safety challenges, it indicates two important research topics for proposing appropriate control design method- ologies. First, the vehicle must handle the interactions with human-driven vehicles, especially safety-critic maneuvers, such as overtaking and crossing intersections [27, 158]. It requests an enhanced environment sensing technology for the estimation of states and intentions of human-driven vehicles [94, 11]. Second, the high number of automated vehicles can have impact on the traffic flow, which incorporates in human-driven vehicles. On the global level of transportation, the exploitation of the result of the traffic flow analysis in the modeling and control of automated vehicles is one of the hot topics, see e.g., [29]. The most important approaches of traffic flow modeling are summarized by [73]. The analysis of the traffic flow, in which semi-automated and automated vehicles are traveled together with human-driven vehicles, is proposed by [132]. Stability issues of the traffic flow of connected and automated vehicles are examined by [144]. In [30] it has been shown that automated vehicles have only slight negative effects but significant positive effects on the traffic flow, depending on the penetration rate of automated vehicles and on the traffic scenario.

The need for the coordination of vehicle control and transportation systems, together with the consideration of human factors have posed the problem of distinguishing between these two areas. Conventionally, the design of automated vehicle control is based on physical microscopic motion models, while the control design for transportation systems requires statistics-based macroscopic models. Due to the different structures of models, constraints and the distinct forms of performance requirements, the number of applicable control methods on the joint design problem is limited. Bridging the gap between design methods on the local and on the global levels has led to the application of unconventional control methods, which have been based on the increased number of information sources. The high number of available signals on the automated vehicle and in the transportation system has motivated the application of data-driven methods for the joint design problem, especially learning-based techniques. Based on huge amount of data on the traffic, a novel data-driven approach for the analysis and modeling of traffic flow dynamics is proposed by [139]. Traffic flow prediction using a deep-learning algorithm is presented by [99]. In that research, a deep-learning architecture model is applied by using auto-encoders as building blocks to represent traffic flow features for prediction. Similarly, Lasso regression is used for traffic flow prediction in [85]. Cell phone information-based big data analysis and control for transportation purposes is proposed by [40]. The work of [24] focused on generating models for microscopic traffic simulation, which is built upon real world data. Identification and prediction of traffic flow states based on big data analysis method are presented by [97].

The presented challenges indicate not only control theoretical research activity, but they also imply the vehicle-oriented applications of the methods. In Hungary, it is motivated by the fact that autonomous vehicle technology may have considerable economic

and social impacts [34, 130, 18]. Nevertheless, the benefits of automation cannot be achieved without significant research, development and innovation process. For example, the Autonomous Vehicles Readiness Index is a tool to help measure the level of preparedness for autonomous vehicles in each country. The position of Hungary based on this index is 25 (see [62]), which is suitable from global worldwide aspect, but the open problems provide further growth potential. The goal of Autonomous Systems National Laboratory (ARNL) is to coordinate research activities in a network of several Hungarian research institutes and universities, in cooperation with industrial partnerships. Institute for Computer Science and Control (SZTAKI) has a leading role in the coordination of ARNL and in the providing of novel theoretical results in the field of automated vehicle control methods. The contributions of this thesis fit to the scopes of ARNL on the side of the vehicle control design in coordination with the transportation level. Moreover, the provided control theoretical methods of this thesis by OTKA Grant Agreement No. K 135512 "Robust Control Design for Automated Vehicles with Guaranteed Performances" are motivated. The goal of this project is to provide control theoretical methodologies for achieving prov- able performance guarantees in case of unconventional control systems, e.g., integration of learning-based and model-based control systems.

1.2 Objectives of the thesis

The presented challenges in the coordination of vehicle and transportation systems provide strong motivation for developing novel methods in the field of applied control theory. The goal of this thesis is to provide up-to-date solutions on selected problems of the coordination, focusing on the level of vehicle control.

Robust design methods for providing performance guarantees

The first topic of this thesis reflects to the guaranteed performance level of control systems, which contain unconventional, e.g., learning-based elements. Although the different types of enhanced learning control methods are able to handle various performance requirements effectively, their achieved performance level is not theoretically guaranteed. The quantity and quality of learning samples can be chosen to any size, but it does not guarantee the avoidance of performance degradation in an emergency scenario or robustness against faults and disturbances.

The aim of the thesis is to provide a hierarchical supervisory control structure, with which the minimum level on selected primary (i.e., safety) performances for systems with unconventional elements can be guaranteed. The proposed design method is independent from the internal structure of the unconventional element, and thus, it can be used for various control problems. The contribution is a hierarchical structure, together with the design process of a model-based robust Linear Parameter-Varying (LPV) controller and an optimization-based supervisory algorithm.

Energy-optimal control methods for automated vehicles

The second topic focuses on energy-optimal control design methods for automated vehicles, which can achieve increased number of measured signals from the transportation system. The question of the research is formed as how is it possible to formulate the predictive cruise control with the consideration of road-traffic information for achieving improved energy-consumption performances. Simultaneously, safety performance requirements for the cruise control must be guaranteed, which poses the problem of performance prioritization.

The provided solution of the thesis is a multi-objective constrained optimal cruise control design methodology, with which energy-optimal speed profile for the vehicle can be achieved. The effectiveness of the method through high-fidelity simulation examples is illustrated. Moreover, the method on a test heavy vehicle, as a part of an industrial cooperation has been implemented and has been verified. Furthermore, as a contribution of the thesis, the proposed energy-optimal cruise control in the performance-guaranteed hierarchical control structure has been involved. Using the control structure, the automated vehicle is able to avoid safety-critic situations, while the energy consumption of the vehicle is significantly improved.

Coordinated control design in multi-vehicle context

The third topic of the thesis is related to control of automated vehicles in multi-vehicle context, especially to safety-critical interactions. In case of multiple automated vehicles, the coordination of them is required to achieve time-optimal and energy-optimal motion. An accurate challenge is the coordination of automated vehicles in urban intersection scenarios. The intersections pose the problems of vehicle ordering selection and speed profile design, which lead to a non-convex optimization task with safety and economy performance requirements.

In the thesis coordinated control design methods on the problem of multi-vehicle interactions in intersections have been proposed. First, the problem with the extension of the previously proposed energy-optimal control design framework has been solved. In this method the ordering selection and the speed profile selection methods are divided. Second, the solution within the framework of the performance guaranteed hierarchical design method has been provided. The advantage of this solution is that selection of ordering and selection of speed profile in the same optimization task are formulated. In the hierarchical structure, the unconventional element is designed through a reinforcement learning process, and the supervisory algorithm is based on a constrained quadratic optimization task. In both first and second approaches, the presence of human-driven vehicles in the transportation network is handled.

Analysis and synthesis methods for automated vehicles in traffic

The fourth topic reflects to the coordination of high number of automated vehicles in traffic network context. It leads to an analysis problem, i.e., the impact of automated vehicles with energy-optimal cruise control on traffic flow must be explored. Moreover, it is necessary to form the consequences of the analysis in a traffic flow model, which fits to the

conventional traffic modeling framework. The coordination strategy of automated vehicles in the traffic network requires enhanced control methods, with which performances on the global level (e.g., maximization of the traffic outflow) and the performances on the local level (e.g., minimization of the energy consumption) can be guaranteed.

The thesis proposes methods for finding answers the previous challenges, such as analysis, model formulation and coordinated control design. The analysis of the impact of automated vehicles on the traffic flow through high-fidelity simulations has been performed. The examinations have resulted relationships between the ratio of automated vehicles in the traffic, the setting of the cruise control, the inflow into the traffic network and the average traffic speed. Based on the results of the analysis, a novel control-oriented traffic flow model has been formed. As an important contribution of the thesis, a polynomial stability analysis based on the Sum-of-Squares (SOS) method on the traffic model has been carried out. Finally, a predictive coordination strategy for automated vehicles, based on the results of the stability analysis, has been proposed.

1.3 Structure of the thesis

The structure of the thesis is illustrated in Figure 1.1. In Part I robust control design methods for providing performance guarantees are proposed, which have fundamental roles in the thesis.

Part II focuses on energy-optimal control design for individual vehicles. The design process through two methods is presented. In Chapter 3 a predictive control design method is proposed, which has importance not only in the individual design, but also in the control for multiple vehicles (Chapter 5) and in the analysis of the traffic flow (Chapter 7). Moreover, another design method for individual vehicles using the robust framework with performance guarantees is presented in Chapter 4.

The problem of control design for safety critical interactions of multiple automated vehicles is presented in Part III. The chapters of this part focus on the handling of intersection scenarios using predictive cruise control method (Chapter 5) or learning-based approach (Chapter 6).

Finally, the challenges of coordinated control for automated vehicles in traffic are dealt in Part IV. Macroscopic model for describing relationships between traffic flow dynamics and the energy-optimal cruise control is presented in Chapter 7. Using these achievements, set-based analysis and control design methods for the coordination of automated vehicles in Chapter 8 are proposed.

The new scientific results, the consequences of the thesis, the future goals and the further challenges in Chapter 9 are summarized.

Some supplementary simulations and definitions for Part II-IV are found in the chapters of Appendix.

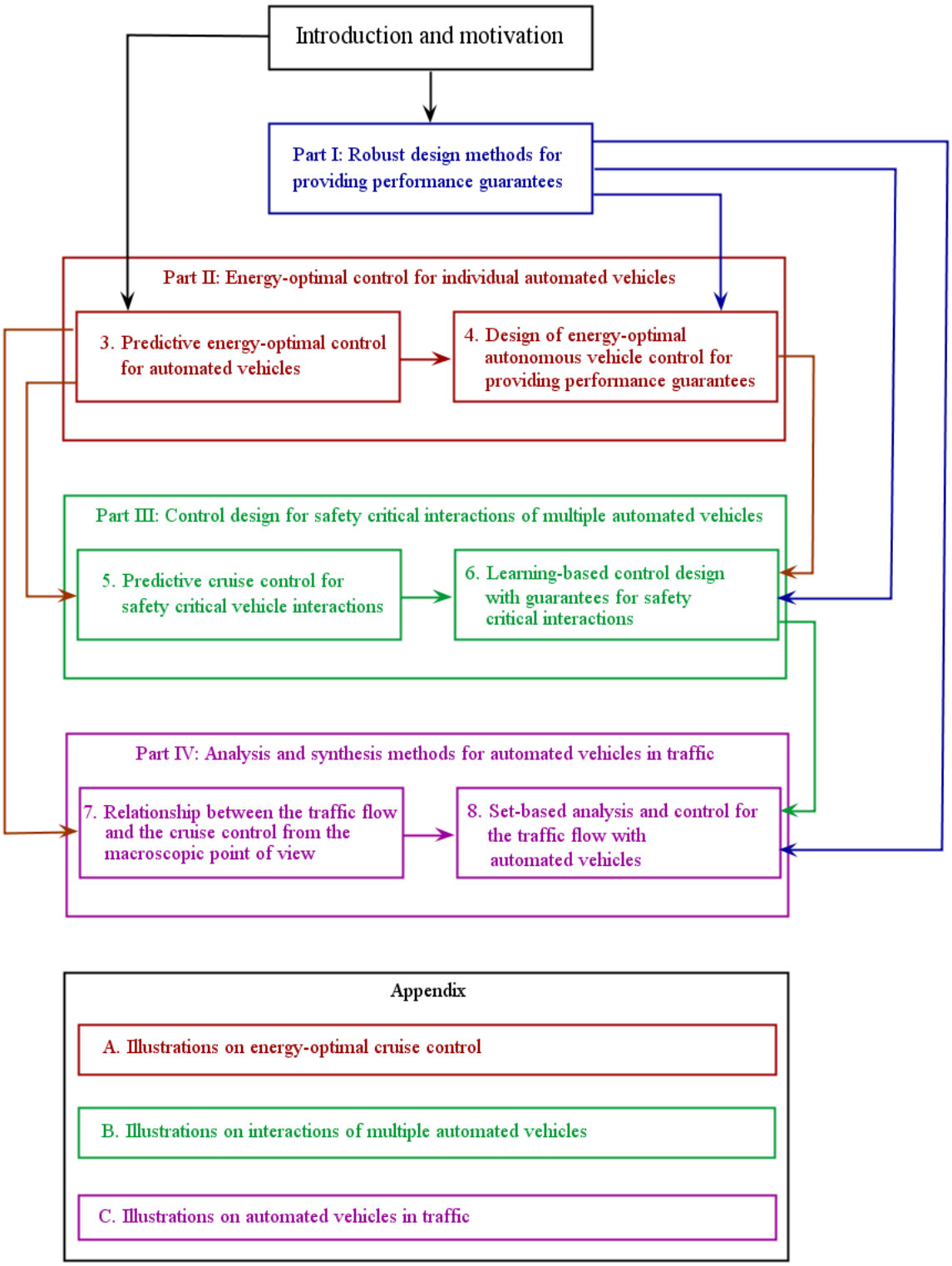

Fig. 1.1: Structure of the thesis

Part I

ROBUST DESIGN METHODS FOR PROVIDING PERFORMANCE GUARANTEES

dc_1992_22

2. ROBUST CONTROL DESIGN FRAMEWORKS FOR ENSURING PERFORMANCE REQUIREMENTS

Unmanned systems require control strategies which various complex human functions can be substituted for. Several deep learning-based methods are able to provide effective control solutions to meet user expectations, e.g., reinforcement learning [92] or imitation learning [121, 135]. One of the most important fields of learning-based control is related to the control of autonomous road vehicles, in which several driving features must be automated to reduce the role of human intervention, e.g., sensing the environment, making decisions, trajectory design, control and intervention with smart actuators. In the case of learning-based control techniques there exist effective methods on the learning process, but the resulting control system may have high complexity, e.g., deep convolutional neural networks. The complex architecture contains conventional control systems (e.g., model-based robust and optimal solutions) and further unconventional solutions, especially machine-learning methods, simultaneously [106]. Nevertheless, increasing complexity of the control systems poses the challenge of performance guarantees for the designers.

The performance requirements against the unmanned control systems can be categorized into two main groups based on their priorities. The primary (safety) performance requirements must be guaranteed during the entire operation of the unmanned system [43]. For example, the limitation of tracking error is a necessary condition in various robotic, vehicle and medical control systems. The secondary performances, e.g., comfort, energy consumption, pollutant emissions, must be considered by the control system, but they can be violated in critical situations, e.g., if a vehicle collision or pedestrian accident is predicted. The consideration of primary and secondary performances leads to a multi-objective optimization problem in the design of the control system. A challenge of control design is to distinguish primary and secondary performances in the control strategy and to provide guarantees on the primary requirements.

Although different types of enhanced learning control methods are able to handle various performance requirements effectively, their achieved performance level is not theoretically guaranteed. The quantity and quality of learning samples can be chosen to any size, but they do not guarantee the avoidance of performance degradation in an emergency scenario or robustness against faults and disturbances. A possible solution on this problem is to provide a control strategy, in which learning-based and model-based control systems are used together. Its motivation is that model-based control design methods have advantages in terms of theoretical guarantees for the performances. In the design of model-based control systems the performances of the system can be defined in a mathematical form and thus, the yielded controller is able to guarantee the performance level of the closed-loop system, which is achieved through the design. Since there may be conflicts between the various performances, a balance between the levels of performances

must be found [173, 74], e.g., the application of weighting functions or iterative tuning etc. Consequently, the complexity of the control-oriented model and the large number of performance specifications in the control design must be limited for numerical reasons in the mathematical computation of the control and the practical implementation possibilities.

Thus, unmanned systems have created gaps in the effectiveness of performance satisfaction and the guarantees between model-based control methods and machine-learning techniques: the model-based control systems are able to provide guarantees, while machine-learning-based control can provide improved performances. Nevertheless, the control of autonomous systems must provide guarantees for safety reasons, while the performances must be satisfied with high efficiency. It requires the combined application of conventional control solutions and machine-learning methods, which is an actual research field in control theory. A reason of this challenge is that the mathematical structure of machine-learning-based algorithms and the formulation of the conventional dynamic controllers are different. This complexity makes difficult to examine the system which, is yielded via their interconnection. Machine-learning-based control systems may be complex for the evaluation of the closed-loop system through the conventional analysis methods of the control theory.

Related works and approaches

In the literature various approaches to provide guarantees on stability and performance issues for machine-learning-based control systems are presented. Most of these studies have been published in recent years, which underlines both the importance and the novelty of the topic. In the following some results of the research area are briefly reviewed.

The application of machine learning with Model Predictive Control (MPC) methods is found, e.g., in [2, 170]. Since computational time may be a crucial problem for the MPC methods, learning methods are able to improve their real-time application. For example, the role of neural networks is to approximate the output of the predictive control through a training process on the optimal solutions of various scenarios. However, a challenge of the approximation is to guarantee stability and constraints, see [57]. In the work of [70] a statistical verification strategy or in [104] a stochastic MPC method has been developed to provide guarantees. A terminal set constraint is used to recursively guarantee the existence of safe control actions at every iteration in [76], which results in a learning-based model predictive control scheme with provable high-probability safety guarantees. Another MPC-based repetitive learning approach is presented in [129]. The goal of the method is to construct recursively terminal set and terminal cost from state and input trajectories of previous iterations, while the feasibility and the nondecreasing property of the performances are guaranteed. This method provides an acceptable solution to the problem of guarantees, because the learning feature is incorporated in the MPC framework, such as the learning of the terminal set and the terminal cost through iterations. However, the method is incompatible with distinct machine-learning structures.

In some other methods conventional control systems and machine-learning agents operate together, while their roles in the control tasks are different. For example, [168] proposes the design for a class of discrete-time single-input single-output nonaffine uncertain nonlinear system. In the design the purpose of the linear dynamic controller is

to stabilize the linearized system, while the state and output feedback adaptive neural network handles nonlinearity. The stability of the closed-loop system is proved through Linear Matrix Inequalities (LMIs). Similarly, a novel switching controller is developed in [171], which consists of a traditional adaptive neural controller and an extra robust controller to pull back the transient from outside of the approximation domain. As a result of the method, the system output converges to a small neighborhood of the reference signal and the closed-loop system is globally stable. Another method for model-reference adaptive controller design with online performance guarantees on tracking success in the presence of a priori dynamic uncertainty is presented in [28].

The overview shows that a general solution on the problem of performances and their guarantees for machine-learning-based control in the existing literature does not exist. The incorporation of the learning process in the control design through iterations and the analysis of the agents have limitations. Since machine-learning-based methods have several well-developed and effective solutions on various problems, it may be fruitful to take them to the part of the control without significant modification. The motivation is to provide a design framework for the problem of performance guarantees, which is independent of the design of the machine-learning-based controller.

2.1 Concept of robust control design frameworks

The aim of this section is to propose control design frameworks for unmanned systems, in which machine-learning-based agents with various structures can be incorporated. The design process is based on robust and Linear Parameter-Varying (LPV) control theories, with which the primary performances are guaranteed and the secondary performances are incorporated in the design process. Since the machine-learning-based agents in unmanned control systems can typically have two important features, two design frameworks are provided.

The agent can provide reference signals for the controller, e.g., the machine-learning-based agent provides reference trajectory and speed for the vehicle through the processing of visual and LiDAR (Light Detection and Ranging) information. In this case the agent is out of the control loop (see Figure 2.1(a)), but the reference signal can have high impact on the performance of the unmanned systems. Thus, the tasks for providing guaranteed performance are (I) to examine the plausibility of the reference signal and (II) to design a robust controller which is able to handle the variation of the reference signal (see Figure 2.1(b)). Thus, in the structure of the controlled system, the plausibility of the reference signal from the learning-based agent is processed by a supervisor. The plausibility process is based on a comparison, the reference signal of the learning-based agent is compared to another reference signal, which is provided by an agent with simplified functionality. The simplified agent is able to provide a reference signal, with which the primary performances are guaranteed, but the secondary performances are not handled. Thus, the supervisor enables the reference signal of the learning-based agent, if the primary performances are not violated, otherwise the reference signal of the simplified agent is enabled. The challenge of the robust control design is to design a controller which is able to track the varied reference signal in the entire range of its enabled variation. The robust control framework for providing performance guarantees in Section 2.2 has been proposed.

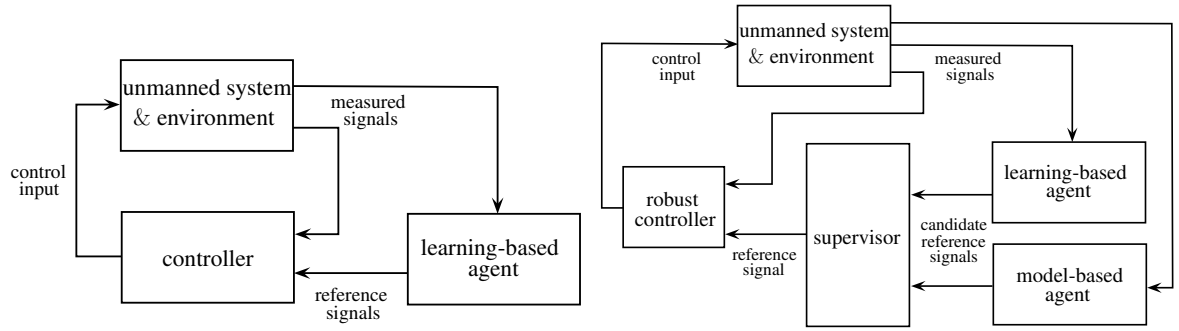

(a) Conventional structure (b) Guaranteed structure

Fig. 2.1: Learning-based agent outside of the control loop

The machine-learning-based agent can be inside of the control loop and it provides control input for the system, see Figure 2.2(a). For example, in the case of an end-to-end learning solution [100] for automated steering a neural network provides the steering signal through camera information. The machine-learning-based agent determines the performance level of the closed-loop systems directly, and thus, the tasks for providing guaranteed performance are (I) to examine the impact of the learning-based control signal on the system and (II) to design a robust controller which is able to provide control signal if the learning-based control signal is unacceptable due to the resulting performance level degradation (see Figure 2.2(b)). Thus, in the structure of the control system a learning-based control and a robust LPV control operate together under the monitoring of a supervisor. In general, especially under normal operation conditions, the supervisor uses a control signal which is calculated by the machine learning control. Nevertheless, emergencies may occur, in which guaranteeing primary performances is essential. In this case, the supervisor uses the control signal of the robust controller and overrides the current control signal. Thus, the theoretically guaranteed performance level is achieved through the application of the robust LPV controller. The robust LPV-based design framework for the solution to the problem of guaranteed performances in Section 2.3 has been provided.

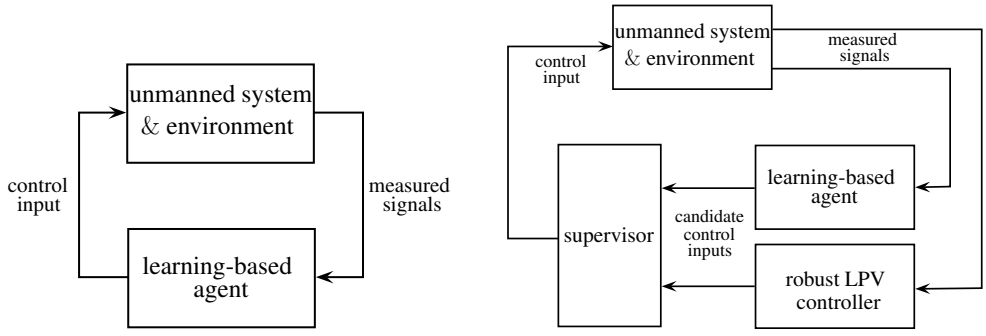

(a) Conventional structure (b) Guaranteed structure

Fig. 2.2: Learning-based agent inside of the control loop

One of the most important advantages of the proposed design frameworks is that they

are independent of the structure of the applied control. Owing to the motivation of automated vehicles machine-learning-based controls are in focus in this thesis. However, in the proposed method none of the structures, i.e., the learning methods or the specialties of the machine learning is considered. Since the proposed method uses only the input and output signals of the applied control system, it can effectively be used for various deep learning methods independently of their internal structure. Furthermore, the robust and LPV framework has well developed design tools and several applications on various control problems, thus the existing experience in the control field provide a beneficial background for the incorporation of machine-learning methods in the novel control context. A drawback of the proposed method is that the design of the robust LPV control requires the formulation of a control-oriented model, whose accuracy can influence the effectiveness of the design.

2.2 Robust control framework with learning-based agent in the reference signal generation

A conventional application of learning-based methods is to design agents with enhanced functionalities, which are able to provide reference signals for the controller, see Figure 2.1. In this section a design framework is proposed with which the primary performances of the unmanned system can be guaranteed if the learning-based agent provides the reference signal. First, the supervisor is designed and second, the design of the robust controller is presented.

2.2.1 Examinations on the reference signals through a supervisor

In this structure the reference signal, which is the output of the learning-based agent, is noted as r_L. Moreover, there is also a model-based reference signal generator in the structure (see Figure 2.1(b)), whose output is r_0. The reference signal for the controller r is provided by the supervisor, whose inputs are r_L and r_0.

The purpose of the supervisor is to decide on the plausibility of r_L. The examination of the signal is based on the comparison of r_L with r_0. The output of the supervisor is the reference signal r, which is formed as

$$r = r_0 + \Delta_l^*, \text{ if } \Delta_l^* \in \Lambda_l, \tag{2.1}$$

where Δ_l^* is a scalar design parameter and Λ_l is a domain.

The value of Δ_l^* is selected in such a way that if the condition $\Delta_l^* \in \Lambda_l$ of (2.1) is guaranteed, then $r = r_L$, such as

$$\Delta_l^* = r_L - r_0. \tag{2.2}$$

But, if the condition on the relation is not guaranteed in (2.1), then Δ_l is limited with the boundary of the domain Λ_l. It means that the general rule of the reference signal formulation is

$$r = r_0 + \Delta_l, \tag{2.3}$$

where

$$\Delta_l = \min\big(\max(\Delta_l^*; \Delta_{l,max}); \Delta_{l,min}\big), \tag{2.4}$$

where $\Delta_{l,min}, \Delta_{l,max}$ are the boundaries of Λ_l. The presented rule in (2.3)-(2.4) expresses that r is inside of a limited environment of r_0. If r_L is inside of the environment, $r = r_L$, but for other cases r_L is overridden through the boundaries.

The relation of the reference signal and the guaranteed performances can be formed from the aspect of the supervisor design problem and from the aspect of the control design problem, as follows.

- There are given the learning-based agent, the model-based agent for the computation of r_L, r_0 and the robust controller (see Figure 2.1(b)). The task of the supervisor design is to determine the maximum of Λ_l, with which the robust performance of the system is guaranteed. This type of design problem is relevant if the controller of the system is fixed and it cannot be changed.

- There are given the learning-based agent, the model-based agent for the computation of r_L, r_0 and the supervisor with a predefined Λ_l. The task of the robust control design is to design a controller which is is able to guarantee the robust performance of the system against varying r. This type of design problem is relevant if there are predefined requirements on the reference signals.

The rest of the section is focused on the second problem, i.e., on the design of the robust controller. Thus, it is assumed that requirements on Λ_l are given and a robust controller must be designed.

2.2.2 Design process of the robust controller

The design of the robust controller requires the description of the system via state-space representation as

$$\dot{x} = Ax + B_1 w + B_2 u, \tag{2.5}$$

where x is the state vector, w is the disturbance vector and u is the vector of the control inputs. The goal of the control design is to guarantee the performance requirements, which are composed in the vector $z = \begin{bmatrix} z_1 & \dots & z_n \end{bmatrix}^T$ as

$$|z_i| \to min, \qquad \forall i = 1 \dots n. \tag{2.6}$$

The formulation of z_i depends on the current control problem. Nevertheless, due to the reference tracking structure in Figure 2.1 there are performances, which are in relation with the reference signal r. It is assumed that z_j, $1 \leq j \leq n$ has the form

$$z_j = \mathtt{x_j} - r, \tag{2.7}$$

where $\mathtt{x_j}$ is the signal from the convex combination of x, w and u, which must track reference r. Performance z_j can be reformed using (2.3) as

$$z_j = \mathtt{x_j} - r_0 + \Delta_l, \tag{2.8}$$

in which r_0 and Δ_l are considered to be measured disturbances. There is an important difference between the measured disturbances:

- r_0 is generated by the model-based agent. The mathematical structure of the model-based agent is considered to be known and using r_0 the primary performances of the system are guaranteed. Therefore, the control designer can have exact knowledge about the properties of r_0, i.e. the range of its value or the frequency content of the signal.

- Δ_l depends on the model-based and the learning-based agents and their bounds are determined by Λ_l. Since there can be more uncertainties in the determination of the properties of the learning-based agent, the characterization of Δ_l can be a complex problem. In the practice of the robust control design, the characteristics of Δ_l can be covered by a conservative approximation.

Since the dynamics of the measured disturbance signals are different, it is recommended to handle them separately in the control design.

The dynamic equations, the performance and the measurement equation are transformed into a joint state-space representation

$$\dot{x} = Ax + B_1 w_{ext} + B_2 u, \tag{2.9a}$$
$$z = C_1 x + D_{11} w_{ext} + D_{12} u, \tag{2.9b}$$
$$y = C_2 x + D_{21} w_{ext} + D_{22} u, \tag{2.9c}$$

where A, B_1, B_2 and $C_1, C_2, D_{11}, D_{12}, D_{21}, D_{22}$ are matrices and the disturbance vector w is extended as $w_{ext} = \begin{bmatrix} w & r_0 & \Delta_l \end{bmatrix}^T$. The measurement vector y contains the signals, which are measured for the output generation of the robust controller.

The control design is based on the robust $\mathcal{H}_\infty$ method, with which the robust stability and the performance requirements of the system against the disturbances can be guaranteed. The design method requires the augmentation of the closed-loop system with weighting functions, see an illustration for three performances in Figure 4.1. The inter-

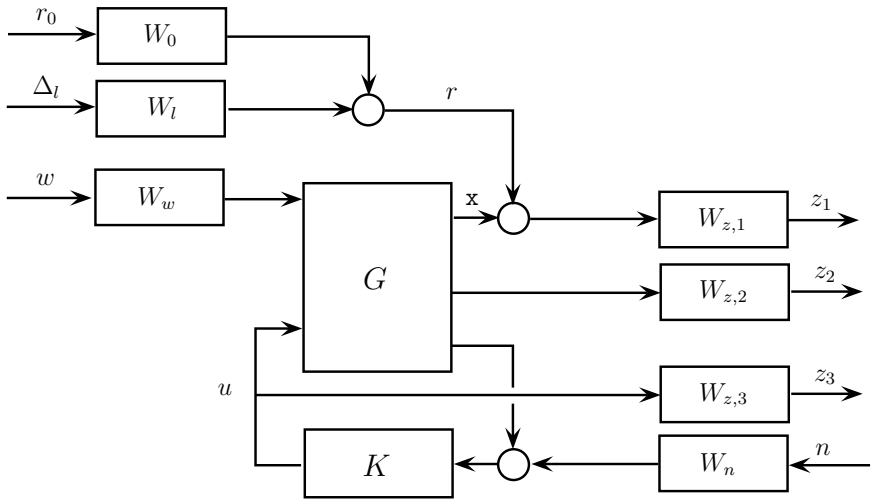

Fig. 2.3: Illustration of closed-loop interconnection structure for $\mathcal{H}_\infty$ design

connection structure contains several weighting functions, whose roles are to guarantee

the trade-off between the performances and to scale the signals. The weight W_n is related to the sensor characteristics on the measurement, where n represent noises, W_{dist} scales the longitudinal disturbance force.

The role of weight W_0 is to consider the dynamics of the reference signal r_0. Similarly, W_1 scales the disturbance Δ_l. This weight is selected in the form of

$$W_l = \frac{\max(\Delta_{l,min}; \Delta_{l,max})}{T_{12}s^2 + T_{11}s + 1}, \tag{2.10}$$

where T_{12}, T_{11} are design parameters, which represent the dynamics of the signal. The selected forms guarantee that the values of the disturbances are $\Delta_{l,1,m}, \Delta_{l,2,m}$ in steady state.

$W_{z,1}, W_{z,2}$ and $W_{z,2}$ are the weights for the performances in (2.6), which represent the minimization of them. Weight $W_{z,1}$ has important role from the aspect of the overall performance of the control, because it scales the tracking error (2.8). The form of the weight is

$$W_{z,1} = \frac{\bar{e}_j}{T_2 s + 1}, \tag{2.11}$$

where T_2 is a design parameter and $\bar{e}_j$ is the expected maximum tracking error. The selected form guarantees that the tracking error is $\bar{e}_j$ in steady state.

The state space representation of the closed-loop control system is formulated in the following way:

$$\dot{x}_{cl} = A_{cl}x_{cl} + B_{cl}w, \tag{2.12a}$$
$$z = C_{cl1}x + D_{cl1}w. \tag{2.12b}$$

The objective of control design is to minimize the $\mathcal{H}_\infty$-norm of the transfer function $T_{z,w}$, which represents the relationship between the disturbances and the performances. More precisely, the problem can be stated as follows [133, 25]: the closed-loop RMS (power-to-power) gain from w to z does not exceed γ, if and only if there exists a symmetric matrix X_∞ such that

$$\begin{bmatrix} A_{cl}P + PA_{cl}^T & PB_{cl} & C_{cl}^T \\ B_{cl}^T P & -\gamma I & D_{cl}^T \\ C_{cl} & D_{cl} & -\gamma I \end{bmatrix} < 0. \tag{2.13}$$

For the system P, find an admissible control K which satisfies the following design criteria:

- the closed-loop system must be asymptotically stable,
- the closed-loop transfer function from w_{ext} to z satisfies the constraint:

$$\|T_{z,w}(s)\|_\infty < \gamma, \tag{2.14}$$

for a given real positive value γ.

New result 2.2.1: Robust control design framework for systems with learning-based agent in the reference signal generation has been provided. The result of the method is a supervisory control system, with which requirements on selected performances are guaranteed. The design of the robust control is based on the $\mathcal{H}_\infty$ method, in which the variation of the reference signal as a disturbance has been incorporated.
References: [Németh and Gáspár, 2021, Németh et al., 2020, Németh and Gáspár, 2020, Németh et al., 2021b, Fényes et al., 2021b]

2.3 Robust control framework with learning-based agent in the control loop

The application of learning-based agents inside of the control loop is an innovative solution on several control problems in the field of automated vehicles. In this case the agent has control purposes, which means that it provides the control input using measured signals, see Figure 2.2. The purpose of this section is to propose the fundamentals of the robust framework, the design of the supervisor and the robust LPV-based controller.

2.3.1 Concept of the design framework

The aim of the concept is to form the structure of the robust design framework with which requirements on the primary performances can be guaranteed. The idea behind the framework is that the control input of the system is equivalent to the output of the learning-based agent, if the requirements on the primary performances can be guaranteed. But, if the primary performances are violated, the output of the learning-based control is overridden by the supervisor. Decision on the violation of the primary performances is performed through the comparison of the output of the learning-based agent and that of the robust LPV controller.

The output of the learning-based controller is vector u_L with n elements as

$$u_L = \mathcal{F}(y_L), \tag{2.15a}$$

$$u_L = \begin{bmatrix} u_{L,1} & u_{L,2} & \dots & u_{L,n} \end{bmatrix}^T, \tag{2.15b}$$

where y_L vector contains the inputs of the controller with m_L elements. $\mathcal{F}$ represents the learning-based controller itself, e.g., a deep-learning neural network, which is activated on its input layer. Moreover, the output of a robust LPV controller is u_K with n elements as

$$u_K = \mathcal{K}(\rho_L, y_K), \tag{2.16a}$$

$$u_K = \begin{bmatrix} u_{K,1} & u_{K,2} & \dots & u_{K,n} \end{bmatrix}^T, \tag{2.16b}$$

where $\mathcal{K}$ represents the LPV controller and y_K is the vector of the measured signals with m_K elements. In (2.16) $\rho_L \in \varrho_K$ vector contains the scheduling variables of the controller, which is considered to have at least n elements.

The fundamental assumption of the design method is that the control input signal of the system $u = \begin{bmatrix} u_1 & u_2 & \dots & u_n \end{bmatrix}^T$ can be expressed as a function of u_K in a linear

form, under predefined conditions. The parameters in the linear formulation are selected to guarantee $u = u_L$ if the requirements on the primary performances are guaranteed by u_L. Thus, the relationship between u, u_K and u_L with the conditions is formed as

$$u = u_L = I_{n\times n} \circ (\rho_L^* J_{1\times n}) u_K + \Delta_L^*, \text{ if } \rho_{L,i}^* \in \varrho_{L,i}, \ \Delta_{L,i}^* \in \Lambda_{L,i}, \ \forall i = 1 \dots n, \tag{2.17}$$

where $\circ$ represents Hadamard product, $I_{n\times n}$ is an $n \times n$ identity matrix, $J_{1\times n}$ is matrix of ones with one row, ρ_L^* and Δ_L^* are $n \times 1$ vectors as

$$\rho_L^* = \begin{bmatrix} \rho_{L,1}^* & \rho_{L,2}^* & \dots & \rho_{L,n}^* \end{bmatrix}^T, \tag{2.18a}$$

$$\Delta_L^* = \begin{bmatrix} \Delta_{L,1}^* & \Delta_{L,2}^* & \dots & \Delta_{L,n}^* \end{bmatrix}^T, \tag{2.18b}$$

and $\rho_{L,i}^*$, $\Delta_{L,i}^*$, $i = 1 \dots n$ are time-dependent weighting signals. $\varrho_{L,i} = [\rho_{L,i,min}; \rho_{L,i,max}]$, $\Lambda_{L,i} = [\Delta_{L,i,min}; \Delta_{L,i,max}]$ represent domains in (2.17), where $\rho_{L,i,min}$, $\rho_{L,i,max}$, $\Delta_{L,i,min}$, $\Delta_{L,i,max}$ are scalars. The sets of the domains are denoted by ϱ_L, Λ_L. Since $I_{n\times n} \circ (\rho_L^* J_{1\times n})$ in (2.17) leads to an $n \times n$ diagonal matrix with the related elements of ρ_L^*, u_i depends only on $u_{K,i}$.

If the conditions of (2.17) for $\rho_{L,i}^*$ and $\Delta_{L,i}^*$ are guaranteed, the control input of the system u is equal to u_L. But, if there exists at least one $i \in [1; n]$, where $\rho_{L,i}^* \notin \varrho_{L,i}$ or $\Delta_{L,i}^* \notin \Lambda_{L,i}$, the variables $\rho_{L,i}^*$, $\Delta_{L,i}^*$ are limited with the boundaries of $\varrho_{L,j}$ and $\Lambda_{L,j}$ during the computation of the control signal u_i. In this case $u \neq u_L$.

The general control rule, which contains both cases is formed as

$$u = I_{n\times n} \circ (\rho_L J_{1\times n}) u_K + \Delta_L, \tag{2.19}$$

where

$$\rho_L = \begin{bmatrix} \rho_{L,1} & \rho_{L,2} & \dots & \rho_{L,n} \end{bmatrix}^T, \tag{2.20a}$$

$$\Delta_L = \begin{bmatrix} \Delta_{L,1} & \Delta_{L,2} & \dots & \Delta_{L,n} \end{bmatrix}^T, \tag{2.20b}$$

$$\rho_{L,i} = \min \left(\max \left(\rho_{L,i}^*; \rho_{L,i,max} \right); \rho_{L,i,min} \right), \quad \forall i = 1 \dots n, \tag{2.20c}$$

$$\Delta_{L,i} = \min \left(\max \left(\Delta_{L,i}^*; \Delta_{L,i,min} \right); \Delta_{L,i,max} \right), \quad \forall i = 1 \dots n. \tag{2.20d}$$

The relations (2.20c)-(2.20d) guarantee that $\rho_L \in \varrho_L$ and $\Delta_L \in \Lambda_L$. The minimum performance level is determined by the LPV controller in the entire operation domain of the system, while inside of the domains ϱ_L, Λ_L the performance level is enhanced through learning-based control. Thus, the advantages of learning-based control can be achieved, while its drawback, such as performance degradation in some scenarios is eliminated through the minimum performance level.

In Figure 2.4 the structure of the given control architecture is presented. In the proposed concept the feedback loop contains the LPV controller, while the learning-based controller is in an auxiliary loop from the control aspect. The role of the supervisor block is to select ρ_L, Δ_L. The actuated control input u on the system depends on u_K, ρ_L, Δ_L.

The design of the control architecture requires the following steps in the process.

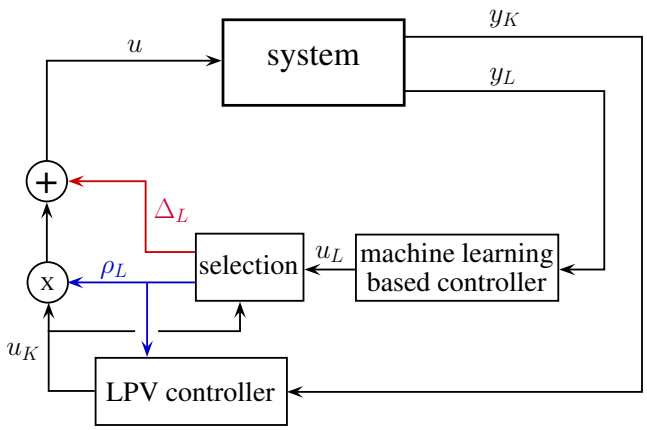

Fig. 2.4: Structure of the control architecture

1. It is necessary to select the values of ρ_L, Δ_L and the domains ϱ_L, Λ_L, as defined in (2.19)-(2.20).

2. The robust LPV control must be designed, in which the domains ϱ_L, Λ_L are incorporated.

The challenge of the control design is that the determination of ϱ_L, Λ_L and the LPV design are not independent from each other. The control design requires the selection of the domains, while the effective selection of the domains requires experience on the performance of the design control. As a solution to this anomaly, an iterative design method is proposed, which incorporates the domain selection and the LPV design in itself. The proposed approach is focused on the iterative design, while the learning-based control is considered to be given.

2.3.2 Selection strategy in the supervisor

The selection strategy of ρ_P and Δ_P is based on the idea that the performance level of the unmanned control system must be maximized. It can be achieved if $u = u_L$ (2.17). However, a predefined minimum performance level for the primary performances must also be guaranteed by the supervisor. The problem of performance level leads to a constrained optimization problem. The maximization of the performance level is achieved through the minimization of the cost function, and the minimum level of primary performances is guaranteed by the constraints. The role of the supervisor is to perform the optimization problem online based on the current signals, e.g., u_L, u_K. The variables of the optimization problem are ρ_P, Δ_P, which are used for the computation of u (2.19).

The objective of the optimization is to minimize the difference between the elements of the control input vector u and the elements of the learning-based agent output u_L. Thus, the cost function is formed as:

$$\sum_{i=1}^{n} \left(u_i - u_{L,i}\right)^2 \rightarrow min. \tag{2.21}$$

The objective (6.4) using (2.19) is rearranged to a quadratic form as

$$\sum_{i=1}^{n}\left(u_i-u_{L,i}\right)^2=\sum_{i=1}^{n}\left(\begin{bmatrix}\rho_{L,i}\\ \Delta_{L,i}\end{bmatrix}^T\begin{bmatrix}u_{K,i}^2 & u_{K,i}\\ u_{K,i} & 1\end{bmatrix}\begin{bmatrix}\rho_{L,i}\\ \Delta_{L,i}\end{bmatrix}+\begin{bmatrix}-2u_{L,i}u_{K,i}\\ -2u_{L,i}\end{bmatrix}^T\begin{bmatrix}\rho_{L,i}\\ \Delta_{L,i}\end{bmatrix}+u_{L,i}^2\right)=$$
$$=\begin{bmatrix}\rho_L\\ \Delta_L\end{bmatrix}^T\beta\begin{bmatrix}\rho_L\\ \Delta_L\end{bmatrix}+\omega^T\begin{bmatrix}\rho_L\\ \Delta_L\end{bmatrix}+u_L^2, \tag{2.22}$$

in which u_L^2 is independent of ρ_L, Δ_L and thus, it can be eliminated during the minimization process (6.4).

The constraints for the optimization are based on the state-space representation of the system:

$$\dot{x}=Ax+\hat{B}_1w+\hat{B}_2u, \tag{2.23}$$

where x represents the state vector and $A, \hat{B}_1, \hat{B}_2$ are matrices in the system representation. The state-space representation of the system is reformulated using the predefined control strategy (2.19) to express u_K instead of u. Therefore, the state-space representation of the system (4.7) is reformulated through the relationship between u and u_K as

$$\dot{x}=Ax+B_1w_K+B_2(\rho_L)u_K, \tag{2.24}$$

where the disturbance vector w_K in the state-space representation (4.8) is composed as $w_K=\begin{bmatrix}w & \Delta_L\end{bmatrix}^T$. The matrices are

$$B_1=\begin{bmatrix}\hat{B}_1 & \hat{B}_2\end{bmatrix}, \tag{2.25a}$$
$$B_2(\rho_L)=\hat{B}_2\big(I_{n\times n}\circ(\rho_L J_{1\times n})\big). \tag{2.25b}$$

Thus, the system is transformed into a LPV representation.

The primary performance requirements on the unmanned control system can typically be formed as inequality constraints on the convex combination of the states and the control input, such as

$$\Theta_{min}\leq\Theta_1x+\Theta_2u\leq\Theta_{max}, \tag{2.26}$$

where $\Theta_{min}, \Theta_{max}$ represent the vectors of the constraints. Θ_1, Θ_2 are matrices, which are formed based on the relationships between x and u. The application of (2.26) in the optimization problem as a constraint requires the reformulation of (2.26), depending on Δ_L, ρ_L.

- The state in the constraint is reformulated as follows. It is assumed that the optimization is solved online with T sampling time. The role of the constraint is to guarantee (2.26) in time step $t+T$, where t denotes the current time. For the computation of $x(t+T)$ the state-space representation (4.8) is transformed into a discrete form with T sampling time as

$$x(k+1)=A_dx(k)+B_{1,d}w_K(k)+B_{2,d}(\rho_L(k))u_K(k), \tag{2.27}$$

where $x(k+1)$ is equal to $x(t+T)$ and $A_d, B_{1,d}, B_{2,d}$ are matrices. It is assumed that the current state vector $x(k) = x$ is known, i.e., it is measured or estimated. Since $w_K(k) = w_K$ is a disturbance vector in the system, not all of its elements can be measured. $B_{1,d}w_K$ can be divided into the components of $\hat{B}_{1,d}w + \hat{B}_{2,d}\Delta_L$. The second term $B_{2,d}\Delta_L$ contains the variable Δ_L of the optimization problem, while the first term $\hat{B}_{1,d}w$ can contain unmeasured disturbances. Therefore, instead of the exact information on $\hat{B}_{1,d}w$, it is covered by the lower and upper limits of the disturbance vector:

$$\Theta_{min,w} \leq \hat{B}_{1,d}w \leq \Theta_{max,w}, \tag{2.28}$$

where $\Theta_{min,w}, \Theta_{max,w}$ are vectors which represent the lower and upper limits of the disturbance vector, respectively. In the composition of the vectors $\Theta_{min,w}, \Theta_{max,w}$, the disturbances are considered elementwise.

- The reformulation of u in (2.26) is provided by (2.19).

The inequalities of constraint (2.26) are reformulated as

$$-\Theta_1\big(A_d x + \Theta_{min,w} + \hat{B}_{2,d}\Delta_L + B_{2,d}(\rho_L)u_K\big) - \Theta_2\big(I_{n\times n} \circ (\rho_L J_{1\times n})u_K + \Delta_L\big) \leq -\Theta_{min}, \tag{2.29a}$$

$$\Theta_1\big(A_d x + \Theta_{max,w} + \hat{B}_{2,d}\Delta_L + B_{2,d}(\rho_L)u_K\big) + \Theta_2\big(I_{n\times n} \circ (\rho_L J_{1\times n})u_K + \Delta_L\big) \leq \Theta_{max}, \tag{2.29b}$$

which can be written in the compact form of

$$\Theta_A \begin{bmatrix} \rho_L \\ \Delta_L \end{bmatrix} \leq \Theta_B, \tag{2.30}$$

where Θ_A is a matrix and Θ_B is a vector.

The constrained optimization problem contains the objective (4.20), the constraint on the states and the control input (2.26) and the constraints on the optimization variables as:

$$\min_{\rho_L, \Delta_L} \begin{bmatrix} \rho_L \\ \Delta_L \end{bmatrix}^T \beta \begin{bmatrix} \rho_L \\ \Delta_L \end{bmatrix} + \omega^T \begin{bmatrix} \rho_L \\ \Delta_L \end{bmatrix}, \tag{2.31a}$$

subject to

$$\Theta_A \begin{bmatrix} \rho_L \\ \Delta_L \end{bmatrix} \leq \Theta_B, \tag{2.31b}$$

$$\rho_L \in \varrho_L, \tag{2.31c}$$

$$\Delta_L \in \Lambda_L. \tag{2.31d}$$

The results of the optimization problem are ρ_L and Δ_L. The output of the supervisor is u, which is computed through (2.19) using ρ_L, Δ and u_K.

2.3.3 Design of the controller via the robust LPV method

The design of the robust LPV controller is based on the state-space representation of the system, which is augmented with Δ_L, ρ_L, see (4.8). Figure 2.5 provides a deeper insight into the idea behind the control architecture from the viewpoint of the robust LPV control design. The control rule (2.19) can be handled as a manipulation of the robust LPV controller output with a known uncertainty Δ_L and a scheduling variable ρ_L (Figure 2.5(a)). Δ_L and ρ_L are the outputs of the supervisor. In the proposed control problem of the design framework the scheme of the controller-uncertainty structure is reformulated, i.e., the plant is augmented with the uncertainty block. Thus, in the design problem of the controller the signals ρ_L, Δ_L and domains ϱ_L, Λ_L are incorporated in the design process, see Figure 2.5(b). The reformulated augmented plant motivates the use of the LPV theory due to parameter variation. The elements of ρ_L are handled as scheduling variables and Δ_L is referred to as a known disturbance vector of the system.

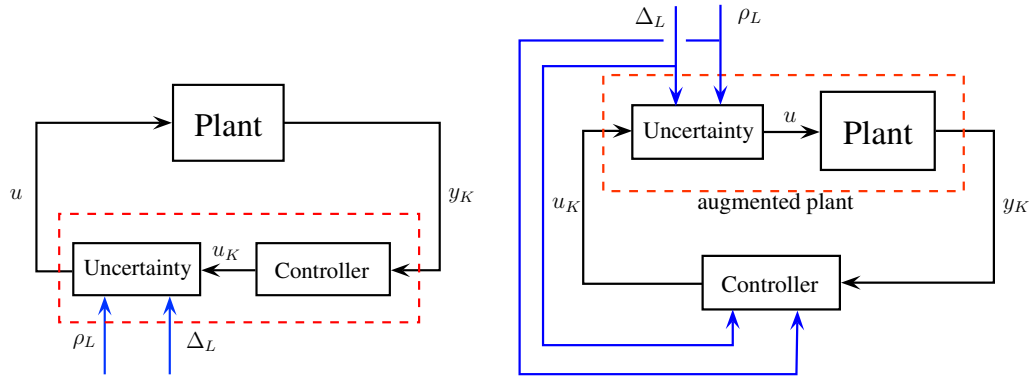

(a) Controller with uncertainty block (b) Plant with uncertainty block

Fig. 2.5: Reformulation of the control design problem

The goal of the robust LPV design is to find a controller with guarantees on the minimum level of primary performances. Nevertheless, in the design of the control further performances can be considered, i.e. secondary performances. These are incorporated in the performance vector z. Performance vector z_K is expressed through the control input u and the existing disturbances w as

$$z = C_2 x + D_{21} w + D_{22} u. \tag{2.32}$$

Similarly to the state-space representation (4.7)-(4.8), the performance equation (8.29) through $u = I_{n\times n} \circ (\rho_L J_{1\times n}) u_K + \Delta_L$ is reformulated as

$$z = C_2 x + D_{21} w_K + D_{22}(\rho_L) u_K, \tag{2.33}$$

where the matrices are

$$D_{21} = \begin{bmatrix} \hat{D}_{21} & \hat{D}_{22} \end{bmatrix}, \tag{2.34a}$$

$$D_{22}(\rho_L) = \hat{D}_{22}\big(I_{n\times n} \circ (\rho_L J_{1\times n})\big). \tag{2.34b}$$

The measured signals for the LPV controller is composed in vector y_K, see Figure 2.4. The model-based design of the controller requires the expression of y_K in the function of x, w and u. The measurement equation is formed as

$$y_K = C_1 x + \hat{D}_{11} w + \hat{D}_{12} u. \tag{2.35}$$

Through the relation $u = I_{n\times n} \circ (\rho_L J_{1\times n}) u_K + \Delta_L$ the measurement equation is reformulated as

$$y_K = C_1 x + D_{11} w_K + D_{12}(\rho_L) u_K, \tag{2.36}$$

where the matrices of (2.36) are

$$D_{11} = \begin{bmatrix} \hat{D}_{11} & \hat{D}_{12} \end{bmatrix}, \tag{2.37a}$$

$$D_{12}(\rho_L) = \hat{D}_{12}\big(I_{n\times n} \circ (\rho_L J_{1\times n})\big). \tag{2.37b}$$

Finally, the augmented plant for the design of the robust LPV controller using (4.8), (2.33) and (2.36) is formulated:

$$\dot{x} = Ax + B_1 w_K + B_2(\rho_L) u_K, \tag{2.38a}$$

$$z = C_2 x + D_{21} w_K + D_{22}(\rho_L) u_K, \tag{2.38b}$$

$$y_K = C_1 x + D_{11} w_K + D_{12}(\rho_L) u_K. \tag{2.38c}$$

The goal of the design method of the LPV control is to provide the quadratic stability of the closed-loop system and the induced $\mathcal{L}_2$ norm from the disturbance vector w_K to z is less than the scalar $\gamma > 0$. The existence of a controller that solves the quadratic LPV γ-performance problem can be expressed as the feasibility of a set of LMIs, which can be solved numerically. The constraints set by the LMIs are not finite. The infiniteness of the constraints is relieved by a finite, sufficiently fine grid. To specify the grid of the performance weights for the LPV design, the scheduling variables are defined through lookup-tables. Gridding reflects the qualitative changes in the performance weights, i.e., the scheduling variables $\rho_L \in \varrho_L$. The stability and the performance level of the closed-loop system are guaranteed by the design procedure [161, 26, 41]. The quadratic LPV performance problem is to choose the parameter-varying controller $\mathcal{K}(\rho_L, y_K)$ in such a way that the resulting closed-loop system is quadratically stable and the induced $\mathcal{L}_2$ norm from the disturbance and the performances is less than the value γ. The minimization task is the following:

$$\inf_{\mathcal{K}(\rho_L, y_K)} \sup_{\rho_L \in \varrho_L} \sup_{\substack{\|w_K\|_2 \neq 0, \\ w_K \in \mathcal{L}_2}} \frac{\|z\|_2}{\|w_K\|_2}. \tag{2.39}$$

The existence of a controller that solves the quadratic LPV γ-performance problem can be expressed as the feasibility of a set of LMIs, which can be solved numerically. Finally, the state-space representation of the LPV control $\mathcal{K}(\rho_L, y_K)$ is constructed, see [161, 138, 109, 20]. The optimization problem (4.23) is solved offline and the resulted controller is $\mathcal{K}(\rho_L, y_K)$ implemented for online control input computation. It leads to the control

input u_K (2.16), which is incorporated in the computation of u (2.19) together with the selection of ρ_L, Δ_L. The control rule results in that the minimum performance level of the closed-loop system is determined by $\mathcal{K}(\rho_L, y_K)$.

The relationship between the selection of ϱ_L, Λ_L and the design of $\mathcal{K}(\rho_L, y_K)$ has been presented in Subsection 2.3.1. The scaling of the performance level through the design of $\mathcal{K}(\rho_L, y_K)$ requires the preliminary selection of ϱ_L, Λ_L. Similarly, the scaling of the performance level through the selection of ϱ_L, Λ_L requires the preliminary design of $\mathcal{K}(\rho_L, y_K)$. Moreover, the design problem of the robust LPV controller (4.23) and the optimization problem in the supervisor (4.21) are not independent of each other due to ϱ_L, Λ_L. A possible solution to the problem is to create an iterative design process, in which the control design, the selection of ϱ_L, Λ_L and the optimization in the supervisor are ordered and performed in an iterative method.

The goal of the iteration is to minimize the difference between u, u_L and to minimize the bounds ϱ_L, Λ_L. The result of the fitting is the reduction of the domains and the reduction of the conservativeness of controller $\mathcal{K}(\rho_L, y_K)$. The fitting of the domains is achieved through an iterative process. Through the iteration a balance between the range of the domains and the characteristics of the control intervention can be achieved. Thus, in the iteration the domains and the characteristics of the intervention are incorporated, which leads to the following optimization task

$$\min_{\substack{\rho_{L,i,min} > 0,\\ \rho_{L,i,max} > 0}} \sum_{i=1}^{n} R_i \Big(\rho_{L,i,max} - \rho_{L,i,min} \Big) + D_i \Big(|\Delta_{L,i,max}| - |\Delta_{L,i,min}| \Big) + T_i \bar{E}_i, \qquad (2.40)$$

with the constraint $\rho_{L,i,max} > \rho_{L,i,min}$, where $\bar{E}_i$ is the average relative error of u_i and $u_{L,i}$. Moreover, $R_i > 0$, $D_i > 0$ and $T_i > 0$, $i = 1 \dots n$ scalars are design parameters.

Through the selection of T the average relative error of u_i and $u_{L,i}$ can be scaled. The motivation behind the increasing of T is to design an LPV controller whose output is as close as possible to the output of the learning-based controller. If u_i is close to $u_{L,i}$, the advantageous dynamics of the learning-based controller is approximated by the LPV controller. Its consequence is that the domains of $\varrho_{L,i}$ and $\Lambda_{L,i}$ are increased. Nevertheless, in a scenario with the performance loss of the learning-based controller, u_i can be close to $u_{L,i}$ for a long time, which can reduce the minimum performance level of the system. It motivates the limitation of T. The roles of R_i, D_i parameters are to scale the domains and to guarantee a balance between them. Thus, the values of R_i, D_i express priority between the reduction of the scheduling variable domain and the disturbance domain. The motivation behind the selection of R, D is to facilitate the LPV control design. If the domain of $\varrho_{L,i}$ is increased, the grid of the LPV design is also increased. Due to the increased difference between the edges of the grid, the design process of the LPV controller can be difficult, because the domains of the systems with the frozen scheduling variables are high. Similarly, if the domain of $\Lambda_{L,i}$ is increased, an increased robustness against the system is required. Both effects can result in unfeasible LMI problems in the design of the LPV control. Therefore, it is necessary to limit R and D.

The solution of the optimization problem (4.24) begins with domains with high ranges, which are reduced through the following iteration process.

1. The domains $\varrho_{L,i} = [\rho_{L,i,min}; \rho_{L,i,max}]$ and $\Lambda_{L,i} = [\Delta_{L,i,min}; \Delta_{L,i,max}]$ are selected high

in the first step. The initial value of $\rho_{L,i,min}$ is selected $\rho_{L,i,min} = \varepsilon_i$, where $0 < \varepsilon_i$ has a small value. Initially, $\rho_{L,i,max}$ is selected high and similarly, $|\Delta_{L,i,min}|$, $|\Delta_{L,i,max}|$ also have high values, which results in a conservative LPV control. The goal of the iterative design process is to reduce the conservativeness through the appropriate selection of the boundaries.

2. The LPV control with the selected domains is designed using (4.23).

3. The closed-loop system with the incorporation of the designed $\mathcal{K}(\rho_L, y_K)$ and the domains ϱ_L, Λ_L are analyzed through various scenarios. It yields the signals u_L and u_K.

4. Due to the results of the scenarios the boundaries are modified to reduce the cost function of the optimization problem (4.24). The new values of $\rho_{L,i,min}, \rho_{L,i,max}$ and $\Delta_{L,i,min}$, $\Delta_{L,i,max}$ for all $i = 1 \dots n$ are selected by the optimization algorithm, e.g., through simplex search or trust-region-reflective methods [80, 35].

5. The LPV design, the scenarios and the evaluation (steps 2-4) are performed until the minimum of (4.24) is reached. If the minimum performance level of the designed control is not suitable, or the ranges of the domains result in frequent control intervention on the bounds, the parameters R_i, D_i and T_i must be modified (step 1) and the iteration must be performed again.

The results of the iteration process are the robust LPV controller and the domains ϱ_L, Λ_L.

New result 2.3.1: Robust control design framework for systems with learning-based agent in the control loop has been provided, with which requirements on selected performances are guaranteed. The novel framework contains two main elements, i.e., the supervisor and the robust controller. The role of the supervisor is to decide on the actual control input, which is based on the comparison of the outputs of the learning-based agent and the robust controller. The algorithm of the supervisor is formed as a constrained quadratic optimization problem. The design of the robust controller based on the Linear Parameter-Varying (LPV) method, in which the difference between the outputs of the learning-based agent and the robust controller through a scheduling variable and a measured disturbance is considered.
References: [Németh and Gáspár, 2021, Németh and Gáspár, 2021c, Németh, 2021, Gáspár and Németh, 2016, Németh, 2019]

Part II

ENERGY-OPTIMAL CRUISE CONTROL FOR INDIVIDUAL AUTOMATED VEHICLES

dc_1992_22

3. PREDICTIVE ENERGY-OPTIMAL CRUISE CONTROL FOR AUTOMATED VEHICLES

Various safety, economy and comfort requirements against automated vehicles pose complex decision and control design challenges. A possible solution on the adaptation to the environment of vehicles is to use increased number of information on the road and traffic through vehicle-to-vehicle (V2V) and infrastructure-to-vehicle (I2V) communication [137].

In the recent years several design methodologies in the field of enhanced energy-efficient driving systems on several vehicle control tasks have been developed. Several methods for considering road conditions have already been proposed, see e.g., [64, 114] and the overview on the principles of the energy efficient cruise controls [53]. The consideration of forthcoming terrain characteristics has been handled by using a receding horizon control under real road conditions in [55, 118]. A study on the implementation of eco-cruise control systems has been published by [5]. In another approach the impact of terrain characteristics and of traffic flow dynamics have been modeled in stochastic framework using a Markov chain model in [77], or [162] has presented a deep learning-based eco-driving solution to electric vehicles.

The motivation of the research is that current cruise control systems are able to take into consideration only instantaneous effects of road conditions and preceding vehicles. Nevertheless, information on the oncoming road can improve the energy-efficient motion of automated vehicles. For example, the effect of longitudinal acceleration on downhill road sections can motivate the reduction of velocity on the previous road sections. It leads to reduced energy consumption on the previous road section and to reduced brake activation on the downhill section.

As a result of my research activity in SZTAKI, systematic design and analysis methods for predictive cruise control systems of automated vehicles with the consideration of road and traffic information have been summarized in book [Gáspár and Németh, 2019]. In this section the fundamentals of the methods and their implementation possibilities are presented.

3.1 Formulation of energy-optimal speed profile using road information

In this section road inclinations and speed limits are formulated for achieving energy-optimal speed profile. Information on road inclinations is a necessary assumption for the calculation. It can be achieved through enhanced digital maps [96], measurements, e.g., cameras, laser/inertial profilometers, differential GPS or a GPS/INS systems [12, 79, 52], or Kalman filtering [91].

The principle of considerating road conditions is illustrated in Figure 3.1. A finite horizon ahead of the vehicle is divided into n number of segments. $v_{ref,i}$ original reference velocities to each segment endpoints are assigned. Moreover, it is assumed that the automated vehicle moves with constant acceleration values along each segments. The dynamics of the vehicle is described on each segments, from the initial point (0) to the endpoint (n) of the horizon. The longitudinal motion of the vehicle is influenced by the traction force F_l as control signal and the disturbance force F_d. Several longitudinal disturbances influence the motion of the vehicle, such as $F_d = F_r + F_{aer} + G_x$, where F_r, F_{aer} and G_x are the rolling resistance, the aerodynamic force and the weighting force, respectively.

The task of the design method is to select modified reference velocity λ for initial point 0, with which the vehicle speed profile guarantees performances requirements on longitudinal control force F_l and on traveling time. The formulation for achieving speed profile is as follows. In the prediction model it is assumed that the velocity in the initial point is equal to the first original reference velocity:

$$\dot{\xi}_0^2 = v_{ref,0}^2. \tag{3.1}$$

The displacement of the vehicle in the first section can be expressed by the velocity differences using kinematic equation $s_1 = \frac{1}{2}(\dot{\xi}_1 + \dot{\xi}_0)t$, where $\dot{\xi}_0$ is the velocity of vehicle at the initial point, $\dot{\xi}_1$ is the velocity of vehicle at the first point and s_1 is the length of first segment [1]. Since in the prediction model the acceleration of the vehicle on each segments is considered to be constant, t is expressed as $t = \frac{\dot{\xi}_1 - \dot{\xi}_0}{\ddot{\xi}}$. Consequently, the velocity of the

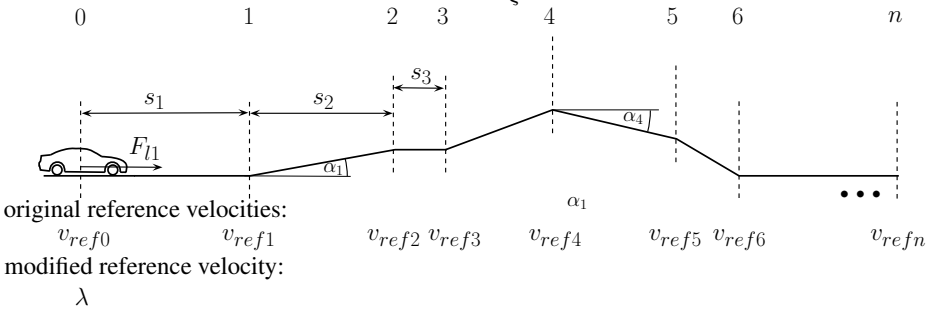

Fig. 3.1: Segment points on the road ahead of the vehicle

first section point can be expressed by the initial velocity and the acceleration as follows:

$$\dot{\xi}_1^2 = \dot{\xi}_0^2 + 2\ddot{\xi}s_1 = \dot{\xi}_0^2 + \frac{2}{m}s_1(F_{l1} - F_{d1}). \tag{3.2}$$

The velocity of the first section point $\dot{\xi}_1^2$ is defined as the reference velocity $v_{ref,1}^2 = \dot{\xi}_1^2$.

The velocity of the vehicle can be formulated for similarly to the next $n-1$ section points. Using this principle, a velocity-chain model, which contains velocities along the way of the vehicle, is constructed. At the calculation of the control force it is assumed that additional longitudinal forces $F_{li}, i \in [2, n]$ will not affect the next sections. The velocities

of vehicle are described at each section point of the road by using similar expressions to (3.2). The velocity of the n^{th} section point is

$$\dot{\xi}_n^2 = \dot{\xi}_0^2 + \frac{2}{m}(s_1 F_{l1} - \sum_{i=1}^{n} s_i F_{di}) = v_{ref,n}^2. \tag{3.3}$$

In the prediction model $F_{di} = F_{di,r} + F_{di,o}$ disturbance force is considered to be divided in two parts: the first part is the force resistance from road slope $F_{di,r}$, while the second part $F_{di,o}$ contains all of the other resistances such as rolling resistance, aerodynamic forces, etc. It is assumes that $F_{di,r}$ is known while $F_{di,o}$ is unknown. The known part of the disturbances contains the longitudinal component of the weighting force, and thus, $F_{di,r} = G_x$ depends on the mass of the vehicle and the angle of the slope α_i. When the control force F_{l1} is calculated, only $F_{d1,o}$ influences the vehicle of all of the unmeasured disturbances. In the control design the effects of the unmeasured disturbances $F_{di,o}$, $i \in \{2, n\}$ are ignored. The consequence of this assumption is that the model does not contain all the information on road disturbances. Therefore it is necessary to design a robust speed controller for handling undesirable effects.

In the next step weights on each segment points are introduced. Weight Q is applied to the current reference velocity, weights $\gamma_1, \gamma_2, ..., \gamma_n$ are applied to the reference velocities at the section points. Weight Q has essential role: it characterizes the tracking requirement of the actual original reference velocity $v_{ref,0}$. Weights γ_i represent the rate of the road conditions ahead of the vehicle. The weights should sum up to one, i.e.,

$$\gamma_1 + \gamma_2 + ... + \gamma_n + Q = 1. \tag{3.4}$$

Weight Q is applied in equation (3.1) and weights $\gamma_1, \gamma_2, ..., \gamma_n$ are applied in order to prioritize the importance of each sections, i.e.,

$$Q\dot{\xi}_0^2 = Qv_{ref,0}^2 \tag{3.5a}$$

$$\gamma_1\dot{\xi}_0^2 + \gamma_1\frac{2}{m}s_1F_{l1} - \gamma_1\frac{2}{m}s_1F_{d1,o} = \gamma_1 v_{ref,1}^2 + \gamma_1\frac{2}{m}s_1F_{d1,r} \tag{3.5b}$$

$$\gamma_2\dot{\xi}_0^2 + \gamma_2\frac{2}{m}s_1F_{l1} - \gamma_2\frac{2}{m}s_1F_{d1,o} = \gamma_2 v_{ref,2}^2 + \gamma_2\frac{2}{m}(s_1F_{d1,r} + \gamma_2 s_2 F_{d2,r}) \tag{3.5c}$$

$$\vdots$$

$$\gamma_n\dot{\xi}_0^2 + \gamma_n\frac{2}{m}s_1F_{l1} - \gamma_n\frac{2}{m}s_1F_{d1,o} = \gamma_n v_{ref,n}^2 + \gamma_n\frac{2}{m}\sum_{i=1}^{n} s_i F_{di,r} \tag{3.5d}$$

Since the sum of Q and γ_i weights are 1, see (3.4), the sum of equations in (3.5) leads to a weighted average of each sub-equations and the following formula is yielded:

$$\begin{aligned}(Q + \gamma_1 + \gamma_2 + ... + \gamma_n)\dot{\xi}_0^2 + \frac{2}{m}s_1(\gamma_1 + \gamma_2 + ... + \gamma_n)F_{l1} - \frac{2}{m}s_1(\gamma_1 + \gamma_2 + ... + \gamma_n)F_{d1,o} \\ = Qv_{ref,0}^2 + (\gamma_1 v_{ref,1}^2 + \gamma_2 v_{ref,2}^2 + ... + \gamma_n v_{ref,n}^2) + \frac{2}{m}s_1F_{d1,r}(\gamma_1 + \gamma_2 + ... + \gamma_n) + \\ + \frac{2}{m}s_2F_{d2,r}(\gamma_2 + ... + \gamma_n) + \ldots + \frac{2}{m}s_nF_{dn,r}\gamma_n\end{aligned} \tag{3.6}$$

Through the rearrangement of (3.6), the following representation of the prediction model is achieved:

$$\dot{\xi}_0^2 + \frac{2}{m} s_1 (1-Q) F_{l1} - \frac{2}{m} s_1 (1-Q) F_{d1,o} = \vartheta, \tag{3.7}$$

where the right hand side, i.e., value ϑ depends on road slopes, original reference velocities and weights

$$\vartheta = Q v_{ref,0}^2 + \sum_{i=1}^{n} \gamma_i v_{ref,i}^2 + \frac{2}{m} \sum_{i=1}^{n} s_i F_{di,r} \sum_{j=i}^{n} \gamma_j. \tag{3.8}$$

Note that weights have important role both in further analysis and synthesis. By making an appropriate selection of the weights, the importance of the road condition is taken into consideration. For example, when $Q = 1, \quad \gamma_i = 0, \ i \in [1, n]$ the control exercise is simplified to a cruise control problem without any road conditions. When equivalent weights are used the road conditions are considered with the same importance, such as $Q = \gamma_1 = \gamma_2 = ... = \gamma_n$. The optimal determination of the weights has an important role, i.e., to achieve a balance between the current velocity and the effect of the road slope. Consequently, a balance between the velocity and the economy parameters of the vehicle is formulated.

The modified reference velocity for the automated vehicle through the rearrangement of (3.7) is yielded:

$$\lambda = \sqrt{\vartheta - 2 s_1 (1-Q)(\ddot{\xi}_0 + g sin\alpha)}, \tag{3.9}$$

where F_{l1} is expressed by the longitudinal motion equation and thus, longitudinal acceleration $\ddot{\xi}_0$ is measured. As a result of the prediction model, road conditions and speed limit information in formulation and tracking of a reference velocity tasks are formulated.

New result 3.1.1: Prediction method for speed profile design of automated vehicles has been developed. In the provided new method several information on the forthcoming road section, i.e., terrain characteristics, speed limitations, traffic information and motion of surrounding vehicles, are incorporated in.
References: [Gáspár and Németh, 2019, Németh et al., 2013a, Gáspár and Németh, 2015, Gáspár and Németh, 2014b]

3.2 Optimization of the cruise control for automated vehicles

In this section the goal is to find an optimal selection of weights $Q, \gamma_i, \ \forall i \in [1; n]$ in such a way that both the minimization of control force and of traveling time are taken into consideration. In the rest of this section, $Q, \gamma_i, \ \forall i \in [1; n]$ are called as prediction weights.

Equations (3.7)-(3.9) show that λ depends on the prediction weights. In the following the longitudinal force is expressed by the weights:

$$F_{l1} = \beta_0(Q) + \beta_1(Q)\gamma_1 + \beta_2(Q)\gamma_2 + \ldots + \beta_n(Q)\gamma_n + K, \tag{3.10}$$

where the members of the expression can be expressed by the weights Q and γ_i and K represents the sum of prediction weight-independent terms. The cruise control optimization problem can be divided into two optimization problems in the following forms:

Optimization 1: The longitudinal control force must be minimized. In practice, the quadratic formulation of F_{l1} is used to express the objective, such as

$$F_{l1}^2 \rightarrow Min! \tag{3.11}$$

Optimization 2: The difference between reference velocity and actual velocity must be minimized, i.e.,

$$|v_{ref,0} - \dot{\xi}_0| \rightarrow Min! \tag{3.12}$$

The two optimization criteria lead to different optimal solutions. In the first criterion the predicted road inclinations and speed limits are taken into consideration by using appropriately chosen weights $\hat{Q}, \hat{\gamma}_i$. At the same time the second criterion is optimal if the predicted information is neglected. In the latter case the prediction weights resulted by Optimization 2 are noted by $\breve{Q}, \breve{\gamma}_i$.

The first criterion (Optimization 1) is met by the formulation of a quadratic optimization problem with the following form:

$$\hat{F}_{l1}^2(\hat{Q}, \hat{\gamma}_i) = (\beta_0(\hat{Q}) + \beta_1(\hat{Q})\hat{\gamma}_1 + \beta_2(\hat{Q})\hat{\gamma}_2 + \ldots + \beta_n(\hat{Q})\hat{\gamma}_n)^2, \tag{3.13}$$

and with the following constrains

$$\hat{\gamma}_1 + \hat{\gamma}_2 + ... + \hat{\gamma}_n + \bar{Q} = 1, \tag{3.14a}$$

$$0 \leq \hat{Q}, \hat{\gamma}_i \leq 1. \tag{3.14b}$$

This task is nonlinear because of the prediction weights. If in the first optimization the prediction weight $\hat{Q}$ is frozen, the optimization task is quadratic in the sense of prediction weights $\hat{\gamma}_i$, and (3.13) is formulated in the following matrix form:

$$\hat{F}_{l1}^2(\Gamma) = \frac{1}{2}\Gamma^T \Phi \Gamma - \kappa\Gamma, \tag{3.15}$$

where the matrix Γ is $\Gamma = \begin{bmatrix}\hat{\gamma}_1 & \cdots & \hat{\gamma}_i & \cdots & \hat{\gamma}_n\end{bmatrix}^T$ and the matrix Φ comes from the rearrangement of (3.13). Thus, the optimization problem leads to a set of quadratic programming tasks for each frozen $\hat{Q}$.

The optimal solution for the second criterion (Optimization 2) can be computed in a relatively easy way, since the vehicle tracks the predefined velocity if the predicted road conditions are not considered. Consequently, the optimal solution is achieved by selecting the prediction weights in the following way: $\breve{Q} = 1$ and $\breve{\gamma}_i = 0, i \in [1, n]$.

Finally, a balance between the two performances must be achieved, which is based on a tuning of the designed prediction weights, i.e., the first criterion is met by selecting prediction weights $\bar{Q}$, $\bar{\gamma}_i$, and the second performance is met by selecting constant prediction weights $\breve{Q}, \breve{\gamma}_i$. For achieving a balance between the two solutions, in the proposed method

two performance weights, i.e., R_1 and R_2, are introduced. The performance weight R_1 ($0 \leq R_1 \leq 1$) is related to the importance of the minimization of the longitudinal control force F_{l1} (Optimization 1) while performance weight R_2 ($0 \leq R_2 \leq 1$) is related to the minimization of $|v_{ref,0} - \dot{\xi}_0|$ (Optimization 2). It is defined a constraint according to the performance weights: $R_1 + R_2 = 1$. The advantage of performance weights compared to prediction weights is that the selection of R_1, R_2, i.e., balance between energy consumption and traveling time, can be better articulated for the operator of the vehicle. The performance weights, which guarantee balance between optimizations tasks, are calculated in the following expressions:

$$Q = R_1\bar{Q} + R_2\breve{Q} = R_1\bar{Q} + R_2 = 1 - R_1(1 - \bar{Q}), \tag{3.16a}$$

$$\gamma_1 = R_1\bar{\gamma}_1 + R_2\breve{\gamma}_1 = R_1\bar{\gamma}_1, \tag{3.16b}$$

$$\vdots$$

$$\gamma_n = R_1\bar{\gamma}_n + R_2\breve{\gamma}_n = R_1\bar{\gamma}_n. \tag{3.16c}$$

Method for selecting performance weights

Although the selection of performance weights is the role of the vehicle operator, e.g., driver, a systematic method for a time-constrained selection is proposed. Since traveling time has great importance for both drivers and logistic services, keeping a scheduled traveling time has impact on the acceptance of such autonomous systems. Hence, managing traveling time is a key element of the proposed method, which is guaranteed by the proper selection of the tuning parameter R_1. Hence, in order to keep the desired traveling time constraints in the optimization of R_1 is needed. For this purpose, the formulation of actual and predicted future motion of the controlled vehicle is necessary. For this reason, the vehicle speed on the forthcoming road horizon must be estimated. The speed in the i^{th} section points is the following:

$$\dot{\xi}_i^2 = \dot{\xi}_0^2 + \frac{2}{m}s_1F_{l1} - \frac{2}{m}F_{d1,o} - \frac{2}{m}\sum_{j=1}^{n} s_jF_{dj}, \quad i = \{1, ..., n\}, \tag{3.17}$$

where $\dot{\xi}_0$ depends on the selected weighting gain R_1 according to (3.9).

The goal of the optimal speed design is to keep traveling time of the vehicles under a required traveling time Δt_{max}, i.e., R_1 must be maximized and simultaneously, this criterion must be guaranteed. Thus, if the time requirement cannot be accomplished, the speed strategy results in $R_1 = 0$ and thus, the maximum speed is applied.

In the following a prediction for the desired traveling time is presented. Assuming constant accelerations on each road sections, it is possible to predict the traveling time between section points as follows:

$$\Delta t_1 = \frac{2s_1}{\dot{\xi}_1 + \lambda}, \quad i = 1; \quad \Delta t_i = \frac{2s_i}{\dot{\xi}_i + \dot{\xi}_{i-1}}, \quad i = 2 \ldots n \tag{3.18}$$

The overall travel time on the look-ahead horizon can be calculated by summing up travel

times between section points:

$$\Delta t = \sum_{i=1}^{n} \Delta t_i. \tag{3.19}$$

Desired traveling time Δt_{min} is calculated by taking speed limits into consideration. It must be compared to both the predicted traveling time Δt and the required traveling time Δt_{max}. For this purpose, based on the speed limits $v_{ref,i}$, the traveling time is computed for each road sections as follows:

$$\Delta t_{i,min} = \frac{2s_i}{v_{ref,i} + v_{ref,i-1}}, \quad i = 1 \dots n \tag{3.20}$$

Hence, the total minimum traveling time can be given as sum of the minimum time values:

$$\Delta t_{min} = \sum_{i=1}^{n} \Delta t_{i,min} \tag{3.21}$$

The computed Δt_{min} results in the minimum traveling time of the vehicle on the horizon.

Next, the differences between the predicted traveling time Δt, the minimum traveling time Δt_{min}, and the required traveling time Δt_{max} are analyzed. From these values, Δt depends on the weighting parameter R_1. If $R_1 = 0$, i.e., the optimization focuses only on the traveling time, the difference is $\Delta t - \Delta t_{min} = 0$. If $R_1 > 0$ then the difference will be positive, since the predicted traveling time increases: $\Delta t - \Delta t_{min} > 0$. Moreover, a maximum value of the acceptable time delay t_{max} is introduced, which is defined by the driver or a fleet management system based on logistics service requirements. In the selection of t_{max}, both the minimum traveling time Δt_{min} and the required traveling time Δt_{max} are taken into consideration.

The purpose of the speed design is to achieve a balance between energy consumption and traveling time. Thus, the design usually leads to the positive value of $R_1 > 0$. Besides, the total delay of the vehicle must be checked, i.e., it must be smaller or equal to t_{max}:

$$\Delta t - \Delta t_{min} \leq t_{max}. \tag{3.22}$$

The formed constraint depends on R_1 according to (3.9), (3.18)-(3.21). The acceptable time delay in (3.22) has high impact, because it influences Δt and Δt_{min}. The longer time horizon is set, the longer road section can be considered. Certainly, if (3.22) cannot be guaranteed, $R_1 = 0$ for the remaining road sections must be selected, i.e., the vehicle moves as high speed as possible.

Handling preceding vehicle in the speed design

Since automated vehicle may catch up with a preceding vehicle, it is necessary to consider speed of the latter v_{lead}. The estimation of the safe stopping distance may be conservative in a normal traffic situation, where the preceding vehicle can also brake, and therefore the distance between the vehicles may be reduced. The safe stopping distance

between the vehicles is determined according to the rule of 91/422/EEC, 71/320/EEC UN and EU directives (in case of M_1 vehicle category, the velocity in km/h):

$$d_{st} = 0.1\dot{\xi}_0 + \dot{\xi}_0^2/150, \tag{3.23}$$

in which $\dot{\xi}$ is the current speed.

The consideration of the preceding vehicle is determined by W, which is selected in the following structure:

$$W = \begin{cases} 1 & \text{if} \quad d < d_{st} \\ (\alpha d_{st} - d)/((\alpha - 1)d_{st}) & \text{if} \quad d_{st} \leq d \leq \alpha \cdot d_{safe} \\ 0 & \text{if} \quad d > \alpha \cdot d_{st} \end{cases} \tag{3.24}$$

where α is a design parameter. For example, $\alpha = 0.5$ means that the speed of the vehicle must be reduced, when the distance is less than $1.5 \cdot d_{st}$. The weight is illustrated in Figure 3.2.

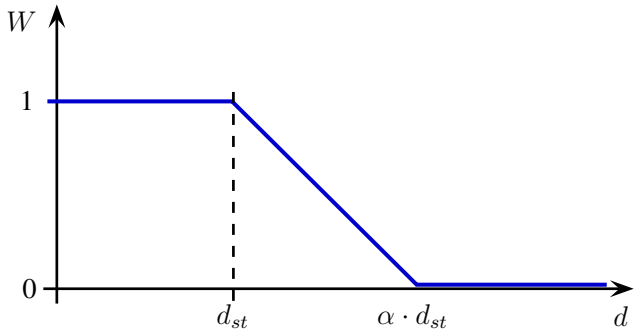

Fig. 3.2: Selection of weight W

The velocity of the vehicle is calculated by using the optimization procedure. It does not modified until the distance from the preceding vehicle is greater than the predefined value αd_{st}. When the distance is reduced, i.e., $d \leq \alpha d_{st}$, the velocity must be modified by applying the weight factor W in the following way:

$$\lambda = W \cdot v_{lead}. \tag{3.25}$$

Consequently, the distance between the vehicles decreases to the safety value. This velocity must be applied, but the velocity is calculated by using the optimization procedure. When the preceding vehicle accelerates and exceeds the calculated velocity, the optimal speed can be applied again.

Because of safety reasons, factor W has priority over the prediction weights Q and γ_i. Thus, in the weighting strategy instead of (3.4), weights should sum up to

$$\gamma_i + \gamma_2 + \ldots + \gamma_n + Q = 1 - W, \tag{3.26}$$

and the new weights must be reduced in the following way:

$$Q_n = Q(1 - W), \quad \gamma_{n,i} = \gamma_i(1 - W),\ i \in [1, n], \tag{3.27}$$

where Q and γ_i are the original weight factors. The designed speed of the vehicle does not exceed the speed, defined in (3.25).

Architecture of energy-optimal cruise control system

The energy-optimal cruise control system can be realized in three layers as Figure 3.3 shows.

Layer 1: The aim of the first, i.e., the high-level layer is the computation of the reference velocity λ (3.9). The results of this computation are prediction weights and the modified reference velocity, which must be tracked by the vehicle. The computation process in block K_0 is compressed in Figure 3.3. The reference velocity is realized through the following layers.

Layer 2: In the second, i.e., control-level layer, the longitudinal control force of the vehicle (F_{l1}) is designed. The role of the high-level controller K_1 is to calculate this required longitudinal force.

Layer 3: In third layer, i.e., actuator-level layer, the real physical inputs of the system, e.g., throttle, gear position and brake pressure are generated by the low-level controller K_2.

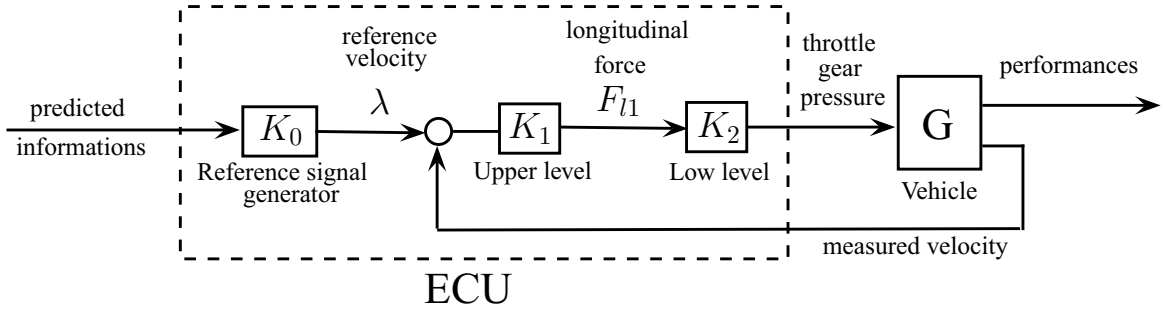

Fig. 3.3: Scheme of control system implementation

In the proposed method the layers are separated from each other. The reference velocity signal generator K_0 can be added to the control-level and actuator-level of the vehicle cruise control, i.e., it is possible to design a reference signal generator unit almost individually, and to attach it to the cruise control system. Thus the reference signal unit can be designed and produced independently from automobile suppliers, only a few vehicle data are needed. The independent implementation possibility is an important advantage in practice.

New result 3.2.1: New advanced energy-optimal solution on the multi-criteria motion profile design problem for automated vehicles has been provided. The method is based on a constrained quadratic optimization, with which the balance between energy consumption and traveling time is achieved. The speed profile computation in the control architecture from the cruise control is separated, which provides increased variability in the implementation of the method.
References: [Gáspár et al., 2017, Németh and Gáspár, 2014, Németh and Gáspár, 2015b, Gáspár and Németh, 2014a]

3.3 Implementation of the energy-optimal cruise control in a truck

The implementation of the proposed cruise cruise control system is evaluated in an incremental manner. First, both the vehicle itself and the control system is realized in TruckSim and Matlab/Simulink simulation environment. In this step, the vehicle and the control system are not separated physically, since both of them exist in the same simulation scheme. Some illustrative simulation results can be found in Appendix A.1. Second, a Hardware-In-the-Loop (HIL) simulation environment has been developed, in which the vehicle dynamics simulation and the control system are physically separated. Third, the validation of the energy-optimal cruise control system has been carried out in cooperation with the Hungarian R&D center of Knorr-Bremse AG. The test vehicle used in the experiment granted by Knorr-Bremse AG is a Volvo FH13 62R 6x2 three-axle truck with total mass of 16 tonnes.

The architecture of the real control system is as follows. The proposed energy-optimal cruise algorithm is running on a MicroAutoBox II system. This device is directly connected to the vehicle via CAN communication system and it is able to control the speed of the vehicle. MicroAutoBox II is also connected to a second industrial on-board computer via RS-232 interface that is used to store or query online maps and other databases on the one hand. It is implemented via a wireless communication unit through a GSM mobile internet connection. On the other hand, the second on-board computer is responsible for receiving data from the GNSS receiver via RS-232 interface and transmitting it to MicroAutoBox II in order to evaluate the cruise control algorithm. The connection to the truck on-board management system is realized via CAN network. Through this, the measurement data of the vehicle can be extracted and the traction power demand for the ECU controlling the engine and a deceleration command for the brake system can be obtained.

The results of the implemented energy-optimal cruise control algorithm have been compared to that of an experienced truck driver. The driver traveled in his own driving style without the use of any cruise control system, thus the throttle and brake pedal has been operated manually. The speed profile used by the driver is illustrated in Figure 3.4 (a). It can be seen that the prescribed speed limit of 80 km/h has not been accurately maintained, often exceeded or gone below by the test driver. The driving style of the truck driver resulted in the consumption shown in Figure 3.4 (b). The entire journey has been completed in 1807 seconds while the fuel consumption of the truck was 10.23 liters. These metrics serve as a benchmark for the energy-optimal cruise control that has been tested with multiple parameter settings.

Based on the measurements carried out in the preliminary vehicle simulations in TruckSim environment, the horizon has been set to $L = 2000m$ with $n = 20$ section points, thus only the optimization weight R_1 was altered during the algorithm testing. Several test runs have been performed with different R_1 weights, and the results have been compared to that of the truck driver. In Figure 3.5 (a) the speed profile of the truck is depicted using the energy-optimal cruise control system and $R_1 = 0.3$ parameter setting. Note, that in order to avoid high deviations from the speed limit, the reference speed for the truck to follow has been limited between $70 - 85$ km/h. The journey has been completed in 1944 seconds, while the fuel consumption of the truck was 9.37 liters, see Figure 3.5 (b). Thus,

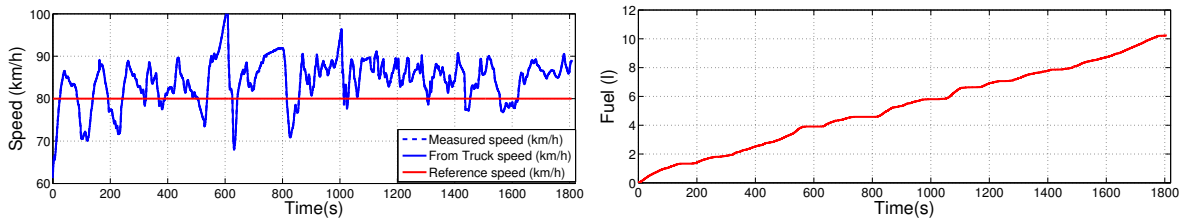

(a) Speed profile (b) Fuel consumption

Fig. 3.4: Tatabánya-Budapest road test with driver

by utilizing the proposed energy-optimal cruise control system with the aforementioned parameter settings, fuel consumption has been reduced by 8.4%, while traveling time with only 137s has been increased.

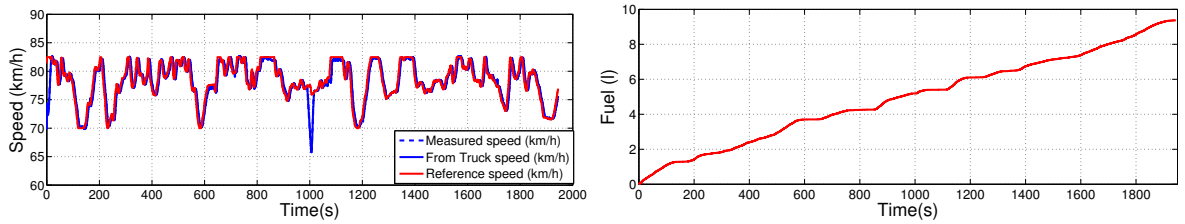

(a) Speed profile (b) Fuel consumption

Fig. 3.5: Tatabánya-Budapest road test with energy-optimal cruise control

New result 3.3.1: The new energy-optimal method of the motion profile design for automated vehicles in simulation and in test vehicle environment has been implemented. The results of the implementations show that the developed design method improves energy and time performances of the automated vehicle motion effectively, under real circumstances.
References: [Gáspár and Németh, 2019, Soumelidis et al., 2018]

4. PERFORMANCE GUARANTEED ENERGY-OPTIMAL CRUISE CONTROL FOR AUTOMATED VEHICLES

Due to various external information sources the achieved performance level of automated vehicle control can depend on the quality of communicated data [61]. Nevertheless, degradation in their quality, i.e., time delays, pocket losses or data manipulation can impair the performance of the cruise control system [Németh et al., 2016d]. A challenge of the enhanced cruise control systems in the automated vehicles is to build reliable architectures, which are less sensitive on the degradation of communicated data and thus, the predefined performances can be guaranteed [157, 81]. In this section the design of a cruise control using various information sources and with guarantees on safety performances are proposed.

Information sources of cruise control systems in automated vehicles can be classified as follows. First, automated vehicle has information from topography database, which provides altitude and road curvature information. The road section ahead of the vehicle is divided into n number of segments, where the lengths of the segments are selected to have constant inclinations. Second, the vehicle has information on speed limitations on the road segments. Since speed limitations can also depend on the actual road construction works and variable speed limit signs in high-speed roads, information from static road map and I2V communication can be required. Third, information on the average traffic speed on the forthcoming road section and the state of the traffic lights expect communication with the traffic control system. Fourth, information on the actual speed and the positions of the surrounding vehicles can require V2V communication and on-board sensors, e.g., radar measurements.

The performances of the predictive cruise control are formed as follows. A primary performance of the vehicle is to keep safe distance from the preceding vehicles in the own lane and from the follower vehicles in the case of a lane change maneuver on the entire horizon. As an assumption, it is considered that the vehicles move in the same directions on the road. Moreover, motion information on the surrounding vehicles are considered in a predefined region of interest, which leads to N_p number of preceding vehicles and N_f number of follower vehicles. Formally, it leads to the conditions

$$e^{k_p} + \sum_{i=1}^{j} \left(\eta_i^{k_p} - \xi_i \right) \geq d_{safe}, \quad \forall j \in \{1, ..., n\}, \quad \forall k_p \in \{1, ..., N_p\}, \tag{4.1a}$$

$$e^{k_f} + \sum_{i=1}^{j} \left(\xi_i - \eta_i^{k_f} \right) \geq d_{safe}, \quad \forall j \in \{1, ..., n\}, \quad \forall k_f \in \{1, ..., N_f\}, \tag{4.1b}$$

where k_p, k_f represent the indexes of the preceding and follower vehicles, e^{k_p}, e^{k_f} are the actual distance between vehicle k_p, k_f and the automated vehicle and d_{safe} is the requested

safe distance. Index j represents the road segment and $\sum_{i=1}^{j} \xi_i$ is the predicted longitudinal displacement of the automated vehicle until step j and $\sum_{i=1}^{j} \eta_i^{k_p}, \sum_{i=1}^{j} \eta_i^{k_f}$ are the predicted displacements of vehicle k_p and k_f. Relations in (4.1) represent that the predicted distance between the automated vehicle and a surrounding vehicle until horizon j cannot be smaller then the predefined safe distance. If the relations are guaranteed, the safe distances from all surrounding vehicles on the entire horizon are kept.

Further primary performance of the control is keeping vehicle speed in a limited range around reference speed $v_{ref,i}$ in segment i. $v_{ref,i}$ is selected based on the speed limitation, road curvature, average traffic speed [Gáspár and Németh, 2019]. The performance is formed as

$$\dot{\xi}_i \in \left[v_{min,i}; v_{max,i}\right], \quad \forall i \in \{1, ..., n\}, \tag{4.2}$$

where $\dot{\xi}$ is the speed of the automated vehicle and $v_{min,i}, v_{max,i}$ values are the minimum and maximum limits of the speed range, in which the vehicle speed can vary. Performance (4.2) guarantees keeping speed limitations. Furthermore, it guarantees the avoidance of the dangerously slow motion of the automated vehicle. The values of $v_{min,i}, v_{max,i}$ are derived from the value of the speed reference $v_{ref,i}$ on each segment, e.g., $-20\%, +5\%$ related to $v_{ref,i}$.

One of the most important secondary performance in the cruise control problem is to achieve minimum control intervention on the road horizon ahead of the automated vehicle, which leads to the criterion

$$\sum_{i=1}^{n} |F_{l,i}| \rightarrow min, \tag{4.3}$$

where $F_{l,i}$ represents traction/braking force on segment i of the horizon.

Another secondary performance is to minimize traveling time of the vehicle. Since the shortest traveling time is equivalent with the maximum speed motion of the vehicle, it can be transformed to the speed objective as

$$|v_{max,i} - \dot{\xi}_i| \rightarrow min, \quad \forall i \in \{1, ..., n\}. \tag{4.4}$$

The motions of the automated vehicles can have impact on the characteristics of the traffic flow, because the speed profiles of automated vehicles can significantly differ from the speed profiles of human-driven vehicles. This impact has increasing importance through the increase of the traffic density and the ratio of the automated vehicles in the traffic flow. A further secondary performance of the control is that motion of the automated vehicles must have advantageous impact on the traffic flow. It means that the output flow of the traffic network q_{out} must be maximized, such as

$$q_{out} \rightarrow max. \tag{4.5}$$

The relationships between q_{out}, the speed selection strategy of the automated vehicles, the ratio of the automated vehicles and the traffic density are characterized in [Gáspár and Németh, 2019].

4.1 Design of the supervisory control strategy

The purpose of the supervisor is to provide control force actuation u through the selection of ρ_P, Δ_P, with which the primary performances during the cruising of the vehicle are guaranteed. The selection is based on the signals u_P, u_K, which are the inputs of the supervisor. The output of the supervisor u is constructed through (2.19), and moreover, the resulted ρ_P is used in the operation of the robust LPV control.

The design of the supervisor is based on the simplified longitudinal model of the vehicle:

$$m\ddot{\xi} = F_l - F_d, \tag{4.6}$$

where m is the mass of the vehicle. The state vector is $x = \begin{bmatrix}\dot{\xi} & \xi\end{bmatrix}^T$, where ξ represents the longitudinal displacement of the vehicle, $w = F_d$ contains the longitudinal disturbances and $u = F_l$ involves the longitudinal control force. The state-space representation of the system is formed as

$$\dot{x} = Ax + \hat{B}_1 w + \hat{B}_2 u, \tag{4.7}$$

where x represents the state vector and $A, \hat{B}_1, \hat{B}_2$ are matrices in the system representation.

The state-space representation of the system is reformulated using the predefined control strategy (2.19), the control input of the robust LPV controller u_K is used in the expression $u = \rho_P u_K + \Delta_P$. Therefore, the state-space representation of the system (4.7) is reformulated through the relationship between u and u_K as

$$\dot{x} = Ax + B_1 w_K + B_2(\rho_P) u_K, \tag{4.8}$$

where the disturbance vector w_K in the state-space representation (4.8) is composed as $w_K = \begin{bmatrix}w & \Delta_P\end{bmatrix}^T$ and the matrices are $B_1 = \begin{bmatrix}\hat{B}_1 & B_2\end{bmatrix}$ and $B_2(\rho_P) = \hat{B}_2 \rho_P$. Thus, the system is transformed into a LPV representation.

Specification of conditions to provide guarantees on primary performances

The conditions to provide primary performances through the supervisor are specified based on the derived system formulation (4.8).

Performance (4.1) in the supervisor design process is focused on keeping safe distance from the closest preceding vehicle and from the closest follower vehicle of another lane, which leads to $N_p = 1, N_f = 1$. The goal of this simplification is to use less communicated data in the computation of ρ_P, Δ_P. The selection of the closest vehicles is performed continuously during the operation of the supervisor based on on-board sensor measurements. If a vehicle in the region of interest of the sensors is not found (e.g., the lane of the automated vehicle is empty ahead or behind), a virtual vehicle is considered to be on the bound of the region.

The prediction of the forthcoming distance d^{k_p} between the preceding vehicle and the automated vehicle is formulated based on their accelerations. The time-dependent

function of $\ddot{d}^{k_p}$ is based on (4.6) as

$$\ddot{d}^{k_p}(t) = \ddot{\eta}^{k_p}(t) - \ddot{\xi}(t) = \ddot{\eta}^{k_p}(t) - \frac{F_l(t)}{m} + \frac{F_d(t)}{m}. \tag{4.9}$$

Through the integration of (4.9) the forthcoming speed difference in time T can be derived as

$$\dot{d}^{k_p}(T) = \int_0^T \ddot{d}^{k_p}(t)dt = \int_0^T \left(\ddot{\eta}^{k_p}(t) - \frac{F_l(t)}{m} + \frac{F_d(t)}{m}\right)dt. \tag{4.10}$$

The integration requires knowledge about the functions $\ddot{\eta}^{k_p}(t)$ and $F_d(t)$. Nevertheless, it is difficult to predict the forthcoming acceleration command of the preceding vehicle and the forthcoming road disturbances. In case of a safe control strategy, these functions are substituted by constant values, which are resulted by worst-case scenarios. It is considered that

$$a_{min} \leq \ddot{\eta}^{k_p}(t) + \frac{F_d(t)}{m}, \tag{4.11}$$

where a_{min} represents the worst-case scenario, when the preceding vehicle has maximum deceleration and the road disturbance has minimum value. The value of a_{min} is a design parameter, which can be selected based on preliminary experimental results. Using a_{min}, (4.10) is computed as

$$\dot{d}^{k_p}(T) = a_{min}T - \frac{F_l}{m}T + \dot{d}^{k_p}(0) = a_{min}T - \frac{F_l}{m}T + \dot{\eta}^{k_p}(0) - \dot{\xi}(0), \tag{4.12}$$

where $\dot{d}^{k_p}(0) = \dot{\eta}(0) - \dot{\xi}(0)$ is the speed difference at time $t = 0$ and $F_l(t)$ is considered to be constant between 0 and T. The predicted distance between the vehicles is resulted by the integration of (4.12), such as

$$d^{k_p}(T) = \frac{a_{min}T^2}{2} - \frac{F_l T^2}{2m} + \dot{\eta}^{k_p}(0)T - \dot{\xi}(0)T + e^{k_p}, \tag{4.13}$$

where e^{k_p} is the measured distance between the preceding vehicle and the automated vehicle in time $T = 0$. The prediction in (4.13) requires measurement on the actual distance e^{k_p} and the relative speed between the automated vehicle and the preceding vehicle $\dot{\eta}^{k_p}(0) - \dot{\xi}(0)$, which can be performed through on-board sensors, e.g., radar.

Similarly, the predicted distance between the automated vehicle and the follower vehicle k_f can be derived from the second derivative of the distance between them as $\ddot{d}^{k_f}(t) = \ddot{\xi}(t) - \ddot{\eta}^{k_f}(t)$. The worst-case scenario is characterized by the acceleration a_{max} through the expression $\ddot{\eta}^{k_f}(t) + \frac{F_d(t)}{m} \leq a_{max}$, which leads to the predicted distance

$$d^{k_f}(T) = \frac{F_l T^2}{2m} - \frac{a_{max}T^2}{2} + \dot{\xi}(0)T - \dot{\eta}^{k_f}(0)T + e^{f_p}. \tag{4.14}$$

The formulation of the primary performances, which means that safe distances from the preceding vehicle and the follower vehicle must be kept, are written as inequalities

$$\frac{a_{min}T^2}{2} - \frac{F_l T^2}{2m} + \dot{\eta}^{k_p}(0)T - \dot{\xi}(0)T + e^{k_p} \geq d_{safe}, \tag{4.15a}$$

$$\frac{F_l T^2}{2m} - \frac{a_{max}T^2}{2} + \dot{\xi}(0)T - \dot{\eta}^{k_f}(0)T + e^{f_p} \geq d_{safe}. \tag{4.15b}$$

Since $u = F_l$ and $u = \rho_P u_K + \Delta_P$ (2.19), the inequalities (4.15) are rewritten as

$$\frac{a_{min}T^2}{2} - \frac{(\rho_P u_K + \Delta_P)T^2}{2m} + \dot{\eta}^{k_p}(0)T - \dot{\xi}(0)T + e^{k_p} \geq d_{safe}, \tag{4.16a}$$

$$-\frac{a_{max}T^2}{2} + \frac{(\rho_P u_K + \Delta_P)T^2}{2m} + \dot{\xi}(0)T - \dot{\eta}^{k_f}(0)T + e^{f_p} \geq d_{safe}. \tag{4.16b}$$

Thus, it is necessary to select ρ_P, Δ_P for given u_K to guarantee inequalities (4.16), with which the primary performance of keeping safe distance is guaranteed.

Performance of keeping vehicle speed in a given speed range (4.2) is also based on the simplified motion model of the vehicle (4.6). The predicted speed of the vehicle in T is resulted through the integration of the acceleration $\ddot{\xi}$ as

$$\dot{\xi}(T) = \int_0^T \left(\frac{F_l}{m} - \frac{F_d}{m}\right) dt. \tag{4.17}$$

Similarly to the derived conditions of keeping safe distance, the worst-case scenario is considered as $|F_d| \leq F_{d,max}$, where $F_{d,max}$ is considered to be the upper bound of the unknown disturbance. If $F_d > 0$, which means that the disturbance has accelerating effect, (4.17) is transformed as $\frac{F_l T}{m} + \frac{F_{d,max}T}{m} + \dot{\xi}(0)$, where $\dot{\xi}(0)$ is the actual speed of the automated vehicle and F_l is considered to be constant. If $F_d < 0$, (4.17) results in $\frac{F_l T}{m} - \frac{F_{d,max}T}{m} + \dot{\xi}(0)$, which means that F_d decelerates the vehicle. The condition for keeping vehicle speed in the given range $\left[v_{min,0}; v_{max,0}\right]$ is formed as

$$\frac{(\rho_P u_K + \Delta_P)T}{m} + \frac{F_{d,max}T}{m} + \dot{\xi}(0) \leq v_{max,0}, \tag{4.18a}$$

$$\frac{(\rho_P u_K + \Delta_P)T}{m} - \frac{F_{d,max}T}{m} + \dot{\xi}(0) \geq v_{min,0}, \tag{4.18b}$$

in which relations $u = F_l$ is transformed to $\rho_P u_K + \Delta_P$ (2.19). Thus, it is necessary to select ρ_P, Δ_P, with which conditions in (4.18) together with (4.16) are guaranteed.

Optimization in the supervisor strategy

In the supervisory process ρ_P, Δ_P are selected during the operation of the energy-optimal cruise control system. The objective of the supervisor is to provide control input u, which is as close as possible to u_P:

$$\left(u - u_P\right)^2 \rightarrow min. \tag{4.19}$$

Through (6.4) the control force intervention of the enhanced cruise control system approximates the output signal of the predictive cruise control. Moreover, during the selection of ρ_P, Δ_P the criteria of (4.16) and (4.18) must be guaranteed and the constraints $\rho_P \in \varrho_P$, $\Delta_P \in \Lambda_P$ must also be satisfied.

Objective (6.4) using (2.19) is rearranged to a quadratic form as

$$(u-u_P)^2 = \begin{bmatrix}\rho_P\\ \Delta_P\end{bmatrix}^T \begin{bmatrix}u_K^2 & u_K\\ u_K & 1\end{bmatrix} \begin{bmatrix}\rho_P\\ \Delta_P\end{bmatrix} + \begin{bmatrix}-2u_Pu_K\\ -2u_P\end{bmatrix}^T \begin{bmatrix}\rho_P\\ \Delta_P\end{bmatrix} + u_P^2 =$$
$$= \begin{bmatrix}\rho_P\\ \Delta_P\end{bmatrix}^T \beta \begin{bmatrix}\rho_P\\ \Delta_P\end{bmatrix} + \omega^T \begin{bmatrix}\rho_P\\ \Delta_P\end{bmatrix} + u_P^2, \tag{4.20}$$

in which u_P^2 is independent from ρ_P, Δ_P and thus, it can be eliminated during the minimization process (6.4).

The strategy of the supervisor is to compute ρ_P, Δ_P during the operation of the cruise control. In each steps the following constrained optimization problem must be solved, which is yielded from (4.20) and the constraints (4.16), (4.18) together with the bounds on ρ_P, Δ_P:

$$\min_{\rho_P,\Delta_P} \begin{bmatrix}\rho_P\\ \Delta_P\end{bmatrix}^T \beta \begin{bmatrix}\rho_P\\ \Delta_P\end{bmatrix} + \omega^T \begin{bmatrix}\rho_P\\ \Delta_P\end{bmatrix}, \tag{4.21a}$$

subject to

$$-\frac{(\rho_P u_K + \Delta_P)T^2}{2m} + \frac{a_{min}T^2}{2} + \dot{\eta}^{k_p}(0)T - \dot{\xi}(0)T + e^{k_p} \geq d_{safe}, \tag{4.21b}$$
$$\frac{(\rho_P u_K + \Delta_P)T^2}{2m} - \frac{a_{max}T^2}{2} + \dot{\xi}(0)T - \dot{\eta}^{k_f}(0)T + e^{f_p} \geq d_{safe}, \tag{4.21c}$$
$$\frac{(\rho_P u_K + \Delta_P)T}{m} + \frac{F_{d,max}T}{m} + \dot{\xi}(0) \leq v_{max,0} + S, \tag{4.21d}$$
$$\frac{(\rho_P u_K + \Delta_P)T}{m} - \frac{F_{d,max}T}{m} + \dot{\xi}(0) \geq v_{min,0} - S, \tag{4.21e}$$
$$\rho_P \in \varrho_P, \tag{4.21f}$$
$$\Delta_P \in \Lambda_P. \tag{4.21g}$$

In (4.21d)-(4.21e) S is a slack variable. The role of S is to set a hierarchy in the constraints and to ensure that the optimization problem returns a feasible solution [149]. For example, if the automated vehicle must be stopped to avoid the collision with a preceding vehicle and $v_{min,0} > 0$, constraint (4.21e) cannot be guaranteed. It leads to the infeasibility of the optimization problem of (4.21). It must be avoided by setting S to a high value. Since the avoidance of the collision has higher priority than keeping the speed is the predefined range, the following process must be performed for the selection of S.

- $S = 0$ is selected as a default value. If (4.21) has feasible solutions ρ_P, Δ_P, control input $u = \rho_P u_K + \Delta_P$ is computed.
- If (4.21) is not feasible with $S = 0$, S is selected for a high value to guarantee the feasibility. Then, (4.21) with the new value of S is solved. The resulted ρ_P, Δ_P are applied to provide control input $u = \rho_P u_K + \Delta_P$.

4.2 Design of the robust LPV-based cruise control system

The aim of the robust LPV control is to provide u_K control input signal for the supervisor. The design process using the proposed method in Section 2.3.3 is carried out. The robust LPV control has importance in the situations, when the output of the predictive cruise control can violate the primary performances. Nevertheless, in most of the operation of the enhanced cruise control, u_P might be acceptable. Therefore, u_K has importance mainly in critical situations, and in these scenarios the maintenance of the secondary performances has low priority. Consequently, it is enough to use the simplified control-oriented model (4.6) for the robust LPV control design, with which the objective of the main functionality in cruise control, such as speed tracking can be specified as $z_1 = v_{ref,0} - \dot{\xi}, \quad |z_1| \rightarrow min$. Moreover, the minimization of the control input u_K must be considered as an objective of the robust control design $z_2 = u_K, \quad |z_2| \rightarrow min$. The consideration of u_K has the role to guarantee the quantification of z_1 through the balance between the objectives. Furthermore, through z_2 the insufficiently high longitudinal control force is avoided. The objectives z_1, z_2 are composed in a vector of objectives, such as $z_K = \begin{bmatrix} z_1 & z_2 \end{bmatrix}^T$. Using the state-space formulation of the system (4.8), z_K is formed as $z_K = C_1 x + D_{11} w_K + D_{12} u_K$, where w_K is extended as $w_K = \begin{bmatrix} F_d & \Delta_P & v_{ref,0} \end{bmatrix}^T$, C_1, D_{11}, D_{12} are matrices.

The measurement equation for the robust LPV control design is formed as $y_K = v_{ref,0} - \dot{\xi} = C_2 x + D_{21} w_K$, where C_2, D_{21} are matrices. The value of $v_{ref,0}$ in (2.33)-(2.36) is selected as follows. If $N^p = 0$, $v_{ref,0}$ is get from static map database of speed limits and the camera-based traffic sign recognition system of the vehicle. If $N^p > 0$, the speed information of database and the speed information of the recognition system are limited by radar measurement about $\dot{\eta}^p$. Thus, in the robust LPV control low number of external information is incorporated and most of the information is based on own sensors.

Finally, the plant for the robust LPV control design is formed as follows:

$$\dot{x} = Ax + B_1 w_K + B_2(\rho_P) u_K, \tag{4.22a}$$

$$z_K = C_1 x + D_{11} w_K + D_{12} u_K, \tag{4.22b}$$

$$y_K = C_2 x + D_{21} w_K, \tag{4.22c}$$

in which ρ_P is the scheduling variable of the system.

The control design is based on the resulted control-oriented model (4.22). Scaling of w_K and providing a balance between the elements of z_K require a weighting strategy in the control design method. The closed-loop interconnection structure is presented in Figure (4.1). The interconnection structure contains several weighting functions. The weight W_n is related to the sensor characteristics on the velocity error measurement, where n represent sensor noise. W_d scales the longitudinal disturbance force F_d. The bound of F_d also has role in the supervisor design. Weight W_d is characterized as $W_d = \frac{F_{d,max}}{T_d s+1}$, where T_d is a tuning parameter, which represents the dynamics of F_d variation. Similarly, W_{Δ_P} scales uncertainty Δ_P. This weight is selected in the form $W_{\Delta_P} = \frac{\max(|\Delta_{P,min}|;|\Delta_{P,max}|)}{T_{\Delta 2} s^2 + T_{\Delta 1} s + 1}$, where $T_{\Delta 2}, T_{\Delta 1}$ are design parameters, which represent the dynamics of the signal. The role of weight $W_{ref,0}$ is to scale the reference signal $v_{ref,0}$. It is considered as a constant parameter with the supreme of $v_{max,0}$.

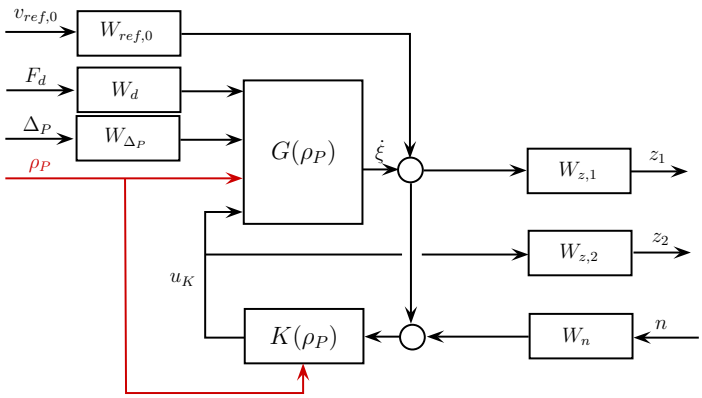

Fig. 4.1: Closed-loop interconnection structure for robust LPV control design

$W_{z,1}, W_{z,2}$ are the weights on the control performances, which provide a balance between them. Weight $W_{z,1}$ has important role from the aspect of the minimum performance level of the cruise control, because it scales the tracking error $v_{ref,0} - \dot{\xi}$. The form of the weight is $W_{z,1} = \frac{e_v}{T_z s+1}$, where T_z is a design parameter and e_v is the expected maximum tracking error. The selected form guarantees that the tracking error is e_v in steady state. The selection of e_v must guarantee $e_v \leq v_{max,0} - v_{ref,0}$ and $e_v \leq v_{ref,0} - v_{min,0}$ to avoid the degradation of performance (4.2). Weight $W_{z,2}$ scales the control input u_K. Its value is selected as a constant parameter, which represents the supreme of $|u_K|$.

The quadratic LPV problem is to choose the parameter-varying controller $\mathcal{K}(\rho_P, y_K)$ in such a way that the resulted closed-loop system is quadratically stable and the induced $\mathcal{L}_2$ norm from the disturbance w_K to the objectives z_K is less than the value γ [161, 26]. The minimization task is the following:

$$\inf_{\mathcal{K}(\rho_P, y_K)} \sup_{\rho_P \in \varrho_P} \sup_{\substack{\|w_K\|_2 \neq 0, \\ w_K \in \mathcal{L}_2}} \frac{\|z_K\|_2}{\|w_K\|_2}. \tag{4.23}$$

The optimization problem shows that the resulting controller depends on the domains ϱ_P, Λ_P, which demonstrates that the selection process of ϱ_P, Λ_P and the LPV design are not independent from each other. During the control design it is necessary to find a balance in the selection of the domain, which is based on an iteration process.

The goal of the iteration is to find domains ϱ_P, Λ_P, with which u approximates u_P. It provides that the enhanced cruise control system operates with u_P as most as possible, without the violation of primary performances. The following optimization is based on scenarios, which are performed in each steps of the iterations:

$$\min_{\substack{\rho_{P,min}, \rho_{P,max} \\ \Delta_{P,min}, \Delta_{P,max}}} \sum_{j=1}^{N} \big(u(j) - u_P(j)\big)^2 = \min_{\substack{\rho_{P,min}, \rho_{P,max} \\ \Delta_{P,min}, \Delta_{P,max}}} \sum_{j=1}^{N} \big(\rho_P(j) u_K(j) + \Delta_P(j) - u_P(j)\big)^2, \tag{4.24}$$

where j expresses the time step and N is the length of a given scenario.

4.3 Illustration of the enhanced cruise control strategy

In the simulation example the automated vehicle travels on a section of the hilly Hungarian M1 highway, which interconnects capital cities Budapest and Vienna. In the example there is an accident on the highway (see $5000m$ segment point in Figure 4.2(a)), which results in a congestion. The traffic control system provides information about the reduction of the traffic speed between $3500m - 5000m$, see Figure 4.2(a).

The automated vehicle incorporates the traffic speed information in its enhanced cruise control strategy through $v_{ref,i}$. Since the automated vehicle has $1000m$ prediction horizon in the example, the information about the reduced traffic speed is considered from $2500m$. It results in the reduction of the vehicle speed (see Figure 4.2(b)), with which an energy-efficient motion can be achieved through the approaching to the accident [Németh and Gáspár, 2017]. Moreover, there is a preceding vehicle ahead of the automated vehicle, which stops at $3800m$, when the congestion is reached, see its speed profile in Figure 4.2(b). The goal of the enhanced cruise control is to provide minimum control force in the cruising, while the safe distance $d_{safe} = 20m$ from the preceding vehicle is guaranteed, especially at the stop of the preceding vehicle. The distance between the vehicles is illustrated in Figure 4.2(c). It can be seen that the safety distance $20m$ is guaranteed in the given example. The control signal u and the values of ρ_P, Δ_P are illustrated in Figure 4.2(d)-(f). At the end of the simulation, when the distance is reduced, ρ_P is set to zero and Δ_P is also reduced. It results in the tracking of the preceding vehicle speed (close to zero) through the control input of the robust LPV control.

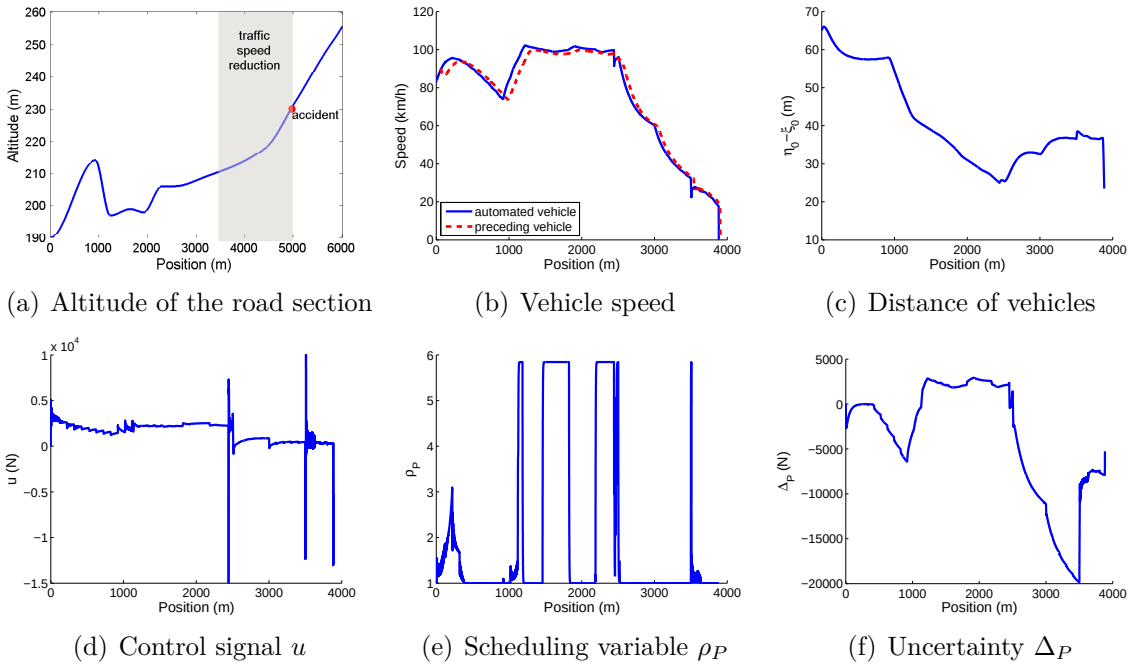

(a) Altitude of the road section (b) Vehicle speed (c) Distance of vehicles

(d) Control signal u (e) Scheduling variable ρ_P (f) Uncertainty Δ_P

Fig. 4.2: Simulations of lane change scenario

Further simulation examples on the operation of the system under various scenarios, i.e., degradation in V2V communication or impact of computational issues, are found in

Appendix A.2.

New result 4.3.1: Energy-optimal motion profile with the consideration of forthcoming road and traffic information in a performance guaranteed structure has been designed. The provided new advanced control strategy guarantees safety performance requirements for the vehicle, i.e., keeping safe distance and speed limitations, even if the communicated measured signals are degraded.
References: [Németh and Gáspár, 2021, Németh et al., 2021c, Németh et al., 2021a]

Part III

CONTROL DESIGN FOR SAFETY CRITICAL INTERACTIONS OF AUTOMATED VEHICLES

dc_1992_22

5. PREDICTIVE CRUISE CONTROL FOR SAFETY CRITICAL VEHICLE INTERACTIONS

Handling of intersection scenarios is an important challenge in the research field of autonomous vehicles. From the aspect of control design, several crucial tasks of the automated vehicle control in intersection scenarios should be formulated. For example, the ordering of autonomous vehicles in intersections has an impact on the energy consumption of the vehicles, traveling time, emission or e.g., on traveling comfort due to the acceleration/deceleration maneuvers [108, 172]. It leads to a multi-objective optimization task, which generally has Pareto-optimal solutions. Moreover, the solution of the optimization problem regarding to autonomous vehicles in intersections can require long calculation time. It poses the challenge of the minimization of the computation time, e.g., finding approximations of the optimal solution. The coordination of automated vehicles requires enhanced infrastructure, e.g., Vehicle-to-Vehicle and Vehicle-to-Infrastructure communications [165]. The accurate detection of a vehicle position in intersections [102, 123, 159] or detection and prediction of the human behavior [83, 7] are open problems.

A control-oriented challenge, i.e., ordering of vehicles in unsignalized intersection scenarios, is illustrated through an example, see Figure 5.1. In the scenario it is necessary to modify motion profile for the vehicles to achieve minimum traveling time or energy consumption. Nevertheless, it is not a trivial question, which ordering of the vehicles in the intersection can be an appropriate choice, as it is illustrated by the following example. It is considered that *Vehicle 1* has internal combustion engine and its motion is slow, while *Vehicle 2* is a fast electric vehicle. Moreover, *Vehicle 3* is a truck with high mass. The ordering of the vehicles can differ, depending on the objective function.

- If the goal is the minimization of the traveling time, then the ordering $2-1-3$ of the vehicles is the best choice, which means that the actual speeds of the vehicles have high relevance.

- In case of the minimization of the energy loss the ordering $3-1-2$ is ideal, because the heavy vehicle is not stopped unnecessary.

- If the emission in the intersection must be reduced, the ordering $1-3-2$ is the appropriate selection to avoid the start/stop of the conventional vehicle.

Since the various performances cannot be simultaneously guaranteed, in the control design a balance between the performances can be achieved.

The high number of challenges in the field of autonomous vehicle control in intersections has motivated increased research activity, i.e., several publications with different approaches. One of the most important group of the methods are based on the MPC

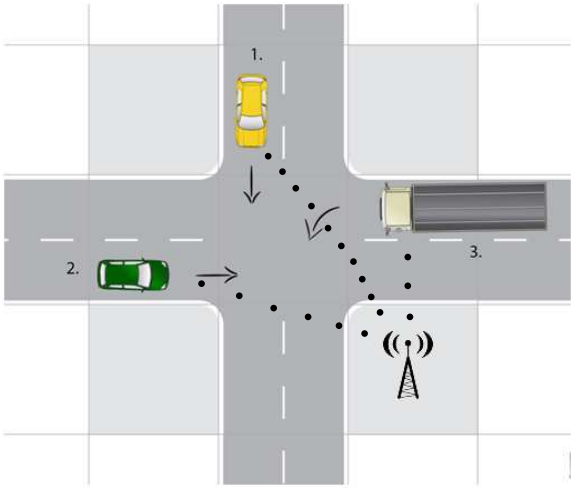

Fig. 5.1: Illustration of intersection scenario without traffic sign

technique [75, 126, 17, 60]. Although it can provide appropriate results, increasing in the number of vehicles can make real-time computation difficult. A possible solution to the problem of increasing computation effort is the approximation of the optimal solution with neural networks, see e.g., [Németh et al., 2018b]. However, in this case it may be difficult to provide guarantees on collision avoidance for all intersection scenarios [Szilassy et al., 2019]. The quadratic programming method is the possibility of real time implementation compared to the convex optimization using space coordinates, see [112]. Collision avoidance is guaranteed through the definition of regions in the intersection with special rules, which reduce the complexity of the problem, but the conservativeness of the solution increases. Due to the ordering problem of the vehicles in the intersection the control problem can be formed as a Mixed-Integer Linear Programming (MILP) task, see e.g., a method on the coordination in [42]. The goal of the control is to find an arrival schedule of the vehicles, which ensures safety while it reduces the number of stops and intersection delays. [111] presents a centralized another MILP-based approach for intersection control in an urban environment of highly automated vehicles, with which the minimum vehicle delay at the intersection can be achieved. Another solution in the predictive control framework is to examine all ordering combinations of the vehicles [Németh and Gáspár, 2019], which can also be difficult for an increased number of vehicles.

The short review on the existing literature shows that several efficient solutions exist, but there are challenges for achieving a reliable control method. The goal of the recent research activities is to find a control design method, with which high number of autonomous vehicles can be handled, the energy consumption and time minimization requirements can be carried out, and the safe motion, i.e., the avoidance of the collision must be guaranteed.

In this dissertation two different methods for the coordinated control design of automated vehicles in intersection scenarios are proposed. The first method in Chapter 5 is an extension of the provided energy-optimal cruise control strategy of Chapter 3. In this method the ordering of vehicles and the computation of their speed profile are different tasks. The second in Chapter 6 method uses learning-based approach in the

guaranteed control design framework of Chapter 2. It provides a method, with which the vehicle ordering and the speed profile computations in the same optimization problem are incorporated.

Although these coordination methods in their approaches are different, the sources of measures signals are similar. In both methods it is considered that motion information (position, velocity, acceleration) on automated vehicles taking part in the interaction through V2V communication is received. The own position, velocity and acceleration signals through on-board measurement are available. In case of human-driven vehicles position and velocity signals on their motion is also considered to be available, e.g., though V2V communication or camera, LiDAR measurement. The forthcoming motions of human-driven vehicles through kinematic and dynamic relationships are predicted.

5.1 Ordering strategy of the vehicles in intersections

It has been shown that the control of automated vehicles in the intersections depends on several factors. However, the proposed predictive control algorithm of Section 3.2 provides an appropriate formulation, in which the energy and the traveling time requirements can be handled together. In the further examination of the intersection problem it is required to find the speed profile of the vehicles, which is able to guarantee a balance between the energy consumption and the traveling time through the performance weight R_1 and W. Moreover, the designed speed trajectories must guarantee the safe motion of the vehicles, which means the avoidance of the collision. It means that the speed of the vehicles with predictive cruise control can be influenced through the weights R_1, W.

The fundamental idea of the vehicle control in the intersection is to find the maximum set of vehicles, in which the vehicles are able to be in cooperation. Cooperation means that the safe motion of the controlled vehicles in the set can be guaranteed without a stopping command. In these sets all of the controlled vehicles can be moved through R_1 and $W \equiv 0$. The controlled vehicles, which are out of the set, can by influenced through R_1 and $W \neq 0$ to guarantee their safety motion. The role of the optimization in the intersection is to find the maximum set of vehicles, in which the cooperation can be guaranteed.

In the real traffic scenario of the intersections human-driven vehicles and automated vehicles with predictive cruise control are together. Due to the human drivers it is necessary to provides some regulations, by which the motion of their vehicles can be controlled. Therefore, the automated vehicles must adapt to the regulations and these constraints must be incorporated in the optimization problem. During the design of automated vehicle control strategy, the motion of the human-driven vehicles are estimated. It results in the predicted speed profile of the human-driven vehicles, which is based on the available signals, e.g., actual position, speed and acceleration, see Section 5.2.

During the optimization process, human-driven vehicles can be the parts of the maximum set of vehicles, in which the vehicles are able to be in cooperation. It means that it can be found speed profiles for automated vehicles, by which the collision with human-driven vehicles can be avoided and stopping commands are not used for the vehicles in the set. Regarding to the conventional vehicles it is considered that humans keep the traffic regulations. Similarly, it must be created confidence in the human participants that

the automated vehicles also keep regulations and the collision is avoided in the intersection. Therefore, an increased safety distance between the conventional and the automated vehicles are guaranteed.

The computation of the maximum set of cooperating vehicles requires to define a quantity, by which the size of the set is defined. It influences the order of the vehicles in the intersection and the number of the cooperating vehicles. Moreover, this quantity can represent the importance of the vehicles regarding to the transportation system or some social aspects. For example, the quantity can be defined as the number of passengers in the vehicles, which means that a public transport buses can have an increased weight. Another example is the presence of high priority vehicles in the traffic (e.g., ambulances, fire brigades), of which motion must be absolutely guaranteed [37, 140, 113]. In this strategy a quasi-kinetic energy is defined as the quantity of the set. The energy of the vehicle i is formed as follows

$$E_i(t) = (1 - \eta_i)\frac{1}{2} m_i v_i^2(t), \tag{5.1}$$

where m_i is the virtual mass of the vehicle and $v_i(t)$ is its actual speed. The parameter η_i is in relation with the efficiency of the driveline recuperation. The parameters of (5.1) are chosen as follows.

- The virtual mass m_i is in relation with the mass of the vehicle. Generally, m_i is equal to the nominal mass of the vehicle, e.g. at passenger cars. However, in case of public transport buses m_i can also contain the mass of the passengers. In this way the number of the passengers in the vehicle can be considered in the optimization problem. Since m_i represents an importance factor, it is enough to estimate the the additional mass, e.g. the number of passenger is multiplied with an average unit-mass. Furthermore, the importance of the high priority vehicles can be scaled through a huge virtual mass.

- The actual speed $v_i(t)$ of the vehicles is considered to be available. Its role is to consider that the stopping of a high speed vehicle results in larger energy loss, compared to a vehicle with slow motion.

- Since there can be several hybrid and electric vehicles in the traffic system, their energy loss can be reduced through the recuperation. Parameter η_i is the average efficiency of the recuperation in the driveline. It represents that the energy loss of hybrid and electric vehicles is smaller, compared to a conventional driveline with internal combustion engine.

During the optimization problem of vehicle ordering, the sum of the quasi-kinetic energy of the set must be maximized:

$$\max_{\omega \in \Omega} \sum_i E_i(t), \tag{5.2}$$

where Ω is the set of all vehicles in the region of interest around the intersection. Since several ω subset of the vehicles from Ω can be generated, it is necessary to order them

according to $\sum_i E_i(t)$. Then, it is necessary to examine, whether the vehicles of ω are able to be in cooperation. The result of the optimization is the maximum ω, in which the cooperation is available.

Summarizing, the process of the speed profile design of the vehicles in the intersection is the following:

1. determination of the region of interest around the intersection,
2. prediction of the speed profile of the human-driven vehicles,
3. determination of the quasi-kinetic energies of the vehicles,
4. ordering of the candidate subset of the cooperating vehicles,
5. selection of the maximum set of the cooperating vehicles through prediction and optimization algorithms,
6. ordering and speed profile design of the vehicles, which are out of the set.

5.2 Formulation of the optimal speed profile design problem

The design of the speed profile for the automated vehicles requires the prediction of the motion of human-driven vehicles and of automated vehicles. In the followings the prediction processes of the vehicles are introduced.

Motion prediction of the human-driven vehicles

In the prediction process of the human-driven vehicles several assumptions are considered. First, it is assumed that automated vehicles has information on the speed and the acceleration of human-driven vehicles ($\dot{\eta}$, $\ddot{\eta}$) and about its actual distance from the intersection e_η. Second, human-driven vehicles accelerate evenly until it reaches the speed limit. When a human-driven vehicle reaches the speed limit $v_{ref,j}$ it does not accelerate further, thus in the oncoming sections the predicted speeds of the vehicle are $v_{ref,j}, \ldots, v_{ref,n}$.

The considered speed profile of the human-driven vehicles is as follows. The following distance and acceleration equations describe the speed profile as

$$e_\eta = \dot{\eta} t_{acc} + \frac{v_{ref,int} - \dot{\eta}}{2} + v_{ref,int}(t_{int} - t_{acc}), \tag{5.3a}$$

$$\ddot{\eta} = \frac{v_{ref,int} - \dot{\eta}}{t_{acc}}, \tag{5.3b}$$

where $v_{ref,inf}$ is the speed limitation on the route of the vehicle. t_{acc} is the time of the acceleration, while t_{int} is the unexpired time until to reach the intersection. t_{int} is expressed from (5.3) as:

$$t_{int} = \frac{v_{ref,int} - \dot{\eta}}{\ddot{\eta}} + \frac{1}{v_{ref,int}} \left[e_\eta - \dot{\eta} \frac{v_{ref,int} - \dot{\eta}}{\ddot{\eta}} - \frac{(v_{ref,int} - \dot{\eta})^2}{2\ddot{\eta}} \right]. \tag{5.4}$$

Since time t_{int} represents the critical situation, when the human-driven vehicle reaches the intersection, this time value is considered at the computation of the automated vehicle motion.

Speed prediction of automated vehicles

Moreover, it is also required to provide a speed prediction method on the controlled vehicles. The prediction is based on the proposed predicted algorithm, see Chapter 3. The ϑ can be rewritten using (3.8) as:

$$\begin{aligned}\vartheta =& Wv_{lead}^2 + (1-W)v_{ref,0}^2 - R_1(1-\bar{Q}-W)v_{ref,0}^2 + R_1\sum_{i=1}^{n}\bar{\gamma}_i v_{ref,i}^2 + \\ &+R_1(\frac{2}{m}\sum_{i=1}^{n}s_i F_{di,r}\sum_{j=i}^{n}\bar{\gamma}_j) = R_1\bar{\vartheta} + v_{ref,0}^2(1-R_1)(1-W),\end{aligned} \tag{5.5}$$

where $\bar{\vartheta}$ contains the value of ϑ calculated with energy-efficient prediction weights $\bar{Q}, \bar{\gamma}_i$.

From (3.9) the reference speed λ is calculated based on the predicted road information. It shows that through Q and ϑ weight R_1 plays an important role in the calculation of the reference speed. Moreover, the predicted values of the weights γ_i also depend on R_1, see (3.16). From (3.7) and (3.8) the square of the reference speed $\dot{\xi}$ is calculated in the following form:

$$\begin{aligned}\lambda^2 =& R_1\bar{\vartheta} + v_{ref,0}^2(1-R_1)(1-W) + 2s_1R_1\left(1-\bar{Q}-W\right)(\ddot{\xi}_0 + gsin\alpha) = \\ =& R_1\left(\bar{\vartheta} - 2s_1(1-\bar{Q}-W\right) + v_{ref,0}^2(1-R_1)(1-W) = \\ =& R_1\bar{\lambda}^2 + v_{ref,0}^2(1-R_1)(1-W)\end{aligned} \tag{5.6}$$

The predicted speed of the vehicle at section point n is formed as:

$$\begin{aligned}\dot{\xi}_n^2 &= \dot{\xi}_0^2 + \frac{2}{m}s_1F_{l1} - \frac{2}{m}s_1F_{d1,o} - \frac{2}{m}\sum_{i=1}^{n}s_iF_{di,r} \\ &= \lambda^2(1-\frac{2}{m}s_1T) + \frac{2}{m}s_1F_{l1} - \frac{2}{m}s_1A - \frac{2}{m}\sum_{i=1}^{n}s_iF_{di,r} = R_1\mathcal{N}_1 + \mathcal{N}_2.\end{aligned} \tag{5.7}$$

According to (5.7) the predicted speed at point n is independent of $v_{ref,n}$. For example when $R_1 = 0$ the predicted speed at point n must be $v_{ref,n}$. However, using (5.7), the value $\dot{\xi}_i$ depends only on the momentary speed limit $v_{ref,0}$, while future speeds $v_{ref,i}$ do not influence it. Based on (5.7) the defined reference speed at section point n must be modified in the following way:

$$\dot{\xi}_n^2 = \left(R_1\mathcal{N}_1 + \mathcal{N}_2\right)R_1 + (1-R_1)v_{ref,n}^2, \tag{5.8}$$

which depends on the weight R_1. In the formula $\mathcal{N}_1$ is independent of the section points ahead, while $\mathcal{N}_2$ contains the road grade information of each section.

The aim of the speed prediction is to determine the position of the automated vehicle in various times. The automated vehicle moves from point ξ_0 to ξ_1, whose distance is s_1 while the traveling time during this section is Δt_1. In the optimization method it is assumed that although the acceleration of the vehicle may change in different intervals, within an interval the acceleration value is constant. Thus, the traveling time in the first interval is expressed as $\Delta t_1 = 2s_1/(\dot{\xi}_1 + \lambda)$, where λ and $\dot{\xi}_1$ are from equations

(5.6) and (5.8), respectively. The traveling time between points ξ_1 and ξ_2 is expressed similarly as $\Delta t_2 = 2s_2/(\dot{\xi}_2 + \dot{\xi}_1)$. Using the computed time values a vector is formed as $\Delta T = \left[\Delta t_1 \dots \Delta t_n\right]^T$. Moreover, the positions of the section points are also arranged in a vector form as $\Xi = \left[\xi_1 \dots \xi_n\right]^T$.

Optimal speed profile design for automated vehicles

The optimization process is based on the modification of R_1 weight of all automated vehicles, which are in a candidate set of cooperating vehicles. The role of R_1 is to guarantee a balance between the energy optimal and the minimum traveling time motion profiles. Similarly to the cruising strategy in the overtaking scenarios, it is necessary to find the maximum R_1 of each vehicles, by which their safety motion regarding to the further vehicles in the intersection can be guaranteed.

However, in case of the intersection problem it is necessary to design R_1 weight for more automated vehicles simultaneously. Therefore, in the followings $R_{1,i}(t)$ represents the performance weight of vehicle i in time t. Moreover, it is necessary to define an objective function, by which the importance of automated vehicles can be scaled. The previously defined $E_i(t)$ can be a good choice, because that value has the same role. Thus, the objective function of the optimization is

$$\max_{R_{1,i}(t)\in[0;R_{1,max}]} \sum_{i\in\omega} E_i(t) R_{1,i}(t), \tag{5.9}$$

where $R_{1,max}$ is the upper limit of $R_{1,i}(t)$.

The objective of the optimization is constrained by some safety criteria, which guarantee the avoidance of the collision between the vehicles in set ω. Regarding to the constraints a safety distance s_{safety} between the vehicles is predefined. The value s_{safety} depends on the speed limits $v_{ref,i}$ in the intersection and the number of the routes connected to the intersection. The constraint between vehicle i and j represents the following. If vehicle j reaches the intersection in the predicted time t_j, then vehicle i must be out of the intersection area at least the distance s_{safety}. The form of the constraints is defined as

$$e_i - \xi_i(t_j) > s_{safety}, \qquad \forall i \neq j, \tag{5.10}$$

where i represents vehicle i and e_i is the actual distance of vehicle i from the intersection. $\xi_i(t_j)$ is the predicted distance of vehicle i from its actual position in time t_j.

Thus, the optimization problem is formed as

$$\max_{R_{1,i}(t)\in[0;R_{1,max}]} \sum_{i\in\omega} E_i(t) R_{1,i}(t), \tag{5.11}$$

such that

$$e_i - \xi_i(t_j) > s_{safety}, \qquad \forall i \neq j.$$

The solution of the optimization problem (5.11) requires some prediction processes. It is necessary to select candidate $R_{1,j}$ values for each vehicle j and to provide a prediction

as follows. Using $R_{1,j}$ the vectors of the prediction for automated vehicle j Ξ, ΔT are computed, see Section 5.2. Using e_j actual distance of vehicle j from the intersection, t_j is computed as

$$t_j = interp(\Xi_j, \Delta T_j, e_j). \tag{5.12}$$

Then, $\xi_i(t_j)$ can be determined for all vehicles $i \neq j$. In case of automated vehicles Ξ_i and ΔT_i are computed. Then, $\xi_i(t_j)$ is computed as

$$\xi_i(t_j) = interp(\Delta T_i, \Xi_i, t_j). \tag{5.13}$$

In case of human-driven vehicles $\xi_i(t_j)$ is computed through the prediction of the motion profile. Thus, the constraints regarding to vehicle j and i are computed using (5.10).

An example on the formulation of the optimization problem with three vehicles is found in Appendix B.1.

5.3 Simulation results under multi-vehicle scenarios

The effectiveness of the proposed method through a simulation scenario with automated vehicles is illustrated. Further example on the interactions of human-driven and automated vehicles is found in Appendix B.1.

In this scenario there are three automated vehicles with predictive cruise control, of which positions and turning intentions are illustrated in Figure 5.2. Moreover, the speed limit is 50 km/h on the network, but it is varied on two routes. Although the intersection is considered to be flat, due to the varying speed limits the speed profile of the vehicles must be optimized. In the example the mass of the vehicles are different, and their distance from the middle of the intersection ξ_0. The initial speeds of the vehicles are considered to be equal to the speed limit, such as 50 km/h for Vehicle 1 and Vehicle 2, while it is 60 km/h for Vehicle 3.

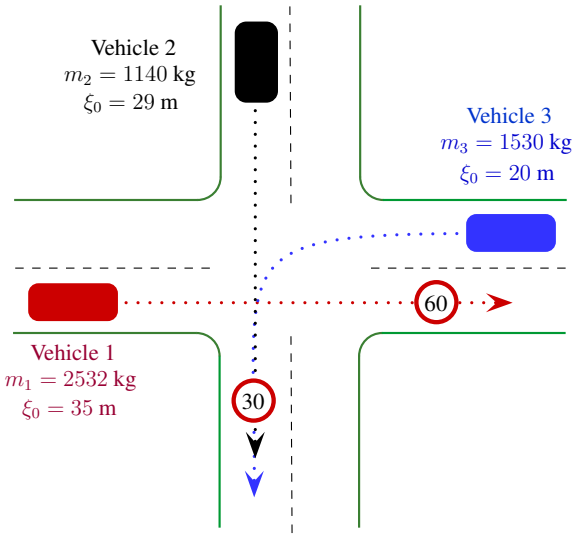

Fig. 5.2: Scenario of the vehicles with their initial position

The determination of the maximum set of cooperating vehicles is based on the energy values of the vehicles, as proposed in Section 5.1. Considering $\eta_i = 0$ for all vehicles, the energy values in $t = 0$ are $E_1(0) = 244$ kJ, $E_2(0) = 109$ kJ, $E_3(0) = 212$ kJ. Therefore, the ordering of the sets are for all vehicles are in cooperation: ω_3 with 565 kJ, and if two vehicles are in cooperation: $\omega_{2,1}$ (Vehicle 1 - Vehicle 3) with 456 kJ, $\omega_{2,2}$ (Vehicle 1 - Vehicle 2) with 353 kJ, $\omega_{2,3}$ (Vehicle 2 - Vehicle 3) with 321 kJ. If cooperation cannot be reached, the values are $\omega_{1,1}$ (Vehicle 1) with 244 kJ, $\omega_{1,2}$ (Vehicle 3) with 212 kJ, $\omega_{1,3}$ (Vehicle 2) with 109 kJ.

The simulation resulted that Vehicle 3 is the first in the order of the intersection, Vehicle 1 is the second, while Vehicle 2 is the last vehicle, see Figure 5.3. During the simulation the safety distance is selected as $s_{safety} = 3$ m, which must be guaranteed in all interactions.

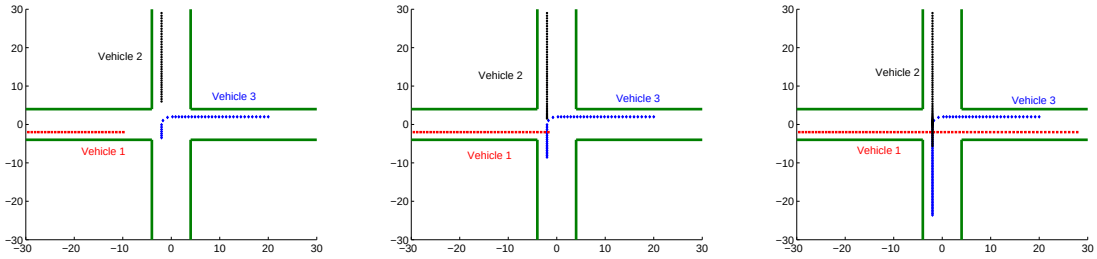

(a) Vehicle 3 turns to left (b) Vehicle 1 cruises straight in the intersection (c) Vehicle 2 cruises as the last vehicle

Fig. 5.3: Cruising of the automated vehicles in the intersection

The most important results of the simulations regarding to the predictive cruise control strategy are found in Figure 5.4. The speed values of the vehicles are illustrated in Figure 5.4(a). It shows that the speed profile of Vehicle 3 is smoothly decreasing, while Vehicle 2 must be stopped to avoid the collision with Vehicle 1. The $R_{1,i}$ values are illustrated in Figure 5.4(b). It shows that $R_{1,3}$ has the maximum value during the simulation, which means that Vehicle 3 is able to cruise with its minimum energy consumption. However, $R_{1,1}$ is reduced between $1.2s \dots 1.7s$, which results in its increased acceleration to guarantee the s_{safety} between Vehicle 1 - Vehicle 2. Vehicle 2 has the most varying $R_{1,2}$ signal, as shown in Figure 5.4(b). Moreover, Figure 5.4(c) presents that W for Vehicle 2 must be modified at several times. It results in that in the most of the simulation time ω_3 can be reached, but in some time periods (e.g., $0.6s \dots 0.9s$, $1.1s \dots 1.3s$, $1.7s \dots 2.6s$) $\omega_{2,1}$ is the maximum set with the coordination of Vehicle 1 and Vehicle 3. Nevertheless, the proposed strategy is able to guarantee the predefined safety distance between the vehicles.

New result 5.3.1: The extension of the new energy-optimal motion profile design method for the interaction of multiple automated vehicles has been provided. The coordination of the automated vehicles in intersection scenarios through the extended optimization problem has been solved, i.e., the ordering of the vehicles and the selection of their speed profiles in a joint optimizations process have been formed. In the coordination of the automated vehicles the motion of the human-driven vehicles in the intersection has been

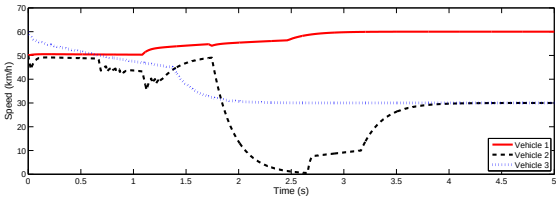

(a) Speed of the vehicles

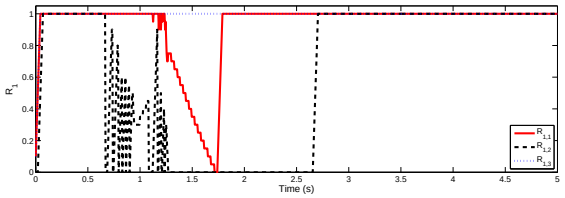

(b) $R_{1,i}$ values

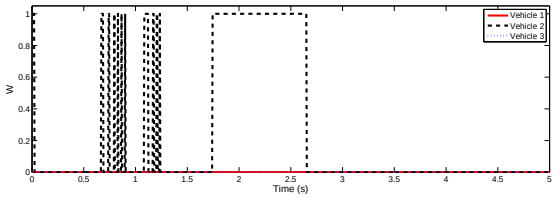

(c) Weight W_i of the vehicles

Fig. 5.4: Results of the simulation with three vehicles

incorporated.
References: [Gáspár and Németh, 2019, Németh and Gáspár, 2019, Németh and Gáspár, 2015a, Szilassy et al., 2019]

6. LEARNING-BASED CONTROL DESIGN WITH GUARANTEES FOR SAFETY CRITICAL INTERACTIONS

The goal of this chapter is to provide a coordinated control strategy for handling automated vehicles in intersections scenarios. In the method of this chapter, the ordering of vehicles and their speed profile computation in a reinforcement learning (RL) based optimization task are incorporated.

The advantage of this method is its model-free property, which can provide solutions to the problem of constraint formulation. Moreover, the training of the control agent through high number of episodes is carried out, which can lead to improved performances. The application of RL for the interactions of automated vehicles is found in [164, 31, 174]. A deep RL method is applied to unsignalized intersections in [63]. It also provides analysis to explore the ability of the system to learn active sensing behaviors and safe navigation in the case of occlusions. [124] also presents a deep RL-based model that considers the effectiveness of leading automated vehicles in mixed-autonomy traffic at a non-signalized intersection. [167] offers a new approach to train of the intelligent agent that simulates the behavior of an unmanned vehicle, based on the integration of reinforcement learning and computer vision. Using full visual information about the road intersection obtained from aerial photographs, it is studied automatic detection the relative positions of all road agents with various architectures of deep neural networks.

In spite of promising achievements, most of the resulting neural-network-based agents cannot provide guarantee on the collision avoidance of the vehicles. In this chapter the RL problem is formed in a guaranteed framework, and thus, the collision of the vehicles during their interaction can be avoided.

The design method with RL-based features strongly connects to the provided robust LPV-based design framework in Section 2.3. In the method of Section 2.3 the goal is to design the robust LPV controller, while the learning-based agent is considered to be given. In the method of this section the RL-based agent must also be designed, while another low-complexity robust control design on the problem of automated vehicles in intersections is also provided. The scheme of the design framework with RL-based agent in Figure 6.1 is illustrated. It contains a robust controller with output a_K, the RL-based agent with output a_L. These signals are used for the computation of Δ by a supervisor. The signal Δ is an addition to a_K, which results in the control input of the vehicle a_1. Through Δ the control input a_1 is able to approximate a_L, i.e., secondary performance level can be improved, and similarly, primary (safety) performance requirements in the computation of Δ are involved. In this structure the parameters of the robust controller and the RL-based agent are computed offline, while the actual value of Δ in each steps is computed online.

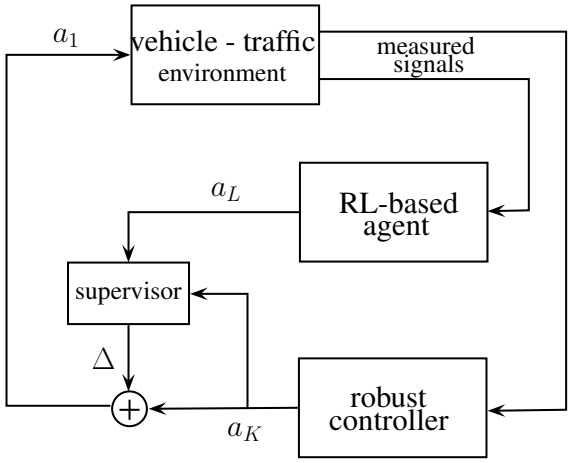

Fig. 6.1: Scheme of guaranteed design framework with RL-based agent

6.1 Formulation of the supervisory strategy for the environment of reinforcement learning

The goal of this section is to formulate collision-free motion of the vehicles in intersection scenarios. The formulation includes the longitudinal motion model of the vehicles and the constraints on their motion to avoid collision.

The longitudinal motion of the vehicles is formulated through the simplified kinematics of vehicles, such as

$$v_i(k+1) = v_i(k) + Ta_i(k), \tag{6.1a}$$

$$s_i(k+1) = s_i(k) + Tv_i(k) + \frac{T^2}{2}a_i(k), \tag{6.1b}$$

where $_i$ index represents the number of the vehicle, n is the number of vehicles, v_i is longitudinal velocity, s_i is longitudinal displacement. a_i represents the longitudinal acceleration of the vehicle, which is handled as a control input command and T is the time step of the discrete motion model. The longitudinal displacement is related to the center point of the intersection and thus, it is defined as $s_i = 0$ for all i in the center point. The longitudinal displacement of the approaching vehicle has negative value and the displacement of the vehicle moving away has positive value.

In the environment model of the intersection the automated ego vehicle is numbered with 1. Thus, for example in the case of $n = 5$ in the environment the ego vehicle and four surrounding vehicles are incorporated. The control input of the automated vehicles is separated into two elements, as

$$a_1(k) = a_K(k) + \Delta(k), \tag{6.2}$$

where a_K is the control input command of the robust longitudinal controller and $\Delta(k)$ is the additional input from the supervisor in the model.

The purpose of the supervisor in the collision-free motion model is to select $\Delta(k)$ for the automated ego vehicle with the following objectives and constraints.

- The objective of the selection is to minimize the difference between the current control input $a_1(k)$ and the output of the learning-based controller $a_L(k)$. The aim of the minimization is to preserve the performance level of the learning-based controller, if possible.

- Some of the vehicles can intercross their route in the intersection. Thus, intervention with $a_1(k)$ must provide motion for the automated vehicle, with which the safe distance s_{safe} between the automated vehicle and the further surrounding vehicles with intercrossing routes can be guaranteed. Since the number of vehicles n can be high, a limited number of surrounding vehicle motion must be simultaneously considered, i.e. n_s represents the number of vehicles which are incorporated in the design process. It is a constraint in the selection of Δ.

- The velocity of the vehicles must be inside of a predefined range. The upper bound of the range is defined by the speed limit v_{max} or the curvature of the intersection. The lower bound is represented by the stopping of the vehicle. Thus, it is necessary to select Δ for all vehicles to keep velocities inside of the range. It is also a constraint in the selection process.

The selection process of Δ for the automated ego vehicle is formed as an optimization problem as follows:

$$\min_{\Delta(k)} \big(a_1(k) - a_L(k)\big)^2 \tag{6.3a}$$

subject to

$$s_1(k+1)^2 + s_j(k+1)^2 \geq s_{safe}^2, \qquad \forall j \in n_s, \tag{6.3b}$$

$$0 \leq v_1(k+1) \leq v_{max}, \tag{6.3c}$$

$$\Delta \in \boldsymbol{\Delta}, \tag{6.3d}$$

where j represents the surrounding vehicles, whose motion can be in conflict with the automated vehicle, i.e., their routes are intercrossed. $\boldsymbol{\Delta}$ represents the domain of the optimization variable. In the optimization problem the kinematics of the vehicle motion (6.1) is considered through the formulation of the constraints, the separation of the control input (6.2) is involved in the objective function.

The objective (6.3a) is transformed using (6.2) as

$$\begin{aligned} &\big(a_1(k) - a_L(k)\big)^2 = \big(a_K(k) + \Delta(k) - a_L(k)\big)^2 = \\ &= \Delta(k)^2 + 2f(k)\Delta(k) + (a_K(k)^2 + a_L(k)^2 - 2a_L(k)a_K(k)), \end{aligned} \tag{6.4}$$

where f vector is formed as $f(k) = a_K(k) - a_L(k)$. Since $(a_K(k)^2 + a_L(k)^2 - 2a_L(k)a_K(k))$ is independent of $\Delta(k)$, it is omitted in the rest of the optimization problem.

The constraint for collision avoidance (6.3b) is formed to achieve keeping s_{safe} between the vehicles. The distance is measured in the sense of the longitudinal displacement of the vehicles on their route. Geometrically, the quadratic constraints (6.3b) represent that the trajectories of the automated vehicle s_1 and the related surrounding vehicles must be out of a circle. The radius of the circle is defined by s_{safe}, see Figure 6.2(a). For example,

it there are two surrounding vehicles with the automated vehicle (e.g., see Figure 6.5), the trajectories must be out of a sphere, whose radius is represented by s_{safe}, see Figure 6.2(b).

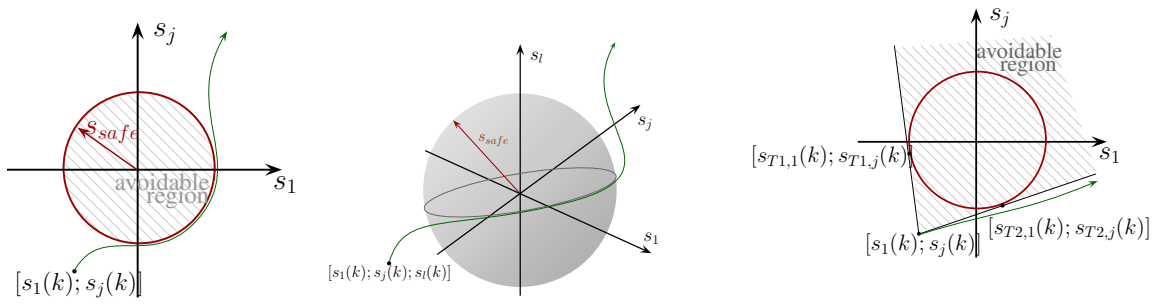

(a) Constraint illustration of a related pair (b) Constraint illustration on an example (c) Illustration of constraint approximation

Fig. 6.2: Geometrical illustration of the quadratic constraints

Although the circle perfectly describes the region of the state-space, which must be avoided, it leads to a quadratic constraint in the optimization problem (6.3). Since the optimization problem must be solved in each k time step during the motion of the vehicles, the quadratic constraint can make the solution of the optimization more complex and it can make the real-time solution more difficult. It motivates the transformation of the quadratic constraints into linear constraints. In this paper it is performed through the approximation of the avoidable regions of circles to the avoidable regions of half-planes.

The method of the approximation is illustrated in Figure 6.2(c). First, the tangent lines to the circle from the actual state $\begin{bmatrix} s_1(k) & s_j(k) \end{bmatrix}^T$ are assigned. The avoidable half-plane is determined by the region between the tangent lines, i.e., the trajectories must be out of it. Second, two linear inequality constraints are specified, which represent that the trajectory of the state must be out of the avoidable half-plane, such as

$$\begin{bmatrix} s_{T1,1}(k) \\ s_{T1,j}(k) \end{bmatrix}^T \begin{bmatrix} s_1(k) \\ s_j(k) \end{bmatrix} \leq \begin{bmatrix} s_{T1,1}(k) \\ s_{T1,j}(k) \end{bmatrix}^T \begin{bmatrix} s_1(k+1) \\ s_j(k+1) \end{bmatrix}, \tag{6.5a}$$

or

$$\begin{bmatrix} s_{T2,1}(k) \\ s_{T2,j}(k) \end{bmatrix}^T \begin{bmatrix} s_1(k) \\ s_j(k) \end{bmatrix} \geq \begin{bmatrix} s_{T2,1}(k) \\ s_{T2,j}(k) \end{bmatrix}^T \begin{bmatrix} s_1(k+1) \\ s_j(k+1) \end{bmatrix}, \tag{6.5b}$$

where $\begin{bmatrix} s_{T1,1}(k) & s_{T1,j}(k) \end{bmatrix}$, $\begin{bmatrix} s_{T2,1}(k) & s_{T2,j}(k) \end{bmatrix}$ are the tangent points on the circle in time step k. Note that the linear constraints result in an outer approximation of the avoidable set. There are regions of the half-space which cannot be reached due to the linear constraints, but they are out of the circle.

The longitudinal displacement of the automated vehicle at $k+1$ in (6.5) is transformed to express the linear constraints in terms of Δ. The transformation is based on the motion equation (6.1) and the relation of actuation separation (6.2). Moreover, the motions of

surrounding vehicles for $k+1$ with their actual velocity $v_j(k)$ are predicted, such as

$$s_1(k+1) = s_1(k) + Tv_1(k) + \frac{T^2}{2}a_K(k) + \frac{T^2}{2}\Delta(k), \tag{6.6a}$$

$$s_j(k+1) = s_j(k) + Tv_j(k), \tag{6.6b}$$

which can be substituted into (6.5). It leads to the linear constraints

$$\begin{bmatrix} s_{T1,1}(k) \\ s_{T1,j}(k) \end{bmatrix}^T \begin{bmatrix} -Tv_1(k) - \frac{T^2}{2}a_K(k) \\ -Tv_j(k) \end{bmatrix} \leq \frac{T^2}{2} \begin{bmatrix} s_{T1,1}(k) \\ 0 \end{bmatrix}^T \Delta(k), \tag{6.7a}$$

or

$$\begin{bmatrix} s_{T2,1}(k) \\ s_{T2,j}(k) \end{bmatrix}^T \begin{bmatrix} -Tv_1(k) - \frac{T^2}{2}a_K(k) \\ -Tv_j(k) \end{bmatrix} \geq \frac{T^2}{2} \begin{bmatrix} s_{T2,1}(k) \\ 0 \end{bmatrix}^T \Delta(k). \tag{6.7b}$$

Figure 6.2(c) illustrates that the reachable set for the state $\begin{bmatrix} s_1(k+1) & s_j(k+1) \end{bmatrix}^T$ is non-convex, which means that (6.7) formulates disjunctive inequalities. However, each constraint in (6.7) leads to convex reachable sets, which means that the optimization problem can be divided, as it is proposed below.

Another constraint in the optimization (6.3) is on the velocity of the automated vehicle, see (6.3c). In the case of this constraint $v_i(k+1)$ is expressed in terms of Δ using the motion equation (6.1) and the relation of actuation division (6.2). The linear inequality constraint is formed as

$$0 \leq v_1(k) + Ta_K(k) + T\Delta(k), \tag{6.8a}$$

$$v_{max} \geq v_1(k) + Ta_K(k) + T\Delta(k), \tag{6.8b}$$

which leads to

$$\begin{bmatrix} -1 \\ 1 \end{bmatrix} \Delta(k) \leq \begin{bmatrix} \frac{v_1(k)}{T} + a_K(k) \\ \frac{v_{max} - v_1(k)}{T} - a_K(k) \end{bmatrix}, \tag{6.9}$$

where v_{max} is the maximum velocity of the automated vehicle. In an urban environment it is determined by the velocity regulations and in the case of cornering manoeuvres at the intersections the curvature to avoid skidding.

The last constraint in the optimization problem (6.3) is the limitation of the resulting optimization variable, see (6.3d). The value of Δ is limited by the bounds of $a_1(k)$, such as a_{min}, a_{max}, which represent full braking and throttle. Since $a_1(k)$ is also influenced by $a_K(k)$, the constraints on $\Delta(k)$ are formed as

$$a_{min} - a_K(k) \leq \Delta(k), \tag{6.10a}$$

$$a_{max} - a_K(k) \geq \Delta(k), \tag{6.10b}$$

which leads to the constraint

$$\begin{bmatrix} -1 \\ 1 \end{bmatrix} \Delta(k) \leq \begin{bmatrix} a_K(k) - a_{min} \\ a_{max} - a_K(k) \end{bmatrix}. \tag{6.11}$$

The optimization task (6.3) using (6.4), (6.7), (6.9) and (6.11) is reformulated as

$$\min_{\Delta(k)} \ \Delta(k)^2 + 2f^T\Delta(k) \tag{6.12a}$$

subject to

$$\begin{bmatrix}-1\\1\end{bmatrix}\Delta(k) \leq \begin{bmatrix}\frac{v_1(k)}{T} + a_K(k)\\ \frac{v_{max}-v_1(k)}{T} - a_K(k)\end{bmatrix} \tag{6.12b}$$

and

$$\begin{bmatrix}-1\\1\end{bmatrix}\Delta(k) \leq \begin{bmatrix}a_K(k) - a_{min}\\ a_{max} - a_K(k)\end{bmatrix} \tag{6.12c}$$

and

$$\begin{bmatrix}s_{T1,1}(k)\\ s_{T1,j}(k)\end{bmatrix}^T \begin{bmatrix}-Tv_1(k) - \frac{T^2}{2}a_K(k)\\ -Tv_j(k)\end{bmatrix} \leq \frac{T^2}{2}\begin{bmatrix}s_{T1,1}(k)\\ 0\end{bmatrix}^T \Delta(k), \ \ \forall j \in n_s \tag{6.12d}$$

or

$$\begin{bmatrix}s_{T2,1}(k)\\ s_{T2,j}(k)\end{bmatrix}^T \begin{bmatrix}-Tv_1(k) - \frac{T^2}{2}a_K(k)\\ -Tv_j(k)\end{bmatrix} \geq \frac{T^2}{2}\begin{bmatrix}s_{T2,1}(k)\\ 0\end{bmatrix}^T \Delta(k), \ \ \forall j \in n_s. \tag{6.12e}$$

The quadratic optimization in (6.12) contains disjunctive inequalities. It means that the optimization task for the solution can be reformulated to a mixed-integer optimization problem [16]. In practice, the optimization problem (6.12) can be solved as a set of quadratic optimization problems, which has only *and* conditions between the constraints. Thus, in the case of n_s number of surrounding vehicles 2^{n_s} number of distinct constrained optimization problems can be formed. Since the objective functions for each problem is the same, the global minimum solution with the comparison of their solutions can be found. Finally, the solution is yielded by $\Delta(k)$, which leads to the minimum value of the objective function, considering all of the optimization tasks. The optimization problem during the motion of the automated vehicle is continuously solved.

6.2 Cruise control design with learning-based and robust control methods

The intervention in the longitudinal dynamics of the automated vehicle in the intersection has high importance in achieving the required motion profile for time step $k+1$. The control input of the vehicle is composed by two elements, such as $a_K(k)$ and $\Delta(k)$, see (6.2). The computation of $\Delta(k)$ in Section 6.1 has already been proposed. In this section the design of the control intervention $a_K(k)$ is proposed.

The most important requirements for the controller are formed as follows.

- The control system must guarantee safe longitudinal motion for the vehicle, even if a_L has degradation or a fault scenario. The safe motion is guaranteed through a_K and Δ.
- The longitudinal controller must have robust characteristics, because $a(k) \neq a_K(k)$, if $\Delta(k) \neq 0$. Robustness must also be guaranteed in extreme vehicle dynamic

scenarios. For example, if $a_K(k)$ suggests full throttle, but it has been overridden by $\Delta(k)$ to be full braking. Similarly, robustness must be guaranteed if $a_K(k)$ suggests full braking, but it has been overridden by $\Delta(k)$ to be full throttle.

- The control signal $a_K(k)$ must be computed to avoid the saturation of the control actuation $a(k)$. Since in the computation process the computation of $a_K(k)$ is prior to $\Delta(k)$, the result of (6.12) is not considered in the computation of $a_K(k)$. Thus, the role of the cruise controller is to guarantee $a_{min} \leq a_K(k) \leq a_{max}$.

The design of the longitudinal controller is based on the simplified vehicle model (6.1) with one state, such as the longitudinal velocity $v_1(k)$. The controller is formed as a gain P for velocity tracking, whose input is the velocity error, see Figure 6.3. The reference signal for the tracking is v_{ref}. The idea behind the formulation of the control design as a tracking problem is as follows. The vehicle must adapt to the environment, which determines the achievable velocity of the vehicle, e.g., through maximum speed limits. The aim of the cruise control is to consider the regulations and the motion of the further vehicles to achieve safe motion. The maximum speed limit information is provided by $v_{ref}(k)$ and information on the motion of the vehicles in the environment in the computation of $\Delta(k)$ is included. Thus, through the selections of $v_{ref}(k)$ and $\Delta(k)$ the safe motion is guaranteed.

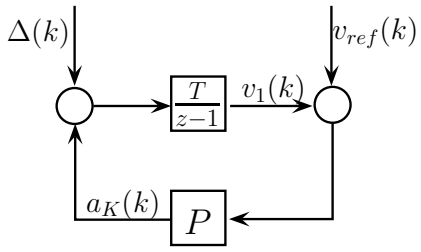

Fig. 6.3: Closed-loop structure of the longitudinal control

The selection of P is determined by the requirement of the robustness for the controlled system. In the presented structure $\Delta(k)$ is handled as a disturbance and the performance of the systems is the minimization of the tracking error, such as $|v_{ref}(k) - v_1(k)|$. Thus, for the robustness issue, it is necessary to limit the impact of $\Delta(k)$ disturbance on the performance. The robustness criterion is based on the small-gain theorem [173]. As a consequence, the $\mathcal{H}_\infty$ norm transfer function from $\Delta(k)$ on the velocity error must be smaller than 1, which guarantees disturbance attenuation.

In the computation of the transfer function the maximum value of the $\bar{\Delta} = |\Delta(k)|$ is also considered. The maximum is determined by the vehicle dynamic scenario, if $\Delta(k)$ implies full throttle instead of full braking or full braking is implied instead of full throttle. Thus, the value of $\bar{\Delta}$ is $|a_{min}| + |a_{max}|$. The transfer function from $\Delta_i(k)$ to the velocity error is

$$G(z) = \frac{\bar{\Delta}\frac{T}{z-1}}{1 + \frac{P \cdot T}{z-1}}. \tag{6.13}$$

The criterion on the selection of P is to guarantee $||G(z)||_\infty < 1$.

The constraint on the control input $a_1(k)$ is influenced by the limitation of the reference signal. The reference velocity in Figure 6.3 represents the maximum speed limit $v_{max}(k)$ for the vehicle on the given road section. Nevertheless, it is necessary to provide a reference velocity for the vehicle, with which the constraint on $a(k)$ is kept. Thus, $v_{ref}(k)$ is computed as

$$v_{ref}(k) = v_1(k) + \min\left(\frac{a_{max}}{P}, \max\left(\frac{a_{min}}{P}, v_{max} - v_1(k)\right)\right). \tag{6.14}$$

The expression represents that the reference velocity can differ from that actual velocity with a limited value. The value of P has a role in the computation of the reference signal.

Finally, the method of the selection of P is as follows. It is recommended to select the value of P as high as possible, which can result in a fast operation of the tracking control. However, the value of P is constrained by the robustness criterion, such as

$$\max P, \tag{6.15a}$$

subject to

$$||G(z)||_\infty < 1. \tag{6.15b}$$

The output of the robust longitudinal controller is $a_K(k)$, which is used in the computation of the control input (6.2) and in the computation of $\Delta(k)$ (6.12).

6.2.1 Design of motion profile using reinforcement learning

In the previous sections a control strategy is formed with which the safe motion of the automated vehicle in an intersection can be guaranteed. Nevertheless, in the design problem of the vehicle motion there are economy aspects, which are recommended to consider during the design process, i.e., it is recommended to minimize the control energy of the vehicles. In this section the consideration of the economy performance in the design process is proposed.

The goal of the design process is to find an agent which is able to generate the control signal $a_L(k)$. The agent is trained through a reinforcement learning process. The structure of the design process is illustrated in Figure 6.4. The model for the learning process contains the optimization task (6.12) together with the result of the robust control design (6.15). The model guarantees the avoidance of the collision in the intersection for every $a_L(k)$ signal. Thus, during the training process of the agent in every episode the safety performances are guaranteed and similarly, the economy performance is improved. The output of the motion model is reward $r(k)$, which is composed by $a(k)$ and $v_1(k)$ as follows

$$r(k) = -Q_1 a_i^2(k) + Q_2(s_1(k) - s_1(0)), \tag{6.16}$$

where Q_1 and Q_2 positive values are design parameters, which scale the importance of each term in $r(k)$. The reward contains the control inputs in the vehicles $a(k)$, which represent the economy performance of the vehicles. If the reward contains only $a(k)$, it can result in unacceptably slow motion for the automated vehicle, because $a(k) = 0$ is the best choice for the maximization of the reward. Thus, in the reward the traveled distance

of the automated vehicle $(s_1(k) - s_1(0))$ is also incorporated, where $s_1(0)$ is the initial position of the automated vehicle. The observation for the agent includes the position of the automated vehicles $s_1(k)$ and of the surrounding vehicles $s_j(k)$ $j \in n_s$ and their velocities $v_1(k), v_j(k)$ $j \in n_s$.

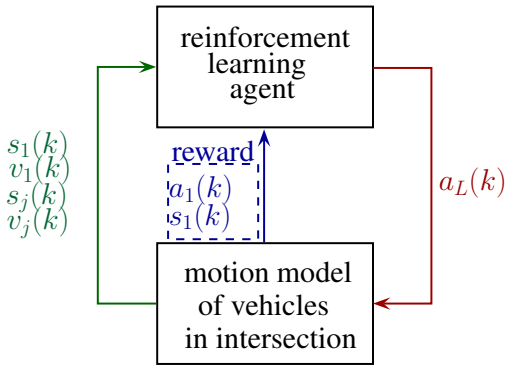

Fig. 6.4: Control structure in the learning process

The goal of the reinforcement learning process is to maximize reward (6.16) during episodes. In this paper the training process through the deep deterministic policy gradient (DDPG) is carried out, which is a model-free, online, off-policy reinforcement learning method [89]. A DDPG agent is an actor-critic reinforcement learning agent that computes an optimal policy that maximizes the long-term reward. In the method actor and critic approximators are used. Both approximators use the observations, which are represented by S. The purpose of the actor approximator $\mu(S)$ is to find the action A with $a_L(k)$, which maximizes the long-term future reward. The role of the critic $Q(S, A)$ is to find the expected value of the long-term future reward for the task.

The result of the training process is an agent whose output is $a_L(k)$. In the control process of the automated vehicle the agent works together with the control strategy (6.12). As a result, the collision avoidance of the vehicles in the intersection is guaranteed and similarly, the economy performance of the vehicles is improved.

6.3 Simulation scenarios in multi-vehicle context

Comparative simulation examples are shown to illustrate the effectiveness of the designed controller. In the rest of this section, the first and the second examples show simplified scenarios, in which three vehicles are in the intersection. The further analysis on the three vehicle scenario under varying traffic environments, i.e., depending on the initial velocities and positions of the vehicles, are found in Appendix B.2. Moreover, in Appendix B.2 a complex scenario seven vehicles is found. In all of these simulations, the closest $n_s = 3$ vehicles in the constraints of the optimization tasks are incorporated in.

The RL-based agent is trained through 500 simulation scenarios, in which the number of vehicles, their initial velocities and positions are selected randomly, i.e., the vehicle number is varied between 1 and 7, the initial positions are selected between $-20m \ldots -40m$ and the initial velocities are varied between 10 $km/h \ldots 50$ km/h. In the learning process

of the neural networks the following structures have been trained. The actor network has 8 neurons in the input layer, 3 fully connected layers with 48 neurons and Rectified Linear Unit (ReLU) functions in each layer and 1 neuron with hyperbolic tangent functions in the output layer. The critical network has the same structure. In the structure and parameter selection of the neural networks the k-fold cross-validation technique [51] and a hidden-layer number optimization process [166] can be used. The sampling time in each episode is selected as $T = 0.05s$. The terms in the reward function are considered with the same design parameters, such as $Q_1 = -0.1$, $Q_2 = 10$. The training process has been performed through Matlab 2020a Reinforcement Learning Toolbox [101] on Intel i7 CPU.

In the simplified examples, the first and second scenarios are illustrated in Figure 6.5. In these cases Vehicle 1 is the ego vehicle, Vehicle 2 and Vehicle 3 are the surrounding vehicles on the perpendicular road section. Both surrounding vehicles cross the route of Vehicle 1, which results in a conflict situation. In the first scenario the following initial conditions are set: $s_1 = -40\ m$, $s_2 = -36\ m$, $s_3 = -41\ m$ and all of the vehicles have 50 km/h initial velocity. In the second scenario Vehicle 3 has different settings, while the further vehicles have the same initial conditions, i.e., $s_2 = -48\ m$ and $v_2 = 30\ km/h$. The safe distance is set to $s_{safe} = 8\ m$.

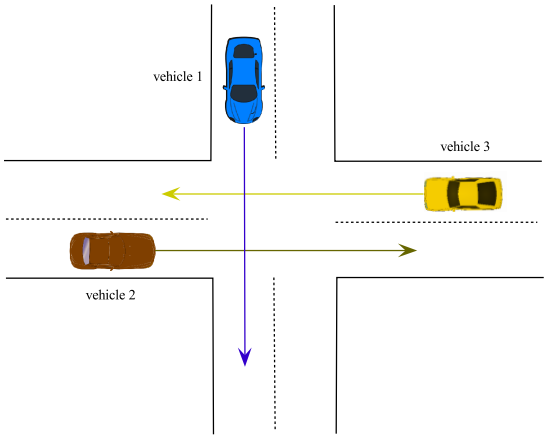

Fig. 6.5: Illustration on the simplified intersection scenarios

The results of the simplified scenarios are found in Figure 6.6. Figures 6.6(a),(b) show that the automated ego vehicle is able to guarantee keeping s_{safe}. Nevertheless, in the two scenarios the ordering of the vehicles in the intersection is different. Since in scenario 1 the surrounding vehicles have increased velocity, the automated vehicle decides to reduce its velocity to 18 km/h and allows the surrounding vehicles with right of way to enter the intersection. But, in scenario 2 the automated vehicle has enough time to go through the intersection before Vehicle 3 enters it. Thus, in this case v_1 can be increased after Vehicle 2 leaves the intersection, see Figure 6.6(d). The differences in the motion of Vehicle 1 also influence the trajectories in Figure 6.6(a),(b). Moreover, the control input signals for each scenarios are found in Figure 6.6(e),(f). In case of scenario 2 the acceleration of the ego vehicle is increased to $3m/s^2$ in $2.6s$ to avoid the collision with Vehicle 2, while in scenario 1 the acceleration is increased later in $3s$ by a lower value.

New result 6.3.1: A novel energy-optimal motion profile design method for intersection

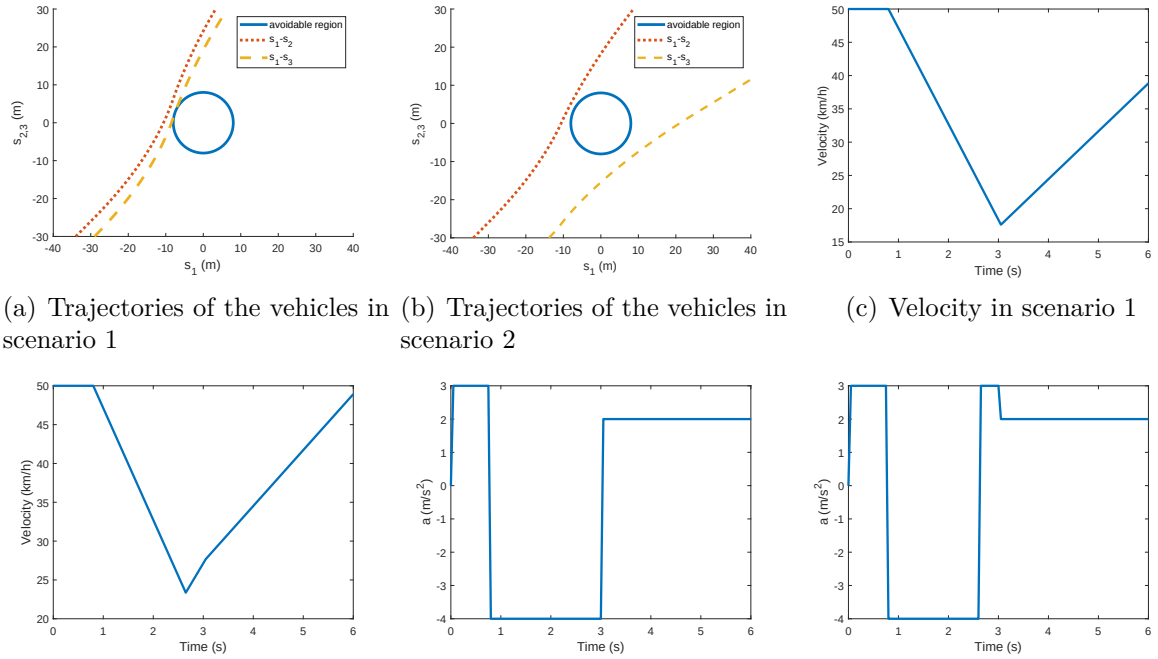

(a) Trajectories of the vehicles in scenario 1

(b) Trajectories of the vehicles in scenario 2

(c) Velocity in scenario 1

(d) Velocity in scenario 2

(e) Control input in scenario 1

(f) Control input in scenario 2

Fig. 6.6: Signals of the simplified scenarios

scenarios of automated vehicles in a performance guaranteed structure has been provided. The developed design framework contains three elements, such as a robust cruise control, a supervisor and a reinforcement-learning-based agent. The role of the robust cruise control in cooperation with the supervisor is to provide guarantee on the collision avoidance with the further vehicles in the intersection. The learning-based agent improves economy and time performances of the vehicle. In the novel control structure the advantages of the robust control, i.e., the performance guarantees, and the benefits of the learning-based methods, i.e., the improved performance level are combined.

References: [Németh and Gáspár, 2021b, Németh and Gáspár, 2021a, Németh et al., 2018b]

Part IV

ANALYSIS AND SYNTHESIS METHODS FOR AUTOMATED VEHICLES IN TRAFFIC

dc_1992_22

7. RELATIONSHIP BETWEEN THE TRAFFIC FLOW AND THE CRUISE CONTROL FROM THE MACROSCOPIC POINT OF VIEW

Research on automated vehicles goes beyond vehicle control, i.e., high number of automated vehicles can have impact on the dynamics of entire traffic flow. Due to the strict rules of the vehicle control, e.g., keeping speed limits, the speed profile of the automated vehicle can differ from the speed profile of the human-driven vehicles [13]. In case of a mixed traffic, which contains human-driven and automated vehicles simultaneously, the ratio of automated vehicles and their settings influence the motion of human-driven vehicles [148, 98]. In the rest of this thesis, the analysis of this relationship through simulation-based and set-based approaches is carried out. Moreover, the formed relationships in the control design of automated vehicles and in the control design for improving traffic flow are involved.

Modeling and analysis of the mixed traffic, in which automated controlled vehicles and conventional uncontrolled vehicles are traveling together, require novel methodologies. The traffic flow model, which was characterized by the automated vehicles, was proposed by [84]. The analysis of the traffic-flow, in which semi-automated and automated vehicles were traveling together with human-driven vehicles were proposed by [132, 155]. Since the semi-automated vehicles supported a smooth traffic flow through their filtering effects, a control law was proposed by [23]. Similar results in the field of mixed traffic were achieved by [169]. The cooperative cruise control of multiple cars in mixed traffic, in which the motion of the conventional uncontrolled vehicles was considered as the continuous approximation of hybrid dynamical systems was examined by [32]. That paper illustrated, the cooperative control was able to improve the overall stability. Similarly, the connection of the cruise controlled vehicles was able to improve the string stability through the prevention of shockwave formation and propagation as presented by [143]. The mixed traffic was also modeled and examined from the aspect of the vehicle clusters. A method which was able to predict the distribution of the small clusters in the mixed traffic was proposed by [67]. Based on this information the effect of the vehicles with cruise control on the mixed traffic was examined. However, in several cases the traffic flow signals were not measured directly, see e.g., [68]. A method for the estimation of the total density and flow of vehicles for mixed traffic based on the Kalman filtering was proposed by [15]. The results were also used for the analysis and control of the vehicles in the traffic.

This chapter analyzes the impact of automated vehicles with energy-optimal cruise control strategy on the traffic flow. Since the speed profile of the proposed energy-optimal cruise control in Chapter 3 may differ from that of human-driven vehicles, the modeling and control of mixed traffic flow is a hot research topic. In this thesis an analysis method based on high-fidelity macroscopic simulations is applied, in which three parameters concerning to the cruise control and to the traffic flow are taken into consideration. Through

the contributions of the analysis, the proposed energy-optimal cruise control is extended for creating a balance between traffic flow and energy-efficient cruising. Thus, the proposed method guarantees an energy-efficient motion for automated vehicles in the traffic, while an extreme reduction of the traffic speed can be avoided.

7.1 Analysis of the predictive cruise control in the traffic

In the research the traffic model and the measurements of a test network are built in the VISSIM microscopic traffic simulation system. In the demonstration example, a 20 km-long 3-lane segment of the Hungarian M1 highway between Budapest and Tatabánya is modeled in VISSIM, in which the terrain characteristics (see Figure 7.1) and the speed limits are taken into consideration. The speed limit on the section is 130 km/h, although there is a 90 km/h limitation between 5.6 $km \dots 8.5$ km segments. Using this model several simulations with different traffic densities are performed. Moreover, traffic contains a significant number of automated vehicles, in which the energy-optimal optimization method have been built in. The further vehicles in the mixed traffic are conventional vehicles, i.e., in this context conventional vehicle means human-driven vehicles with trying to keep constant maximum speed.

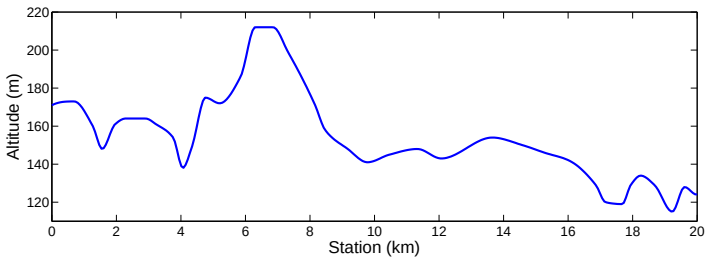

Fig. 7.1: Terrain characteristics of the highway section

During the research several traffic simulations are performed to analyze the impact of the automated vehicles with energy-optimal cruise control on the entire traffic. In these simulations the effects of three parameters are examined through their variations, such as

- q_{in}: the inflow of the vehicles on the highway section,
- κ: the ratio of automated vehicles in the traffic,
- $R_{1,max}$: the upper limit of the energy-efficient parameter in the speed profile optimization.

In the following the most representative scenarios are presented. The scenarios and the impacts of the controlled vehicles are interpreted, while the numerical results are summarized in Table 7.1. The aims of the analysis are to examine the average speed and the traction forces of the vehicles depending on $q_{in}, \kappa, R_{1,max}$.

The first scenario is proposed in Figure 7.2. In this case the selected parameters are $q_{in} = 3000$ veh/h, $R_{1,max} = 0.7$ and $\kappa = 1\%$. It means that a low number of automated

Tab. 7.1: Results of the analyses

q_{in}	$\kappa[\%]$	$R_{1,max}$	Mean of force $[N]$			Traveling time [s]	Average speed $[km/h]$
			conventional	automated	overall		
3000	1	0.7	678.1	622.1	677.5	608.3	118.4
3000	20	0.7	676.2	629.4	666.8	609.9	118.1
3000	50	0.7	673.4	630.4	651.9	610.0	118.0
5000	20	0.7	662.8	623.8	566.1	627.3	114.8
3000	20	0.9	674.8	598.7	659.6	613.5	117.4
3000	50	0.9	667.4	598.9	633.2	622.4	115.7

vehicles are on the highway. Consequently, the impact of the automated vehicles on the entire traffic flow is negligible. Thus, the average speed of the traffic is close to its maximum 130 km/h, see Figure 7.2(a). However, in the outer lane the speed is slightly reduced, because the slowest cruise-controlled vehicles are all in this lane. It means that a small κ value has a very slight impact on the traffic flow. The average traction forces of the

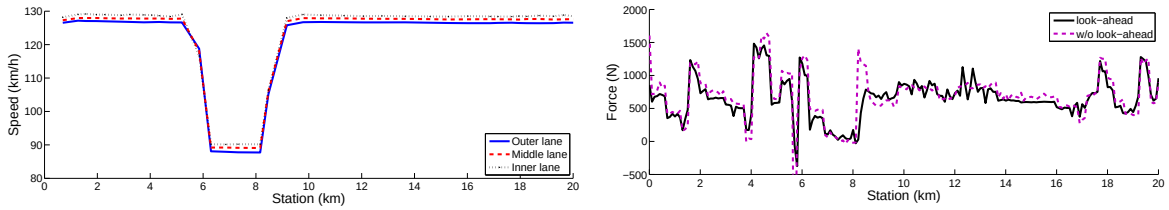

(a) Average speed (b) Traction force

Fig. 7.2: Scenario 1: $q_{in} = 3000\ veh/h$, $\kappa = 1\%$, $R_{1,max} = 0.7$

conventional and the automated vehicles are illustrated in Figure 7.2(b). Since the motions of the automated vehicles are not disturbed by each other or the conventional vehicles, they can achieve their optimal speed. This optimal speed results in force reduction on the entire route, which means that the average traction force is decreased by 8.6%.

In the second scenario the ratio of the automated vehicles is increased to $\kappa = 20\%$. In this case the automated vehicles have high impact on the traffic flow. Figure 7.3(a) shows that the average speed in the lanes significantly varies, see e.g., in the section between $13 - 20\ km$. As a result of the increased κ, not all of the automated vehicles are able to realize their speed trajectory. Furthermore, the speed profiles of the conventional vehicles are also influenced by the automated vehicles. The effect of the higher κ on the traction forces is illustrated in Figure 7.3(b). It can be seen that the traction forces of the automated vehicles are closer to those of the conventional vehicles. Thus, due to the increased traffic, not all of the automated vehicles are able to guarantee the fuel-economy motion. Furthermore, the traction force of the conventional vehicles slightly decreases. Thus, in this scenario the automated vehicles have a low impact on the traffic flow: the speed profile and the traction force of the vehicles without energy-optimal cruise control are not modified significantly.

In the third simulation scenario κ is increased to 50%, which has a high impact on the traffic flow. The results of the this scenario are presented in Figure 7.4. The energy-

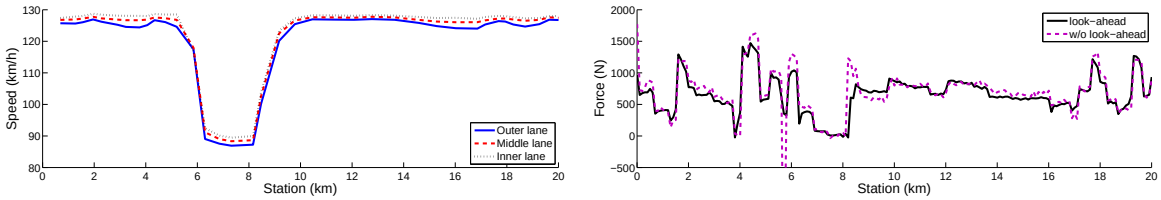

(a) Average speed (b) Traction force

Fig. 7.3: Scenario 2: $q_{in} = 3000\ veh/h$, $\kappa = 20\%$, $R_{1,max} = 0.7$

optimal speed profile is forced upon the conventional vehicles in all lanes, see Figure 7.4(a). As a result the average traction force in the traffic flow decreases, as shown in

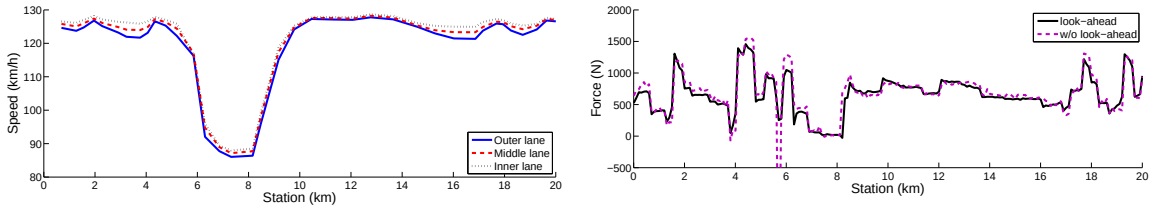

(a) Average speed (b) Traction force

Fig. 7.4: Scenario 3: $q_{in} = 3000\ veh/h$, $\kappa = 50\%$, $R_1 = 0.7$

Figure 7.4(b). This scenario illustrates that the energy consumption of the traffic flow can be influenced by using a high κ ratio. Comparing the results to the first scenario, which contains 99% conventional vehicles, the average traction force of the conventional vehicles decreases from $678.1N$ to $673.4N$.

In the fourth scenario the impact of q_{in} on the traffic flow is illustrated. It means that the inflow increases to $q_{in} = 5000\ veh/h$ value, which represents rush hour traffic. Figure 7.5 presents the results of this scenario. The result of the rush hour traffic is the

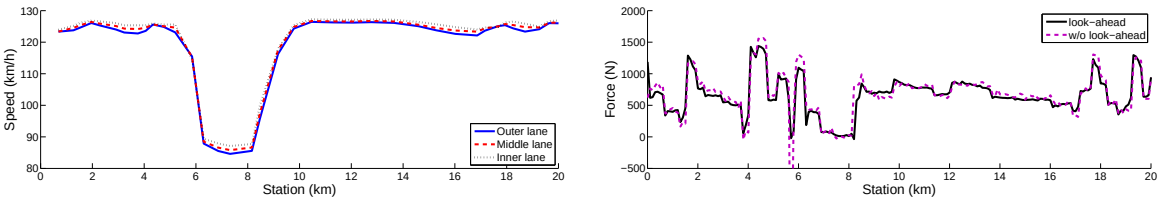

(a) Average speed (b) Traction force

Fig. 7.5: Scenario 4: $q_{in} = 5000\ veh/h$, $\kappa = 20\%$, $R_{1,max} = 0.7$

adaptation of the automated and the conventional vehicles to each other. Since the motion of the automated vehicles is closer to the conventional vehicles, it leads to a slight increase in their traction force, compared to the similar scenario with $q_{in} = 3000\ veh/h$. Moreover, the motion of the conventional vehicles also varies, which results in their force reduction

by 2.3% compared to $q_{in} = 3000\ veh/h$. Thus, in heavier traffic the energy-optimal cruise control has a significant impact on all the vehicles in terms of force requirement.

The last scenarios presents the impact of $R_{1,max}$ increase on the traffic speed and the average traction force, see Figure 7.6 and Figure 7.7. Due to the increased optimization parameter the energy-efficiency in the motion of the automated vehicles has a priority. As a consequence the average speed of the vehicles in the outer lane significantly decreases, compared to the results of the second and third scenarios,see Figure 7.6(a) and Figure 7.7(a). However, in the other lanes the average speed is close to the scenario with the

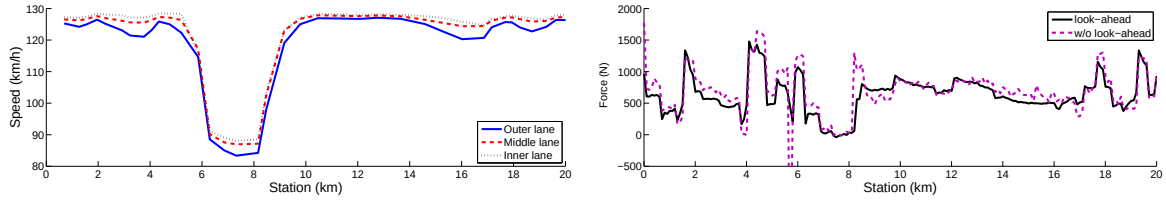

(a) Average speed (b) Traction force

Fig. 7.6: Scenario 5: $q_{in} = 3000\ veh/h$, $\kappa = 20\%$, $R_{1,max} = 0.9$

parameter $R_{1,max} = 0.7$. Thus, most of the automated vehicles move into the outer lane. As a consequence of these scenarios, the traction forces of the automated vehicles are smaller, and they have slight impact on the traction force of the conventional vehicles, as presented in the numerical values of Table 7.1. Thus, the increase in $R_{1,max}$ results in a low energy consumption reduction for the entire traffic.

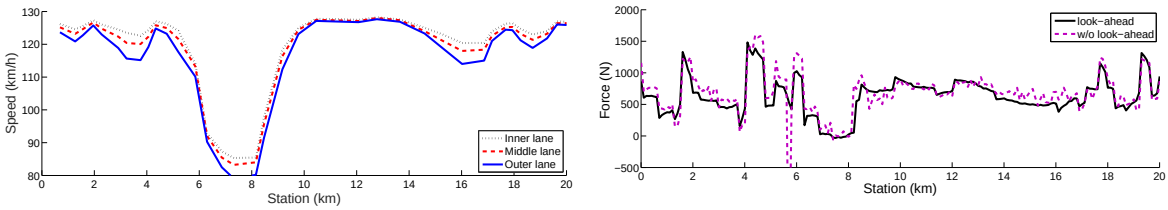

(a) Average speed (b) Traction force

Fig. 7.7: Scenario 6: $q_{in} = 3000\ veh/h$, $\kappa = 50\%$, $R_{1,max} = 0.9$

The force, traveling time and average speed requirements are summarized in Table 7.1. It shows the mean forces of the conventional and the automated vehicles, and their differences are also presented. The following conclusions on the traction forces based on the simulations are drawn:

- The increase in the traffic flow q_{in} can lead to the reduction of the traction forces of the conventional and the automated vehicles simultaneously. However, it increases the traveling time of the vehicles due to the dense traffic.
- If the ratio of the automated vehicles increases, it is slightly disadvantageous for the motion of the automated vehicles, but it improves the force reduction of the conventional vehicles.

- The increase in the $R_{1,max}$ leads to the significant reduction of the automated vehicle traction forces, and it has high impact on the conventional vehicles.

7.2 Improvement of the energy-optimal cruise control with the results of the traffic flow analysis

Previously the effects of three parameters on the traffic flow have been examined. It has been demonstrated that ratio κ of automated vehicles in the traffic flow has significant impact on the energy consumption of all the vehicles. The weight R_1 reduces the traction force of the automated vehicles substantially, and modifies the average speed of the traffic flow. Moreover, the increase of the traffic volume q_{in} results in the reduction of the traffic speed and the traction force simultaneously.

Since parameters q_{in}, κ and R_1 have impacts on traffic speed and on traction force, an appropriate speed profile design for the automated vehicles must be found. In a real traffic scenario the measurement of q_{in} and the information about κ are available. Furthermore, the weight R_1 in the energy-optimal cruise control is a parameter, whose setting has impact on the entire traffic flow. With an appropriate choice of R_1 the energy efficiency and the average speed of the traffic flow can be improved. In the following a strategy for the selection of R_1 is proposed, by which the effect of the energy-optimal cruise control on the traffic flow is considered.

The core of the strategy is based on the design of $R_{1,max}$. This parameter has a relevance in the design of R_1. It means that $R_{1,max}$ determines the maximum value of R_1. In the optimization $R_{1,max}$ is an upper bound of the optimization variable R_1. Since the weight R_1 has a high impact on the traffic flow (see Figure 7.6), the bound $R_{1,max}$ is also important in the limitation of the traffic flow speed reduction.

In the $R_{1,max}$ selection strategy the information about q_{in} and κ are involved.

- Through the appropriate selection of $R_{1,max}$ the disadvantageous effect of the high q_{in} on the traffic speed can be reduced, see Figure 7.5. If the R_1 weight is reduced in rush hour traffic, the speed profile of the automated vehicle is closer to that of the conventional vehicle. As a result, the adaptation of the automated vehicles to the conventional vehicles leads to an increase in the traffic speed.

- The ratio κ has a high impact on the traffic, see Figure 7.4. If κ is high, the average speed of the entire traffic decreases. Although it results in an energy saving traffic flow, the motion of the conventional vehicle can be significantly inhibited. Therefore, it is recommended to limit $R_{1,max}$ to avoid the disadvantageous effect of the high κ values.

The assumptions of q_{in} and κ are formulated in a function, such as:

$$R_{1,max} = \mathrm{f}(q_{in}, \kappa) \tag{7.1}$$

where f is an appropriately chosen function. f may depend on the current road section and the traffic requirements. For example, there are some road sections where the fast motion of the vehicles is more important than saving energy. In this case f must be chosen as a

function with low values. A typical form of the function f(q_{in}, κ), derived from the results of the analysis, is illustrated in Figure 7.8. The function indicates that at low κ and N values the high $R_{1,max}$ value is preferred, which results in saving energy. If κ or q_{in} values increase, f is reduced. However, the inequality $R_{1,max} > 0$, $\forall \kappa, N$ must be guaranteed to improve the energy efficiency of the traffic flow.

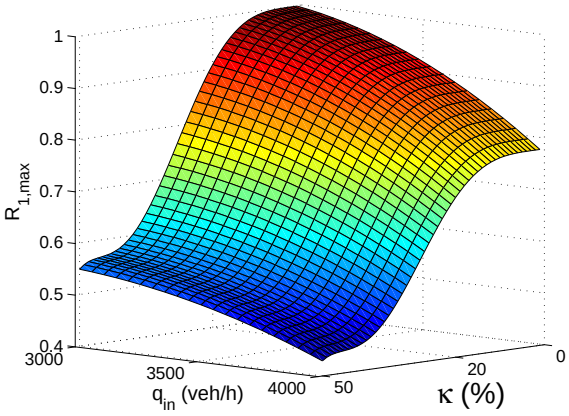

Fig. 7.8: Typical form of f(q_{in}, κ) function

7.3 Illustration on the improved energy-optimal cruise control

In this section the enhancement of the traffic flow based on the improved energy-optimal cruise control strategy is illustrated. A traffic simulation scenario is presented in which the traffic volume along the highway section varies. The aim of the demonstration is to show that the automated vehicles are able to adapt to the variation of q. Thus, the energy efficiency of the entire traffic flow is improved.

The simulation scenario contains the analyzed $20km$ section of the Hungarian M1 highway, see Figure 7.9. At the $2km$ point of this highway section an entrance ramp is found, where vehicles merge into the highway. Furthermore, at $4km$ an exit ramp is located. It results in an increased traffic on the section $2 \ldots 4km$ of the highway. Since q

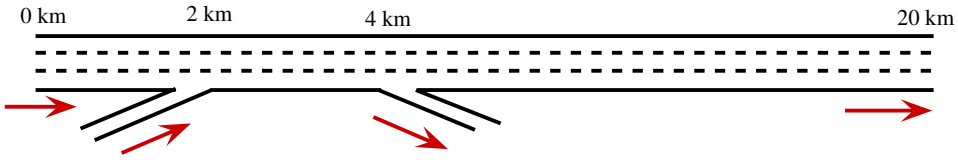

Fig. 7.9: Traffic flow on the highway section

increases, $R_{1,max}$ of the energy-optimal cruise control must be reduced, see the control rule in Figure 7.8. Thus the relationship between q and $R_{1,max}$ by a second-order polynomial is defined, see Figure 7.10. It guarantees that the maximum of R_1 is reduced at increasing traffic volume.

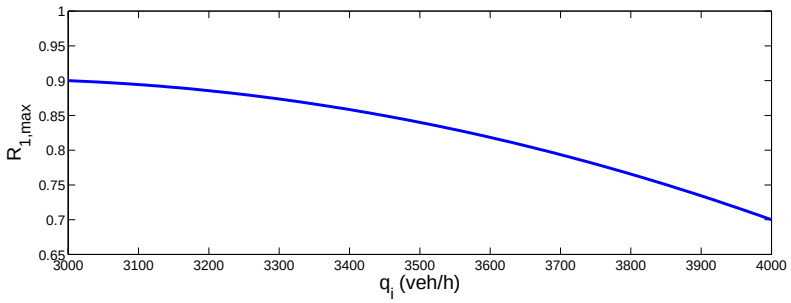

Fig. 7.10: Relationship between q and $R_{1,max}$

In this section three scenarios are presented. In the first case $R_{1,max} = 0.7$, which means that the faster motion of the vehicles is preferred. The second scenario $R_{1,max} = 0.9$ prefers the energy-efficient cruising, while in the third case $R_{1,max}$ is varied. The ratio of the automated vehicles in the traffic flow is constant $\kappa = 20\%$. Figure 7.11(a) presents the volume of the traffic for all simulations. It demonstrates the effect of the entrance

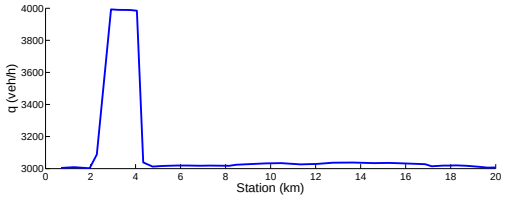

(a) Traffic volume on the highway section

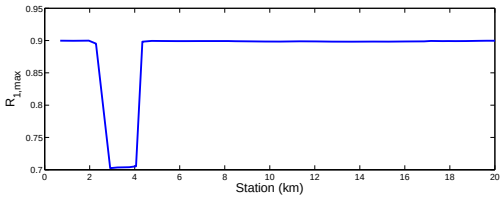

(b) Variation of $R_{1,max}$ in the third scenario

Fig. 7.11: Volume and $R_{1,max}$ values through the simulations

and exit ramps, see the values of q in the $2 \dots 4km$ section. As a result of the ramps, the traffic volume increases significantly in a short section, which may have impact on the average speed of the traffic. Therefore, in the third simulation scenario the value of $R_{1,max}$ is varied based on the relationship in Figure 7.10. As a result, $R_{1,max}$ is reduced to 0.7 between $2 \dots 4km$. It means that in this $2km$ long section the priority of energy-efficient cruising is modified to faster motion.

Figure 7.12 presents the average speeds in the lanes, in which automated vehicles have different $R_{1,max}$ strategies. If $R_{1,max} = 0.7$ is set, automated vehicles have a limited effect on the traffic. In this case the average speed values are close to the maximum speed limit in all lanes. However, at the second strategy, $R_{1,max}$ has a high impact on the average speed, e.g., in the section $14 \dots 20\ km$. In this case the speed of the vehicle varies significantly based on the forthcoming road terrain characteristics, speed limits and the current traffic volume. Between the entrance and the exit ramps the speed of the vehicles is unnecessary decreased, which is disadvantageous from the aspect of the traffic flow. The varying $R_{1,max}$ solution in the third scenario combines the advantages of the two solutions: it guarantees a fast speed on rush hour traffic section, while the energy saving speed profile is realized on the further sections, see all of the lanes in Figure 7.12. In this scenario the $R_{1,max}$ is varied as Figure 7.11(b) shows. For example, in Figure 7.12(a) the speed profile of the improved energy-optimal cruise control strategy is equal to the

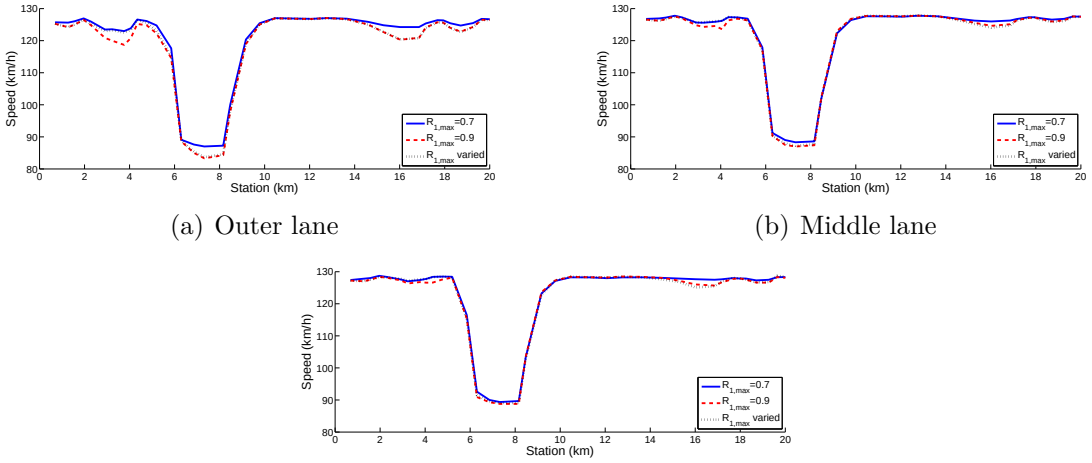

(a) Outer lane

(b) Middle lane

(c) Inner lane

Fig. 7.12: Average speed of the vehicles

speed in the constant $R_{1,max} = 0.9$ scenario, except in the section $2 \dots 4km$, where the speed profile is close to the constant $R_{1,max} = 0.7$ strategy. Thus, it is possible to avoid the unnecessary deceleration in the rush hour traffic section, while the benefits of the energy-optimal cruise control are achieved.

The similar conclusions are drawn in the examination of the traction forces, see Figure 7.13. In these figures the green points are related to the traction forces of the conventional vehicles, while the red points are connected to the automated vehicles. Figure 7.13(c) shows that the force values in the section $2 \dots 4km$ are close to the $R_{1,max} = 0.7$ strategy (Figure 7.13(a)), while in the further sections the forces are equal to those in the second strategy, see Figure 7.13(b). This conclusion is reinforced by the section between $14km$ and $20km$ points, where the similarity between the combined $R_{1,max}$ and the constant $R_{1,max} = 0.9$ strategy is demonstrated. Thus, the varying $R_{1,max}$ is able to guarantee reduced traction forces, while the average speed of the traffic is not degraded. The numerical results of the simulations are found in Table 7.2. It proposes that in the $R_{1,max} = 0.9$ strategy the mean forces are smaller than in the first scenario $R_{1,max} = 0.7$. In the case of the varied $R_{1,max}$ scenario, the mean force of the automated vehicles is between the results of the constant scenarios, while the value for the conventional vehicles is slightly higher than the result of the $R_{1,max} = 0.7$. It is the consequence of the varying speed of automated vehicles, which results in the accelerating and decelerating motion of the conventional vehicles in the section $2 \dots 4km$, increasing the traction force. However, the strategy of the $R_{1,max}$ variation leads to the overall reduction of the mean forces compared to the $R_{1,max} = 0.7$ strategy. Moreover, comparing the results to the negligible number of automated vehicles in the traffic flow (scenario $\kappa = 1\%$) the benefits are more significant, see Table 7.2. Through the use of the energy-optimal cruise control strategy the force saving of the overall traffic is 2.2%. Thus, the proposed energy-optimal cruise control strategy can be effective in the traffic flow, where automated vehicles are in minority.

New result 7.3.1: Analysis method on the impact of automated vehicles with energy-

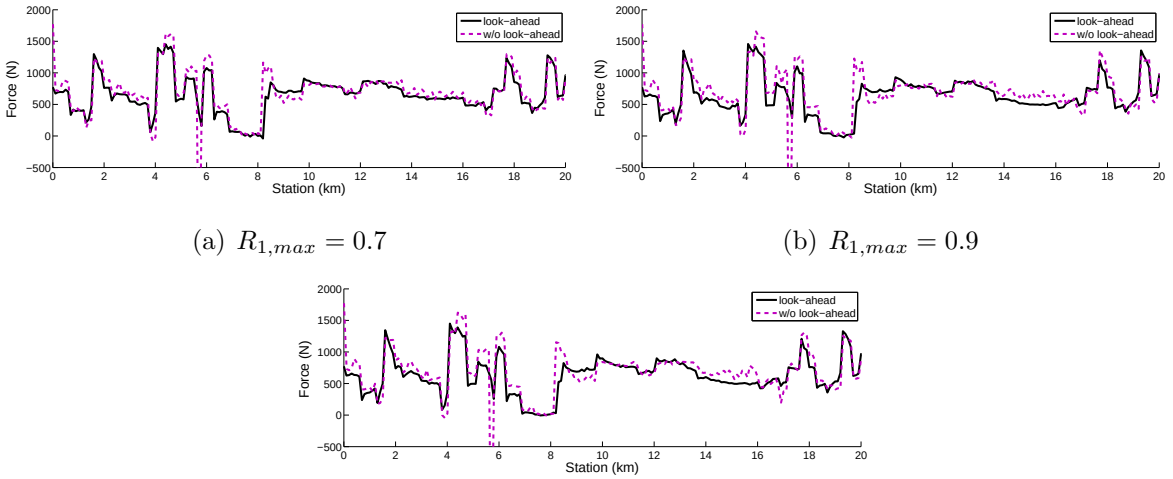

(a) $R_{1,max} = 0.7$

(b) $R_{1,max} = 0.9$

(c) $R_{1,max}$ varied

Fig. 7.13: Traction force of the vehicles

Tab. 7.2: Results of the simulations

$\kappa[\%]$	$R_{1,max}$	Mean of force $[N]$			Traveling time [s]	Average speed $[km/h]$
		conventional	automated	overall		
20	0.7	675.5	629.0	666.2	611.8	117.8
20	0.9	673.3	598.7	658.4	612.0	117.6
20	varied	676.5	604.7	662.1	611.9	117.7
1	0.7	677.7	621.8	677.1	609.1	118.2

optimal cruise control on the time-domain properties of the traffic flow has been provided. Through the analysis of high-fidelity simulation scenarios the following contributions have been formed. The selection of design parameter on energy-optimal motion for automated vehicles has impact on the energy consumption of all vehicles in the traffic network. Increasing ratio of automated vehicles has increased advantage on the energy consumption of all vehicles. Moreover, this advantageous impact at increased traffic flow is more significant. Through the contributions a strategy for the parameter selection of the energy-optimal cruise control has been formed and thus, a balance between the energy, time performances of the individual automated vehicles and the traffic flow maximization performance has been achieved.

References: [Németh and Gáspár, 2017, Németh et al., 2019a, Bede et al., 2017a, Bede et al., 2017b, Németh et al., 2016b, Németh and Gáspár, 2016, Németh and Gáspár, 2015b, Németh et al., 2022b]

8. SET-BASED ANALYSIS AND CONTROL FOR THE TRAFFIC FLOW WITH AUTOMATED VEHICLES

Relationships between the motion and control of automated vehicles and the dynamics of traffic flow have impact on both systems, i.e., automated vehicles and traffic control systems. The relationships have been formed through simulation-based tools in the previous chapter, and the contributions in the design of energy-optimal cruise control of automated vehicles have been incorporated. In this chapter the relationship has been examined from another viewpoint, which is the view of macroscopic traffic dynamics. Due to the nonlinear characteristic of the traffic flow dynamics [9], Sum-of-Squares (SOS) programming tool for the analysis of polynomial systems has been used.

In SOS programming the problem of finding feasible solutions to polynomial inequalities is transformed into semi-definite optimization task. Important theorems in SOS programming, such as the application of Positivstellensatz, were proposed in [117]. In this way the convex optimization methods can be used to find appropriate polynomials for the SOS problem. The approximation of nonnegative polynomials by a sequence of SOS was presented in [82]. The SOS polynomials incorporate the original nonnegative polynomials in an explicit form. [122] showed sufficient conditions for the solutions to nonlinear control problems, which were formulated in terms of state dependent Linear Matrix Inequalities (LMI). In the method the semidefinite programming relaxations based on the SOS decomposition were then used to efficiently solve such inequalities. The application of the SOS decomposition technique to non-polynomial system analysis was summarized in [115]. [66] introduced the application of SOS programming to several control problems, e.g., reachable set computation and control design algorithms. A local stability analysis of polynomial systems and an iterative computation method for their region of attraction were presented in [145]. In [134] the SOS method was applied to two non-convex problems, for example polynomial semi-definite programming and the fixed-order $\mathcal{H}_2$ synthesis problem. In [142] the performance analysis of polynomial systems was presented, by which sufficient conditions were provided for bounds on reachable sets and $\mathcal{L}_2$ gain of nonlinear systems subject to norm-bounded disturbance inputs. Robust performance in polynomial control systems was analyzed in [150]. This method considered the effects of neglected dynamics and parametric uncertainties. Numerical computation problems of convex programming based on the SOS method in practical applications were analyzed in [95]. As a new result the maximum Controlled Invariant Sets of polynomial control systems were calculated in [78].

The fundamental definitions and theorems for the set-based analysis of traffic flow dynamics are found in Appendix C.1. First, in this chapter the formulation of finding maximum Controlled Invariant Set using SOS programming is proposed. Second, it has been applied for the stability analysis of traffic flow dynamics. Third, the resulted con-

tributions of the analysis in the synthesis method of control on mixed traffic flow are incorporated.

8.1 Formulation of the of set-based analysis methods for discrete-time systems

In case of road traffic systems the representation of its flow dynamics is conventionally formulated through discrete time relationships. Therefore, in the followings the SOS-based computation method of Controlled Invariant Sets is reformulated to discrete time systems. The fundamental definitions and theorems are found in Appendix C.1. The goal of the analysis is to determine the maximum inflow $q_{in,max}(k)$, at which the stability of the system can be preserved, i.e., congestion of the network can be avoided. The analysis problem leads to an optimization process, in which the $u_{max}(\rho(k)) = q_{in,max}(k)$ function must be found, where ρ represents scheduling variable.

The state space representation of the system with $u_{max}(\rho(k))$ is given in the following form:

$$x(k+1) = f(\rho(k), x(k)) + g u_{max}(\rho(k)), \tag{8.1}$$

where $f(\rho, x(k))$ is a matrix, which incorporates smooth polynomial functions and $f(\rho, 0) = 0$.

The local stability of the nonlinear system at the origin is guaranteed by the existence of the Control Lyapunov Function of the system [141]. It is rewritten to discrete-time case as:

Definition 1: *A smooth, proper and positive-definite function* $\mathrm{V} : \mathbb{R}^n \to \mathbb{R}$ *is a Control Lyapunov Function for the system* (8.1) *if*

$$\Delta \mathrm{V}(\rho(k), x(k))\Big|_{u(k)=u_{max}(\rho(k))} < 0 \tag{8.2}$$

for each $x(k) \neq 0$ *and* $u_{max}(\rho(k)) \geq 0$, $\mathrm{V}(\rho(k), 0) = 0$ *for all* ρ.

The parameter-dependent Control Lyapunov Function is chosen in the next form:

$$\mathrm{V}(\rho(k), x(k)) = V(x(k)) \cdot b(\rho(k)), \tag{8.3}$$

where $b(\rho(k))$ is an intuitively chosen ρ dependent basis function. The difference in the condition (8.2) is expanded using (8.3):

$$\begin{aligned}\Delta \mathrm{V}(\rho(k), x(k)) &= \mathrm{V}(x(k+1), \rho(k)) - \mathrm{V}(x(k), \rho(k)) + \mathrm{V}(x(k), \rho(k+1)) - \mathrm{V}(x(k), \rho(k)) = \\ &= (V(x(k+1)) - V(x(k))) \cdot b(\rho(k)) + (b(\rho(k+1)) - b(\rho(k))) \cdot V(x(k)) = \\ &= \Delta V(x(k)) \cdot b(\rho(k)) + \Delta b(\rho(k)) \cdot V(x(k)),\end{aligned} \tag{8.4}$$

During the decomposition of $x(k)$ and $\rho(k)$ in the Control Lyapunov Function, the original difference $\Delta \mathrm{V}(\rho(k), x(k))$ is separated to $\Delta V(x(k))$ and $\Delta b(\rho(k))$. The difference $\Delta V(x(k))$ using (8.1) is computed as:

$$\Delta V(x(k)) = V(f(\rho(k), x(k)) + g u(k)) - V(x(k)) \tag{8.5}$$

Considering function $u_{max}(\rho(k))$ in (8.5):

$$\Delta V(x(k))\Big|_{u(k)=u_{max}(\rho(k))} = V(f(\rho(k), x(k)) + g u_{max}(\rho(k))) - V(x(k)). \tag{8.6}$$

The difference $\Delta b(\rho(k))$ depends on the formulation of basis function $b(\rho(k))$. In the further computation the upper limit on $\Delta b(\rho(k))$ is used, such as: $\nu \geq |\Delta b(\rho(k))|$, see [160]. The upper limit is chosen according to the dynamic features of the traffic system.

The local stability criterion (8.2) determines the set of the states x, which are stable and yields that $x_\infty < \infty$, if u_{max} is applied. This set is bounded by the Controlled Invariant Set, defined in the following way:

$$\mathrm{V}(\rho(k), x(k)) = 1. \tag{8.7}$$

For practical reasons the equality definition (8.7) is substituted for by two inequality conditions:

$$1 - \varepsilon \leq \mathrm{V}(\rho(k), x(k)) \leq 1, \tag{8.8}$$

where $\varepsilon > 0$ is an infinitesimally small number.

Further constraints on the stabilization (8.2) are the validity ranges of the scheduling variable ρ and the state x. The choice of the basis function $b(\rho(k))$ is valid in a range

$$\rho_{min} \leq \rho(k) \leq \rho_{max}, \tag{8.9}$$

where ρ_{min} and ρ_{max} are the bounds of the scheduling variable. Moreover, the solution of the urban network gating must be found at the constraint:

$$0 \leq x(k), \tag{8.10}$$

which represents that the number of vehicles in the network is positive or zero.

The local stability condition (8.2) is constrained by the Controlled Invariant Set (8.8), the constraints of the scheduling variable (8.9) and the states (8.10). The stability problem with the constraints is transformed into a set emptiness conditions:

$$\Big\{ \begin{array}{l} (V(f(\rho(k), x(k)) + g u_{max}(\rho(k))) - V(x(k))) \cdot b(\rho(k)) + \nu \cdot V(x(k)) \geq 0, \\ (V(f(\rho(k), x(k)) + g u_{max}(\rho(k))) - V(x(k))) \cdot b(\rho(k)) + \nu \cdot V(x(k)) \neq 0, \\ V(x(k)) \cdot b(\rho(k)) - (1 - \varepsilon) \geq 0, \quad 1 - V(x(k)) \cdot b(\rho(k)) \geq 0, \\ \rho(k) - \rho_{min} \geq 0, \quad x(k) \geq 0, \rho_{max} - \rho(k) \geq 0, \Big\} = \emptyset. \end{array} \tag{8.11}$$

Using generalized S-Procedure, the set emptiness condition (8.11) is transformed into an SOS condition. The optimization problem is to find an $u_{max}(\rho(k))$ solution and feasible $\mathrm{V}(\rho(k), x(k))$ for the following task:

$$\max\ u_{max}(\rho(k)) \tag{8.12}$$

over $s_1, s_2, s_3, s_4, s_5 \in \Sigma_n;\ V(x(k)), b(\rho(k)) \in \mathcal{R}_n$
such that

$$
\begin{aligned}
&- \Big((V(f(\rho(k), x(k)) + g u_{max}(\rho(k))) - V(x(k))) \cdot b(\rho(k)) + \nu \cdot V(x(k)) \Big) - \\
&- s_1 \Big(V(x(k)) \cdot b(\rho(k)) - (1 - \varepsilon) \Big) - s_2 \Big(1 - V(x(k)) \cdot b(\rho(k)) \Big) - s_3 x(k) - \\
&- s_4 \left(\rho(k) - \rho_{min}\right) - s_5 \left(\rho_{max} - \rho(k)\right) \in \Sigma_n. \qquad (8.13)
\end{aligned}
$$

New result 8.1.1: New analysis method for the inner-approximation of controlled invariant sets of discrete-time polynomial systems has been provided. The approximation has been formed as a maximization problem, which is constrained through Sum-of-Squares relations. The result of the maximization is a control Lyapunov function, whose level set results in the approximation of the Maximum Controlled Invariant Set.
References: [Gáspár and Németh, 2019, Németh et al., 2016d, Németh et al., 2016d, Németh et al., 2016c, Németh et al., 2015a]

8.2 Set-based analysis for the design of highway traffic control

The modeling of traffic dynamics in highway systems is based on the law of conservation. The relationship contains the sum of inflows and the outflows for a given highway segment i. The traffic density ρ_i $[veh/km]$ is expressed in the following way:

$$\rho_i(k+1) = \rho_i(k) + \frac{T}{L_i} \left[q_{i-1}(k) - q_i(k) + r_i(k) - s_i(k) \right], \qquad (8.14)$$

where k denotes the index of the discrete time step, T is the discrete sample time, L if the length of the segment, q_i $[veh/h]$ and q_{i-1} $[veh/h]$ denote the inflow of the traffic in segments i and $i-1$, r_i $[veh/h]$ and s_i $[veh/h]$ are the sum of ramp inflow and outflow values, respectively. In (8.14) the inflow $q_{i-1}(k)$ and the ramp outflow $s_i(k)$ are measured disturbance values, while $r_i(k)$ is a controlled ramp metering inflow, which is also known [116]. The outflow $q_i(k)$ of segment i incorporates the core of the traffic dynamics and depends on several factors, see e.g., [105, 152]. In the following $q_i(k)$ is formulated according to the fundamental relationship [9], which is generally derived through historic measurements [46], such as

$$q_i(k) = \mathcal{F}(\rho_i(k)). \qquad (8.15)$$

Note that $q_i(k)$ is not only the outflow of segment i, but it is also the inflow of segment $i+1$. Although $q_i(k)$ is measured as the inflow of segment $i+1$, in the modeling it is required to consider it through the formula (8.15) to receive signals from the dynamics of the traffic flow.

The function $\mathcal{F}(\rho_i(k))$ is formed in a polynomial form, which is fitted to the historic traffic flow data. Since in the mixed traffic flow automated and human-driven vehicles are

traveling together, the ratio of automated vehicles κ and their energy-efficient parameter $R_{1,i}$ must be considered

$$\mathcal{F}(\rho_i(k), R_{1,i}, \kappa) = \sum_{j=1}^{n} c_j(R_{1,i}, \kappa)\rho_i(k)^j, \tag{8.16}$$

where the coefficients in the polynomials are formed as $c_j(R_{1,i}, \kappa) = \sum_{l=1}^{m} \left(d_l R_{1,i}^l \kappa^l\right)$ with constant d_l values. The mixed traffic model using (8.14) and (8.16) is as follows:

$$\rho_i(k+1) = \rho_i(k) + \frac{T}{L_i}[-\mathcal{F}(\rho_i(k), R_{1,i}, \kappa) + q_{i-1}(k) + r_i(k) - s_i(k)] \tag{8.17}$$

Since highways contain several ramps, it is also required to model the dynamics of the queue on the controlled gates. The length of the queues can be calculated through the following linear relationship, see [36]:

$$l_i(k+1) = l_i(k) + T\left(r_{i,dem}(k) - r_i(k)\right), \tag{8.18}$$

where l_i in the units of vehicle denotes the queue length, r_i is the control input [veh/h] and the demand is $r_{i,dem}$.

Based on the mixed traffic model and considering the effects of κ and $R_{1,i}$ parameters, the stability of the traffic system will be analyzed. The examination is based on the Sum-of-Squares method, in which the polynomial characteristics of the fundamental diagram (8.16) can be incorporated [Németh et al., 2015]. One of the purposes of the analysis it to calculate the maximum inflows r_i and q_{i-1} function of $R_{1,i}$ and κ, with which the stability of the traffic flow can be guaranteed.

Using (8.17) the state space representation of the mixed-traffic system is the following form:

$$x(k+1) = f(R_{1,i}(k), x(k)) + g_1 u_{max}(R_{1,i}(k), \kappa(k)) + g_2 d(k), \tag{8.19}$$

where $x(k) = \rho_i(k)$ is the state of the system, $f(R_{1,i}(k), x(k))$ is a matrix, which incorporates smooth polynomial functions and its initial value is $f(R_{1,i}, 0) = 0$. $u_{max}(R_{1,i}(k), \kappa(k))$ is the function of the maximum controlled inflow $r_i(k)$ and $d_i(k) = q_{i-1}(k) - s_i(k)$ includes the measured disturbances of the system.

The stability analysis is based on the computation of the controlled invariant set using the Sum-of-Squares (SOS) programming method [145]. The parameter-dependent Control Lyapunov Function is chosen in the following form:

$$\mathrm{V}(R_{1,i}(k), \kappa(k), x(k)) = V(x(k)) \cdot b(R_{1,i}(k), \kappa(k)), \tag{8.20}$$

where $b(R_{1,i}(k), \kappa(k))$ is an intuitively chosen parameter-dependent basis function, whose form can depend on the analysis problem [71]. The existence of $\mathrm{V}(R_{1,i}(k), \kappa(k), x(k))$ is transformed into set-emptiness conditions. Moreover, the domains of $R_{1,min} \leq R_{1,i}(k) \leq R_{1,max}$ and $\kappa_{min} \leq \kappa(k) \leq \kappa_{max}$ are also formulated in the set-emptiness conditions. Using the generalized S-Procedure [65] the set-emptiness conditions can be transformed into the SOS existence problem, see [Németh et al., 2015].

As a result, an optimization problem is derived, in which the SOS conditions must be guaranteed. The optimization problem is to find an $u_{max}(R_{1,i}(k), \kappa(k))$ solution and feasible $\mathrm{V}(R_{1,i}(k), \kappa(k), x(k))$ for the following task:

$$\max\ u_{max}(R_{1,i}(k), \kappa(k)) \tag{8.21}$$

over $\quad s_{1\ldots7} \in \Sigma_n;\ V(x(k)), b(R_{1,i}(k), \kappa(k)) \in \mathcal{R}_n$
such that

$$\begin{aligned}
&- \Big((V(f(R_{1,i}(k), \kappa(k), x(k)) + g u_{max}(R_{1,i}(k), \kappa(k))) - \\
&- V(x(k))) \cdot b(R_{1,i}(k), \kappa(k)) + \nu \cdot V(x(k)) \Big) - \\
&- s_1 \Big(V(x(k)) \cdot b(R_{1,i}(k), \kappa(k)) - (1-\varepsilon) \Big) - \\
&- s_2 \Big(1 - V(x(k)) \cdot b(R_{1,i}(k), \kappa(k)) \Big) - s_3 x(k) - \\
&- s_4 \left(R_{1,i}(k) - R_{1,min}\right) - s_5 \left(R_{1,max} - R_{1,i}(k)\right) - \\
&- s_6 \left(\kappa(k) - \kappa_{min}\right) - s_7 \left(\kappa_{max} - \kappa(k)\right) \in \Sigma_n.
\end{aligned} \tag{8.22}$$

The result of the optimization (8.21) defines the maximum Controlled Invariant Set, in which the system is stable with the function $u_{max}(R_{1,i}(k), \kappa(k))$. Thus, for the stability of the system the following inequality must be guaranteed:

$$q_{i-1}(k) + r_i(k) - s_i(k) \leq u_{max}(R_{1,i}(k), \kappa(k)). \tag{8.23}$$

The parameters of traffic flow dynamics for the computation of stability domain through VISSIM simulations are tuned. The maximum inflow u_{max} of the system depending on κ and $R_{1,i}$ is illustrated in Figure 8.1, see [Németh et al., 2017]. It is shown that increases in $R_{1,i}$ and κ reduce the maximum number of vehicles of the traffic flow u_{max}. Consequently, in the control design it is necessary to find an appropriate coordination between the stability margin of the traffic system and energy-optimal cruising of the individual vehicles.

New result 8.2.1: A novel method for modeling the dynamics of the traffic flow with the consideration of automated and human-driven vehicles, as a polynomial system has been developed. The new approximation method of the controlled invariant set for the traffic flow has been applied, with which the stable and controllable regions of the state-space have been determined. A stability criteria for the control of the traffic flow with the consideration of the approximation results has been formed.
References: [Gáspár and Németh, 2019, Németh et al., 2016d, Németh et al., 2016d, Németh et al., 2016c, Németh et al., 2015a]

8.3 Predictive coordination strategy for automated vehicles in traffic

In the rest of this chapter the results of the stability analysis in the control strategy of the traffic system are incorporated. A synthesis method for ramp metering through

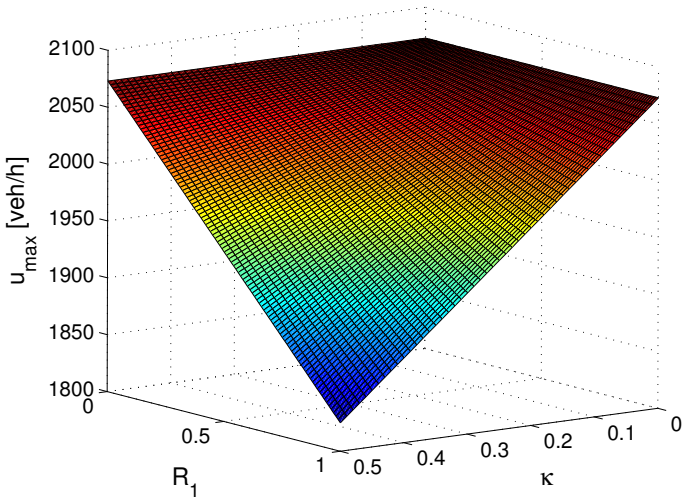

Fig. 8.1: Example on the result of the stability analysis

Model Predictive Control (MPC) design technique is proposed, in which the inequality on the stability as a constraint is built-in. The aim of the MPC design is to consider the prediction of the traffic flow in the design, see e.g., its application to urban traffic systems in [147, 44].

The control design of the highway is based on the the model of the traffic flow (8.17) and the queue dynamics (8.18). In the control-oriented traffic model the nonlinear dynamics (8.17) is linearized around $\rho_i = 0$. Consequently, the traffic model is valid to the maximum of the traffic density ρ_{max}. The mixed traffic flow model is as follows:

$$\rho_i(k+1) = \rho_i(k) + \frac{T}{L}\left(-\alpha(R_{1,i},\kappa)\rho(k) + q(k) + r(k) - s(k)\right), \tag{8.24}$$

where $\alpha(R_{1,i},\kappa)$ is the slope of the fundamental diagram in $\rho_i = 0$. The equation of one highway section is formed as

$$\begin{bmatrix}\rho_i(k+1)\\ l_i(k+1)\end{bmatrix} = \begin{bmatrix}1-\alpha(R_{1,i},\kappa) & 0\\ 0 & 1\end{bmatrix}\begin{bmatrix}\rho_i(k)\\ l_i(k)\end{bmatrix} + \begin{bmatrix}\frac{T}{L} & 0\\ 0 & T\end{bmatrix}\begin{bmatrix}q(k)-s(k)\\ r_d\end{bmatrix} + \begin{bmatrix}\frac{T}{L}\\ -T\end{bmatrix} r_i(k), \tag{8.25}$$

By defining the state vector of one highway section $x_i(k) = \begin{bmatrix}\rho_i(k) & l_i(k)\end{bmatrix}^T$ the state-space representation can be formed. Then all the highway sections f are taken into consideration in order to compress the result in the following matrix form:

$$x(k+1) = A(R_{1,i}(k),\kappa(k))x(k) + B_1 w(k) + B_2 u(k), \tag{8.26}$$

where $x(k) = \begin{bmatrix}x_1(k) & x_2(k) & \dots & x_f(k)\end{bmatrix}^T$ is the state vector, $w(k)$ is the disturbance and $u(k) = \begin{bmatrix}r_1(k) & r_2(k) & \dots & r_f(k)\end{bmatrix}^T$ is the control input vector. In the following, $A(R_{1,i},\kappa)$ simplified denotion will be used instead of $A(R_{1,i}(k),\kappa(k))$.

In the traffic control problem two main performances are defined.

- The total travel distance must be maximized in order to guarantee the maximum outflow of the highway section. In order to achieve this requirement, the maximum critical traffic density of the highway section $\rho_{crit,i}$ is introduced and the following tracking criterion is defined:

$$z_{1,i}(k) = \rho_i(k) - \rho_{crit,i}(k), \qquad |z_1| \to min. \tag{8.27}$$

  Note that $\rho_{crit,i}$ is the reference value in this performance specification.

- The length of the queue on the controlled ramp metering must be reduced to minimize the waiting time of the vehicles:

$$z_{2,i}(k) = l_i(k), \qquad |z_2| \to min. \tag{8.28}$$

Since in the control design all of the highway sections are handled together, the performances of the sections are compressed to a vector

$$z(k) = \begin{bmatrix} z_{1,1} & z_{2,1} & z_{1,2} & z_{2,2} & \dots & z_{1,f} & z_{2,f} \end{bmatrix}^T. \tag{8.29}$$

Since the traffic has relatively slow dynamics, the optimal selection of the current control input has high importance. The expected traffic dynamics or the expected changes in the traffic flow must be incorporated into the control design. Moreover, in the control design constraints must be taken into consideration, e.g., the control inputs $r_i \geq 0$. Consequently, MPC is applied to design the appropriate control interventions.

The MPC problem is described in a finite time horizon $n \cdot T$ ahead. The performance in the given horizon is calculated in the following way

$$\begin{aligned} Z = &\begin{bmatrix} C \\ CA \\ CA^2 \\ \vdots \\ CA^n \end{bmatrix} x(k) - \begin{bmatrix} z_{ref}(k) \\ z_{ref}(k+1) \\ \vdots \\ z_{ref}(k+n) \end{bmatrix} + \begin{bmatrix} 0 & 0 & \cdots & 0 \\ CB_1 & 0 & \cdots & 0 \\ CAB_1 & CB_1 & \cdots & 0 \\ \vdots & \vdots & \ddots & \vdots \\ CA^{n-1}B_1 & CA^{n-2}B_1 & \cdots & CB_1 \end{bmatrix} \begin{bmatrix} w(k) \\ w(k+1) \\ \vdots \\ w(k+n) \end{bmatrix} + \\ &+ \begin{bmatrix} 0 & 0 & \cdots & 0 \\ CB_2 & 0 & \cdots & 0 \\ CAB_2 & CB_2 & \cdots & 0 \\ \vdots & \vdots & \ddots & \vdots \\ CA^{n-1}B_2 & CA^{n-2}B_2 & \cdots & CB_2 \end{bmatrix} \begin{bmatrix} u(k) \\ u(k+1) \\ \vdots \\ u(k+n) \end{bmatrix}. \end{aligned} \tag{8.30}$$

Based on the reference values $\rho_{crit,i}(j)$ in (8.27) the reference signals $z_{ref}(j), j \in \{k, k+n\}$ are defined. The performance in the given horizon in a compact form is as follows:

$$Z = \mathcal{C} - \mathcal{R} + \mathcal{B}_1 W + \mathcal{B}_2 U, \tag{8.31}$$

where $\mathcal{C}$ contains the current states of the system, $\mathcal{R}$ contains the reference values, W contains the disturbance values, U contains the control input values. Note that both W and U also contain the forthcoming disturbances and control inputs, respectively.

In the general MPC design the following cost function is minimized:

$$J(U) = \frac{1}{2}\sum_{i=1}^{n} Z^T(U)QZ(U) + U^T RU, \tag{8.32}$$

where Q and R are weighting matrices. Substituting (8.31) into the function (8.32), the cost function is transformed as

$$\begin{aligned} J(U) =& \frac{1}{2}U^T(\mathcal{B}_2^T Q\mathcal{B}_2 + R)U + (\mathcal{C}^T Q\mathcal{B}_2 + \mathcal{R}^T Q\mathcal{B}_2 + W^T\mathcal{B}_1 Q\mathcal{B}_2)U + \varepsilon \\ =& \frac{1}{2}U^T\phi U + \beta^T U + \varepsilon, \end{aligned} \tag{8.33}$$

where ε consists of all the constant components. Since ε is independent of the effect of U on $J(U)$, it can be omitted from the optimization problem.

Since $J(U)$ contains the forthcoming disturbances and only the current values are measured, the additional elements of W must be estimated. Several methods have been worked out to provide information about the future traffic flow, see e.g., [69]. For example, a deep learning approach based on big data was presented in [99] , a statistics and neural networks were used in [110], while an adaptive Kalman filter approach was proposed by [50].

The minimization of the cost function $J(U)$ also guarantees the performances (8.29). However, the cost function itself does not guarantee the stability of the system. Thus, constrains are built inthe MPC optimization problem by using the results of the SOS-based stability analysis. The SOS analysis results in an inequality (8.23), which must be guaranteed to provide stability.

Moreover, the states of the system $\rho_i(k)$ and $l_i(k)$ must be positive, which is a further constraint on the MPC problem:

$$x(k) \geq 0, \tag{8.34}$$

for all $1 \leq k \leq n$ time steps.

Finally, from (8.23), (8.33), and (8.34) the MPC control design problem is formed in the following way:

$$\min_{u(k)\ldots u(k+n)} \frac{1}{2}U^T\phi U + \beta^T U \tag{8.35}$$

such that

$$\begin{aligned} u_{max}(R_{1,i}(k), \kappa) &\geq q_{i-1}(k) + r_i(k) - s_i(k), \quad \forall i, k \\ x(k) &\geq 0, \quad \forall k \\ U &\in \mathbf{U}, \end{aligned} \tag{8.36}$$

where $\mathbf{U}$ contains the achievable control inputs. The MPC problem can be solved using standard quadratic programming methods, e.g., [47, 136]. The result of the computation (8.35) is a series of control inputs on the horizon $T \cdot n$. The control inputs are computed online during the cruising of the vehicle.

Since the entire traffic system the energy-efficient parameter R_1 has important role, its intervention possibility is also built into the control design. The selection of $R_{1,i}$ in each section is important not only in the force/energy requirement of the vehicles, but also in the dynamics and stability of the traffic system, see (8.17) and (8.23). This parameter is incorporated in the MPC problem through the constraints, see (8.36). Figure 8.2 illustrates the effect of $R_{1,i}$ on the fundamental diagram. It is shown the relationship between $R_{1,i}$ and the outflow of the traffic system $q_i(k)$. If $R_{1,i}$ is reduced, $q_i(k)$ increases. Since outflow $q_i(k)$ significantly influences $\rho_i(k)$ and $l_i(k)$, the parameter $R_{1,i}$ has effects on the state of the system $x_i(k)$.

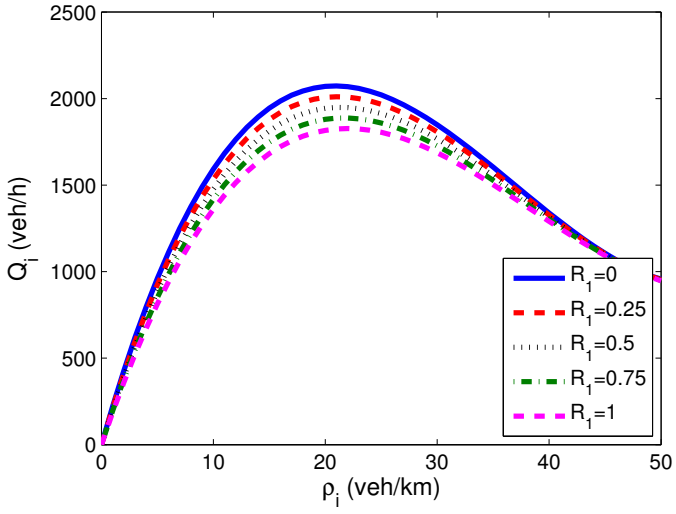

Fig. 8.2: Dependence of fundamental diagram on $R_{1,i}$ at $\kappa = 30\%$

In the coordinated control strategy with the MPC-based control design, the selection of $R_{1,i}$ is proposed. Considering the inflows $q_{i-1}(k)$, $r_i(k)$, $s_i(k)$ and the length of the queue of the controlled ramp metering $l_i(k)$, the energy-efficient parameter $R_{1,i}$ is computed for each section. Depending on the ramp metering two different scenarios are distinguished:

1./ If the highway section i is controlled by the ramp metering r_i, then $R_{1,i}$ must depend on l_i. If l_i increases significantly then $R_{1,i}$ must be reduced to guarantee larger traffic flow on this section. However, the increased flow results in increased r_i, with which the length of queue is reduced, see (8.18). Consequently, the parameter $R_{1,i}$ must be selected as the function of l_i according to Figure 8.3. Here $l_{i,min}$ and $l_{i,max}$ are design parameters.

2./ If the highway section i does not include any controlled ramp metering $r_i(k)$, then $R_{1,i}$ must depend on the inflows and outflows. In this case it is necessary to avoid the instability of the system while the maximum $R_{1,i}$ is selected. From the SOS programing method the maximum traffic flow $u_{max}(R_{1,i}(k), \kappa(k))$ is calculated using (8.21). Exploiting the experience illustrated in Figures 8.1, the maximum traffic flow can be expressed by the following form:

$$u_{max}(R_{1,i}(k), \kappa(k)) = u^0_{max} - u^1_{max} R_{1,i}(k)\kappa(k), \tag{8.37}$$

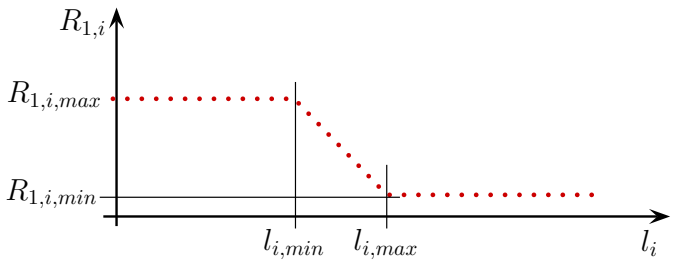

Fig. 8.3: Effect of $l_i(k)$ on $R_{1,i}(k)$

where u^0_{max} and u^1_{max} are selected constants, while $R_{1,i}(k)$ and $\kappa(k)$ are functions of k. Since $r_i(k) = 0$, in the upper limit of (8.23) can be transformed into the following form:

$$u^0_{max} - u^1_{max} R_{1,i}(k)\kappa(k) = q_{i-1}(k) - s_i(k), \tag{8.38}$$

and $R_{1,i}(k)$ is selected as follows:

$$R_{1,i}(k) = \min\left(1, \max\left(\frac{u^0_{max} - q_{i-1}(k) + s_i(k)}{u^1_{max}\kappa(k)}, 0\right)\right), \tag{8.39}$$

Based on the above scenarios, in the coordinated control strategy first the current $R_{1,i}$ values are computed for each section and second the MPC problem (8.35) is solved to achieve the optimal control inputs $r_i(k)$.

Simulation example on coordination of automated vehicles

Finally, the efficiency of the traffic control strategy is illustrated through a simulation example, which is performed in the high fidelity microscopic traffic software VISSIM. The purpose of the example is to show that the MPC-based coordinated strategy is able to control the highway ramps and the energy-efficient parameter of the vehicles guarantees the performances of the traffic system.

In the simulation example, a $20km$ long section of the highway $M1$ between Budapest and Vienna is demonstrated. The highway section is divided into 5 segments, and it contains two controlled on-ramps and one off-ramp, see Figure 8.4. During the simulation it is necessary to minimize the lengths of the queues on the on-ramps, while the traffic flow and the energy-saving of the vehicles are maximized.

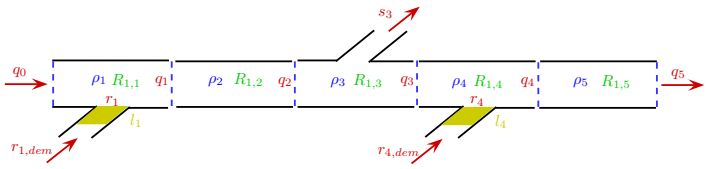

Fig. 8.4: Simulation scenario in the first example

The simulation parameter is $T = 30$ *sec* sampling time in the prediction with $n = 12$ points, which leads to a total of 6 *min* prediction horizon. However, $T = 30$ *sec* is too

small sampling time for the intervention in the traffic control system, thus $T = 120$ *sec* is selected with $n = 3$ points for the control horizon [44]. Since the control input is computed as a flow value, it is transformed into green time with a 120 *sec* cycle. Moreover, in the simulation $\kappa = 20\%$ value along the highway is considered.

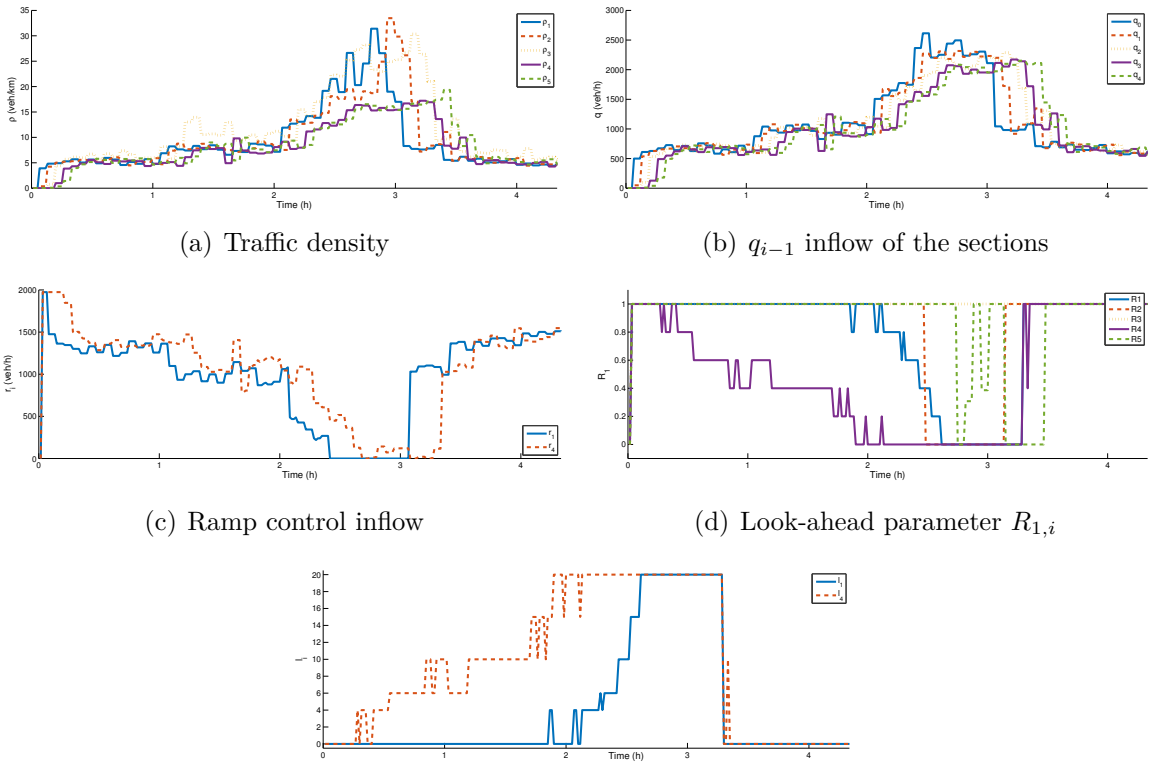

(a) Traffic density

(b) q_{i-1} inflow of the sections

(c) Ramp control inflow

(d) Look-ahead parameter $R_{1,i}$

(e) Queue length on the controlled gates

Fig. 8.5: Results of the VISSIM simulation in the first example

The results of the simulation are shown in Figure 8.5. The simulation shows increasing traffic, whose maximum is approximately 3 *hours*, see the density and the flow values at Figures 8.5(a),(b). The critical density of the traffic is $\rho_{crit} = 25$ veh/km, whose tracking influences the ramps, see Figure 8.5(c). The efficiency of the prediction can be seen in the dynamics of the r_i intervention. For example at time 2.4 h the value of r_1 significantly decreases, because q_0 increases in the future rapidly. However, ρ_1 is approximately 15 veh/km in $t = 2.4$ h.

The variation in economy parameters and the lengths of the queues are illustrated in Figure 8.5(d) and Figure 8.5(e), respectively. The effect of the queue length on $R_{1,i}$ values is shown in the figures. When the queue length increases, the parameters $R_{i,1}$ decreases simultaneously, see the signals of l_1, l_4 and $R_{1,1}, R_{1,4}$. Moreover, $R_{1,2}, R_{1,3}, R_{1,5}$ are selected to avoid the instability of the traffic and improve the flow capacity, e.g., at rush hour traffic their values decrease, see between $2.6 \dots 3.5$ h.

Further example on the coordination strategy is found in Appendix C.2.

New result 8.3.1: A predictive control strategy for the coordination of the motion of automated vehicles and the ramp metering of traffic network has been provided. In the

new control synthesis method the varying characteristics of the traffic flow, depending on the ratio of the automated vehicles, has been incorporated. Moreover, the provided stability criteria as a constraint in the predictive control has been involved. As a result, the provided control strategy guarantees the coordination of the individual vehicle motion and the traffic flow maximization on the global level.
References: [Németh et al., 2017, Németh et al., 2015, Németh and Gáspár, 2019, Németh et al., 2018a, Németh et al., 2022a]

Part V

CONCLUSIONS

dc_1992_22

9. CONCLUSIONS AND FUTURE PROJECTS

Through the proposed novel integration of learning-based and model-based methods several control problems of automated vehicles, especially their coordination with transportation systems, can be solved. Nevertheless, the results lay the path for forthcoming research due to the further open problems and to the limitations of the achieved solutions. In the rest of this dissertation, the new scientific results and the future challenges are summarized.

9.1 New scientific results

Thesis 1. Robust design structures for performance guaranteed control systems

In this dissertation design frameworks for control systems with learning-based agents have been provided. The importance of the frameworks is the design of control systems with guarantees on selected performances. In the context of automated vehicles, through the proposed frameworks, safe and collision-free motion for the vehicles under complex traffic scenarios is guaranteed.

(a) A robust control design framework for systems with learning-based agent in the reference signal generation has been provided. The result of the method is a supervisory control system, with which requirements on selected performances are guaranteed. The design of the robust control is based on the $\mathcal{H}_\infty$ method, in which the variation of the reference signal as a disturbance has been incorporated.

For more details see Section 2.2 and [Németh and Gáspár, 2021, Németh et al., 2020, Németh and Gáspár, 2020, Németh et al., 2021b, Fényes et al., 2021b]

(b) A robust control design framework for systems with learning-based agent in the control loop has been provided, with which requirements on selected performances are guaranteed. The novel framework contains two main elements, i.e., the supervisor and the robust controller. The role of the supervisor is to decide on the actual control input, which is based on the comparison of the outputs of the learning-based agent and the robust controller. The algorithm of the supervisor is formed as a constrained quadratic optimization problem. The design of the robust controller based on the Linear Parameter-Varying (LPV) method, in which the difference between the outputs of the learning-based agent and the robust controller through a scheduling variable and a measured disturbance is considered.

For more details see Section 2.3 and [Németh and Gáspár, 2021, Németh and Gáspár, 2021c, Németh, 2021, Gáspár and Németh, 2016, Németh, 2019]

Thesis 2. Energy-optimal motion profile design for automated vehicles

A novel method for achieving energy-optimal motion profile for automated vehicles has been provided. The importance of the proposed method is in its structure, i.e., various types of forthcoming road and traffic information are incorporated. Furthermore, due to its structure the motion profile design for automated vehicles under various traffic situations is carried out, e.g., cruising on highway, following surrounding vehicles, motion in intersections or optimal speed profile design for overtaking scenarios.

(a) A prediction method for the speed profile design of automated vehicles has been developed. In the provided new method several pieces of information on the forthcoming road section, i.e., terrain characteristics, speed limitations, traffic information and motion of the surrounding vehicles, are incorporated.

For more details see Section 3.1 and [Gáspár and Németh, 2019, Németh et al., 2013a, Gáspár and Németh, 2015, Gáspár and Németh, 2014b]

(b) A new, advanced, energy-optimal solution on the multi-criteria motion profile design problem for automated vehicles has been provided. The method is based on a constrained quadratic optimization, with which the balance between energy consumption and traveling time is achieved. The speed profile computation in the control architecture from the cruise control is separated, which provides increased variability in the implementation of the method. The new energy-optimal method of the motion profile design for automated vehicles in simulation and in test vehicle environment has been implemented. The results of the implementations show that the developed design method improves energy and time performances of the automated vehicle motion effectively, under real circumstances.

For more details see Section 3.2, Section 3.3 and [Gáspár and Németh, 2019, Németh and Gáspár, 2014, Németh and Gáspár, 2015b, Gáspár and Németh, 2014a, Soumelidis et al., 2018]

(c) An energy-optimal motion profile with the consideration of forthcoming road and traffic information in a performance guaranteed structure has been designed. The provided new advanced control strategy guarantees safety performance requirements for the vehicle, i.e., keeping safe distance and speed limitations, even if the communicated measured signals are degraded.

For more details see Chapter 4 and [Németh and Gáspár, 2021, Németh et al., 2021c, Németh et al., 2021a]

Thesis 3. Control design for safety critical interactions of automated vehicles

As a contribution of this dissertation, the proposed control design frameworks and motion profile methods for handling safety critical interactions of automated vehicles have been transformed. The complex multi-vehicle coordinated control problem of cruising vehicles in individual intersections with two novel methods under various scenarios has been solved. In the control solutions the presence of human-driven vehicles in the traffic scenario have been involved.

(a) The extension of the new energy-optimal motion profile design method for the

interaction of multiple automated vehicles has been provided. The coordination of the automated vehicles in intersection scenarios through the extended optimization problem has been solved, i.e., the ordering of the vehicles and the selection of their speed profiles in a joint optimizations process have been formed. In the coordination of the automated vehicles the motion of the human-driven vehicles in the intersection has been incorporated.

For more details see Chapter 5 and [Gáspár and Németh, 2019, Németh and Gáspár, 2019, Németh and Gáspár, 2015a, Szilassy et al., 2019]

(b) A novel energy-optimal motion profile design method for intersection scenarios of automated vehicles in a performance guaranteed structure has been provided. The developed design framework contains three elements, such as a robust cruise control, a supervisor and a reinforcement-learning-based agent. The role of the robust cruise control in cooperation with the supervisor is to provide guarantee on the collision avoidance with the further vehicles in the intersection. The learning-based agent improves economy and time performances of the vehicle. In the novel control structure the advantages of the robust control, i.e., the performance guarantees, and the benefits of the learning-based methods, i.e., the improved performance level are combined.

For more details see Chapter 6 and [Németh and Gáspár, 2021b, Németh and Gáspár, 2021a, Németh et al., 2018b]

Thesis 4. Analysis and synthesis methods for automated vehicles in traffic

The extension of the provided enhanced control design methods for the coordination of automated vehicles in macroscopic traffic context has been developed. Simulation-based and polynomial analysis methods for exploring the impact of automated vehicles on the traffic flow have been elaborated. The results of the analysis in the control synthesis for improving macroscopic traffic performances have been incorporated.

(a) An analysis method on the impact of automated vehicles with energy-optimal cruise control on the time-domain properties of the traffic flow has been provided. Through the analysis of high-fidelity simulation scenarios the following contributions have been formed. The selection of design parameter on energy-optimal motion for automated vehicles has impact on the energy consumption of all vehicles in the traffic network. Increasing ratio of automated vehicles has increased advantage on the energy consumption of all vehicles. Moreover, this advantageous impact at increased traffic flow is more significant. Through the contributions a strategy for the parameter selection of the energy-optimal cruise control has been formed and thus, a balance between the energy, time performances of the individual automated vehicles and the traffic flow maximization performance has been achieved.

For more details see Chapter 7 and [Németh and Gáspár, 2017, Németh et al., 2019a, Bede et al., 2017a, Bede et al., 2017b, Németh et al., 2016b, Németh and Gáspár, 2016, Németh and Gáspár, 2015b, Németh et al., 2022b]

(b) A new analysis method for the inner-approximation of controlled invariant sets of discrete-time polynomial systems has been provided. The approximation has been formed as a maximization problem, which is constrained through Sum-of-Squares relations. The result of the maximization is a control Lyapunov function, whose level set results in the

approximation of the Maximum Controlled Invariant Set. A novel method for modeling the dynamics of the traffic flow with the consideration of automated and human-driven vehicles, as a polynomial system has been developed. The new approximation method of the controlled invariant set for the traffic flow has been applied, with which the stable and controllable regions of the state-space have been determined. A stability criterion for the control of the traffic flow with the consideration of the approximation results have been formed.

For more details see Section 8.1, Section 8.2 and [Gáspár and Németh, 2019, Németh et al., 2016d, Németh et al., 2016d, Németh et al., 2016c, Németh et al., 2015a]

(c) A predictive control strategy for the coordination of the motion of automated vehicles and the ramp metering of traffic network has been provided. In the new control synthesis method, the varying characteristics of the traffic flow, depending on the ratio of the automated vehicles, have been incorporated. Moreover, the provided stability criteria as a constraint in the predictive control has been involved. As a result, the provided control strategy guarantees the coordination of the individual vehicle motion and the traffic flow maximization on the global level.

For more details see Section 8.3 and [Németh et al., 2017, Németh et al., 2015, Németh and Gáspár, 2019, Németh et al., 2018a, Németh et al., 2022a]

9.2 Future challenges and research plans

In the following, three important future challenges which require the continuation of research with the proposed methods will emerge.

The first future challenge is to find connections with implementation and the realization of the proposed methods on clouds. The use of cloud technologies is motivated by the high amount information about the vehicle and traffic control systems, which must be processed, stored and used for control purposes.

A recent hot topic of mobile robot control is cloud-aided learning. There are a high number of cloud robotics solutions, which can vary with tools and technologies used in the build-up of such systems [38]. The aim of clouds for mobile robots is to use a centralized server for performing high complexity computation process, whose realization requires the optimization of data transfer on the network [33]. One of the purpose of learning feature on the cloud is to provide optimal resource allocation, e.g., [93] proposes a resource allocation scheme based on reinforcement learning. A further solution is to utilize the computational capability of the robot, and simultaneously, to consider the latency and CPU availability, which through a RL-based deep Q-network can be achieved [119]. Another purpose of applying learning-based approaches for clouds is the high computation capability of the cloud server [88]. Typical example on the application is route planning, where comfort-based [87] and safety-based [86] route planning approaches on the cloud with access to real-time information on the environment are implemented. Another example is real-time computation of a stochastic model predictive control intervention for a suspension system [49].

The proposed methods of this dissertation provide frameworks with which safety performance requirements on cloud-aided automated vehicle control can be guaranteed.

Through these methods some crucial problems of design [54, 8] and verification [58, 151] can be avoided. The proposed hierarchical frameworks provide an efficient separation of the control system for robust vehicle-level control and for learning-based control in the cloud. The advantage of the solution is that the safe performance specifications even at the degradation of the communication in the network can be guaranteed, see e.g., [Németh et al., 2021c].

The second challenge is related to the practical application of learning-based methods in automated vehicles. The industrial implementation of learning-based, e.g., neural-network-based approaches in automated vehicles requires the provision of systematical methods for verification and validation purposes.

Some properties of neural-network-based systems, e.g., observability [4] can be examined, but the analysis of their highly nonlinear dynamics are difficult. A possible way for achieving guarantees is the using of Hamilton-Jacobi reachability methods, which work in conjunction with an arbitrary learning algorithm [43]. It leads to a least restrictive, safety-preserving control law, which intervenes only when the computed safety guarantees require it, or confidence in the computed guarantees decays in light of new observations. Another answer to the problem of guarantees is the use of Satisfiability Modulo Theory, i.e., an automated verification framework for feed-forward multi-layer neural networks is proposed by [59]. It is proved that the solution of a two-player turn-based game in a predefined form can guarantee the robustness of neural networks [163]. Similarly, in [48] a method for automatically identifying safe regions of the input space is proposed, which is robust against adversarial perturbations within the network. Moreover, another way for the verification of the neural networks is based on the use of realization theory. For example, [39] proposed that the input-output behavior of a continuous-time recurrent neural network can be represented by a rational or polynomial non-linear system. The resulted nonlinear system can be used for the analysis of the neural network.

The proposed design framework of the dissertation incorporates the core of a verification method. The verification is based on the idea behind the design framework of Section 2.3, i.e., methods for the verification of the model-based part of control system exist. Thus, the verification can be performed through safe scenarios, when the intervention of the model-based control is highlighted. It must be extended with the verification of the unconventional part of the control system, with which the maximum performance level of the control system can be verified. For feed-forward neural-network- based control systems an own method using the scenario approach has already been proposed, see [Lelkó et al., 2021a, Lelkó et al., 2021b].

The third challenge is related to the interpretation of automated vehicle control systems with artificial intelligence in a broader context, which poses social, political, and ethical challenges [125]. Most of the problems are related to human-machine interactions and to human resources, which are influenced by the level of automation.

Due to various challenges, in the last years the engineering research field has shown increasing interest in the ethical consequences of innovation [103]. One of the most famous research is Moral Machine for analyzing moral preferences and their dependence on individual, cultural and demographic characters, see [10] and the critique on the approach [45]. Another concept is to build some ethical considerations in a MPC structure of the

automate vehicle control [149], i.e., deontology motivates the development of constraints and through consequentialism the objective function is formed. The motion of automated vehicles in a traffic level context with selfish or altruistic characters can also be described [72]. The character of the vehicle through the setting of the automated control can be set. Another approach of the automated driving is imitation learning [19], where the goal of creating a neural network is to approximate human driving style. Although it can provide an effective solution on the driving task, it poses the problem of preliminary decision on the acceptability of a human driving intervention. The decision requires an a priory rule, which can also require ethical considerations. The ethical challenges of automated vehicles from philosophical [90, 21, 156] and theological sides [Németh, 2022], [6] have also been examined.

The role of the proposed design framework to handle the challenges in broader context is to improve trust in the control system. Through the achieved performance guarantees the safety level of the vehicle is increased. Its reason is that the unwanted control actuation and decision of the learning-based agent through the supervisory concept can be avoided. Similarly, the benefits of the learning-based solutions can improve the performance level, and thus, the risk of accidents can be reduced.

Part VI

REFERENCES

dc_1992_22

dc_1992_22

STATISTICS ON THE PUBLICATIONS OF THE AUTHOR

- Books: 5 [Gáspár and Németh, 2019, Gáspár et al., 2017, Németh et al., 2019c, Németh, 2014, Bokor et al., 2013]
- Book chapter: 1 [Németh and Gáspár, 2021]
- Journal papers: 50
  - D1 ranking: 5 [Németh and Gáspár, 2021c, Fényes et al., 2021a, Németh et al., 2019b, Németh and Gáspár, 2017, Németh and Gáspár, 2013]
  - Q1 ranking: 7 [Németh and Gáspár, 2017, Németh et al., 2018c, Hegedűs et al., 2021, Németh et al., 2016d, Varga et al., 2018, Gáspár and Németh, 2016, Németh et al., 2015d]
- Conference papers: 144
- Independent citations: 425

SELECTED PUBLICATIONS OF THE AUTHOR

[Bede et al., 2017a] Bede, Z., Németh, B., and Gáspár, P. (2017a). Modeling and simulation based analysis of multi-class traffic with look-ahead controlled vehicles. *Transportation Research Procedia*, 27:593–599. 20th EURO Working Group on Transportation Meeting, EWGT 2017, 4-6 September 2017, Budapest, Hungary.

[Bede et al., 2017b] Bede, Z., Németh, B., and Gáspár, P. (2017b). Simulation-based analysis of mixed traffic flow using vissim environment. In *2017 IEEE 15th International Symposium on Applied Machine Intelligence and Informatics (SAMI)*, pages 000347–000352.

[Bokor et al., 2013] Bokor, J., Gáspár, P., Aradi, S., Bauer, P., Csikós, A., Gőzse, I., Luspay, T., Mihály, A., Németh, B., Polgár, J., Soumelidis, A., Szászi, I., and Tettamanti, T. (2013). *Irányítástechnika gyakorlatok*. Typotex Kiadó.

[Fényes et al., 2021a] Fényes, D., Fazekas, M., Németh, B., and Gáspár, P. (2021a). Implementation of a variable-geometry suspension-based steering control system. *Vehicle System Dynamics*, 0(0):1–18.

[Fényes et al., 2021b] Fényes, D., Hegedűs, T., Németh, B., and Gáspár, P. (2021b). Observer design with performance guarantees for vehicle control purposes via the integration of learning-based and LPV approaches. In *32nd IEEE Intelligent Vehicles Symposium*.

[Fényes et al., 2020a] Fényes, D., Németh, B., and Gáspár, P. (2020a). LPV-based autonomous vehicle control using the results of big data analysis on lateral dynamics. In *2020 American Control Conference (ACC)*, pages 2250–2255.

[Fényes et al., 2020b] Fényes, D., Németh, B., and Gáspár, P. (2020b). LPV-based control for automated driving using data-driven methods. *IFAC-PapersOnLine*, 53(2):13898–13903. 21st IFAC World Congress.

[Fényes et al., 2021c] Fényes, D., Németh, B., and Gáspár, P. (2021c). Data-driven modeling and control design in a hierarchical structure for a variable-geometry suspension testbed. In *60th IEEE Conference on Decision and Control*.

[Fényes et al., 2021d] Fényes, D., Németh, B., and Gáspár, P. (2021d). Design of LPV control for autonomous vehicles using the contributions of big data analysis. *International Journal of Control*, 0(0):1–12.

[Gáspár and Németh, 2014a] Gáspár, P. and Németh, B. (2014a). Design of adaptive cruise control for road vehicles using topographic and traffic information. *IFAC Proceedings Volumes*, 47(3):4184–4189. 19th IFAC World Congress.

[Gáspár and Németh, 2014b] Gáspár, P. and Németh, B. (2014b). Design of look-ahead control for road vehicles using traffc information. In *22nd Mediterranean Conference on Control and Automation*, pages 201–206.

[Gáspár and Németh, 2015] Gáspár, P. and Németh, B. (2015). Design of look-ahead cruise control using road and traffic conditions. *American Control Conference, Chicago, U.S.A*, pages 3447–3452.

[Gáspár and Németh, 2016] Gáspár, P. and Németh, B. (2016). Integrated control design for driver assistance systems based on LPV methods. *International Journal of Control*, 89(12):2420–2433.

[Gáspár and Németh, 2019] Gáspár, P. and Németh, B. (2019). *Predictive Cruise Control for Road Vehicles Using Road and Traffic Information*. Springer Verlag.

[Gáspár et al., 2016a] Gáspár, P., Németh, B., Basset, M., and Orjuela, R. (2016a). Implementation of a robust cruise control using look-ahead method. *IFAC-PapersOnLine*, 49(11):505–510. 8th IFAC Symposium on Advances in Automotive Control AAC 2016.

[Gáspár et al., 2012a] Gáspár, P., Németh, B., and Bokor, J. (2012a). Design of a supervisory integrated control for driver assistance systems. *51th IEEE Conference on Decision and Control. Maui, Hawaii*.

[Gáspár et al., 2012b] Gáspár, P., Németh, B., and Bokor, J. (2012b). Design of an integrated control for driver assistance systems based on LPV methods. *Proc. of the American Control Conference , Montréal, Canada*.

[Gáspár et al., 2016b] Gáspár, P., Németh, B., Bokor, J., Sename, O., and Dugard, L. (2016b). The impact of suspension control on the controllability of the lateral vehicle dynamics. In *2016 IEEE 55th Conference on Decision and Control (CDC)*, pages 1576–1581.

[Gáspár et al., 2017] Gáspár, P., Szabó, Z., Bokor, J., and Németh, B. (2017). *Robust Control Design for Active Driver Assistance Systems: A Linear-Parameter-Varying Approach*. Springer International Publishing.

[Hegedűs et al., 2020a] Hegedűs, T., Fényes, D., Németh, B., and Gáspár, P. (2020a). Handling of tire pressure variation in autonomous vehicles: an integrated estimation and control design approach. In *2020 American Control Conference (ACC)*, pages 2244–2249.

[Hegedűs et al., 2021] Hegedűs, T., Fényes, D., Németh, B., and Gáspár, P. (2021). Improving sustainable safe transport via automated vehicle control with closed-loop matching. *Sustainability*, 13(20).

[Hegedűs et al., 2020b] Hegedűs, T., Németh, B., and Gáspár, P. (2020b). Challenges and possibilities of overtaking strategies for autonomous vehicles. *Periodica Polytechnica Transportation Engineering*, 48(4):320–326.

[Hegedűs et al., 2020c] Hegedűs, T., Németh, B., and Gáspár, P. (2020c). Multi-objective trajectory design for overtaking maneuvers of automated vehicles. *IFAC-PapersOnLine*, 53(2):15566–15571. 21st IFAC World Congress.

[Lelkó et al., 2021a] Lelkó, A., Németh, B., and Gáspár, P. (2021a). Stability and tracking performance analysis for control systems with feed-forward neural networks. In *19th European Control Conference*.

[Lelkó et al., 2021b] Lelkó, A., Németh, B., and Gáspár, P. (2021b). A tracking performance analysis method for autonomous systems with neural networks. In *17th IFAC Symposium on Information Control Problems in Manufacturing*.

[Mihály et al., 2017] Mihály, A., Gáspár, P., and Németh, B. (2017). Robust fault-tolerant control of in-wheel driven bus with cornering energy minimization. *Strojniski vestnik - Journal of Mechanical Engineering*, 63(1).

[Németh and Gáspár, 2017] Németh and Gáspár, P. (2017). The relationship between the traffic flow and the look-ahead cruise control. *IEEE Transactions on Intelligent Transportation Systems*, 18(5):1154–1164.

[Németh, 2014] Németh, B. (2014). *Application of LPV methods for integrated vehicle control systems*. Lambert Academic Publishing.

[Németh, 2019] Németh, B. (2019). Robust LPV design with neural network for the steering control of autonomous vehicles. In *2019 18th European Control Conference (ECC)*, pages 4134–4139.

[Németh, 2021] Németh, B. (2021). Coordination of lateral vehicle control systems using learning-based strategies. *Energies*, 14(5).

[Németh, 2022] Németh, B. (2022). Route selection method with ethical considerations for automated vehicles under critical situations. In *IEEE 20th Jubilee World Symposium on Applied Machine Intelligence and Informatics (SAMI)*.

[Németh et al., 2015] Németh, B., Bede, Z., and Gáspár, P. (2015). Control design of traffic flow using look-ahead vehicles to increase energy efficiency. *American Control Conference, Seattle, USA*, pages 3447–3452.

[Németh et al., 2017] Németh, B., Bede, Z., and Gáspár, P. (2017). Modelling and analysis of mixed traffic flow with look-ahead controlled vehicles. *20th IFAC World Congress*.

[Németh et al., 2018a] Németh, B., Bede, Z., and Gáspár, P. (2018a). MPC-based coordinated control design for look-ahead vehicles and traffic flow. In *2018 26th Mediterranean Conference on Control and Automation (MED)*, pages 1–9.

[Németh et al., 2019a] Németh, B., Bede, Z., and Gáspár, P. (2019a). Control strategy for the optimization of mixed traffic flow with autonomous vehicles. *IFAC-PapersOnLine*, 52(8):227–232. 10th IFAC Symposium on Intelligent Autonomous Vehicles IAV 2019.

[Németh et al., 2015a] Németh, B., Csikós, A., Gáspár, P., and Varga, I. (2015a). Analysis of the urban network gating problem: An SOS programming approach. In *2015 European Control Conference (ECC)*, pages 2652–2657.

[Németh et al., 2013a] Németh, B., Csikós, A., Varga, I., and Gáspár, P. (2013a). Multicriteria cruise control design considering geographic and traffic conditions. *Acta Polytechnica Hungarica*, 10(6):119–134.

[Németh et al., 2022a] Németh, B., Fényes, D., Bede, Z., and Gáspár, P. (2022a). Optimal control design for traffic flow maximization based on data-driven modeling method. *Energies*, 15(1).

[Németh et al., 2019b] Németh, B., Fényes, D., Gáspár, P., and Bokor, J. (2019b). Coordination of independent steering and torque vectoring in a variable-geometry suspension system. *IEEE Transactions on Control Systems Technology*, 27(5):2209–2220.

[Németh and Gáspár, 2012] Németh, B. and Gáspár, P. (2012). Mechanical analysis and control design of McPherson suspension. *International Journal of Vehicle Systems Modelling and Testing*, 7(2):173–193.

[Németh and Gáspár, 2013] Németh, B. and Gáspár, P. (2013). Control design of variable-geometry suspension considering the construction system. *IEEE Transactions on Vehicular Technology*, 62(8):4104–4109.

[Németh and Gáspár, 2013] Németh, B. and Gáspár, P. (2013). Design of vehicle cruise control using road inclinations. *International Journal of Vehicle Autonomous Systems*, 11(4):313–333.

[Németh and Gáspár, 2014] Németh, B. and Gáspár, P. (2014). Optimised speed profile design of a vehicle platoon considering road inclinations. *IET Intelligent Transport Systems*, 8(3):200–208.

[Németh and Gáspár, 2015a] Németh, B. and Gáspár, P. (2015a). Design of low confict cruise control for safety critical vehicle interactions. *IFAC-PapersOnLine*, 48(21):1186–1191. 9th IFAC Symposium on Fault Detection, Supervision and Safety for Technical Processes SAFEPROCESS 2015.

[Németh and Gáspár, 2015b] Németh, B. and Gáspár, P. (2015b). Robust look-ahead cruise control design based on the $\mathcal{H}_\infty$ method. *IFAC-PapersOnLine*, 48(14):19 – 24. 8th IFAC Symposium on Robust Control Design ROCOND 2015.

[Németh and Gáspár, 2016] Németh, B. and Gáspár, P. (2016). The impact of traffic flow on the look-ahead cruise control. In *2016 American Control Conference (ACC)*, pages 5988–5993.

[Németh and Gáspár, 2017] Németh, B. and Gáspár, P. (2017). Nonlinear analysis and control of a variable-geometry suspension system. *Control Engineering Practice*, 61:279–291.

[Németh and Gáspár, 2019] Németh, B. and Gáspár, P. (2019). Coordination of automated and human-driven vehicles in intersection scenarios. In *2019 American Control Conference (ACC)*, pages 5278–5283.

[Németh and Gáspár, 2019] Németh, B. and Gáspár, P. (2019). LPV design for the control of heterogeneous traffic flow with autonomous vehicles. *Acta Polytechnica Hungarica*, 16(8):233–246.

[Németh and Gáspár, 2020] Németh, B. and Gáspár, P. (2020). Guaranteeing performance specifications for vehicle systems with learning agents through the robust control theory. *ERCIM News*, 122:18–19.

[Németh and Gáspár, 2021a] Németh, B. and Gáspár, P. (2021a). Design of learning-based control with guarantees for autonomous vehicles in intersections. *IFAC-PapersOnLine*, 54(2):210–215. 16th IFAC Symposium on Control in Transportation Systems CTS 2021.

[Németh and Gáspár, 2021b] Németh, B. and Gáspár, P. (2021b). The design of performance guaranteed autonomous vehicle control for optimal motion in unsignalized intersections. *Applied Sciences*, 11(8).

[Németh and Gáspár, 2021c] Németh, B. and Gáspár, P. (2021c). Ensuring performance requirements for semiactive suspension with nonconventional control systems via robust linear parameter varying framework. *International Journal of Robust and Nonlinear Control*, 31(17):8165–8182.

[Németh and Gáspár, 2021] Németh, B. and Gáspár, P. (2021). *Guaranteed Performances for Learning-Based Control Systems Using Robust Control Theory*, pages 109–142. Springer International Publishing, Cham.

[Németh et al., 2022b] Németh, B., Gáspár, P., and Bede, Z. (2022b). Impact of automated vehicles using eco-cruise control on the traffic flow. *Periodica Polytechnica Transportation Engineering*, 50(1):110.

[Németh et al., 2013b] Németh, B., Gáspár, P., and Bokor, J. (2013b). Integrated control design based on driver-in-the-loop vehicle dynamics. In *52nd IEEE Conference on Decision and Control*, pages 3517–3522.

[Németh et al., 2014] Németh, B., Gáspár, P., and Bokor, J. (2014). Analysis of braking dynamics using parameter-dependent polynomial Control Lyapunov Functions. In *53rd IEEE Conference on Decision and Control*, pages 2536–2541.

[Németh et al., 2016a] Németh, B., Gáspár, P., and Bokor, J. (2016a). LPV-based integrated vehicle control design considering the nonlinear characteristics of the tire. In *2016 American Control Conference (ACC)*, pages 6893–6898.

[Németh et al., 2019c] Németh, B., Gáspár, P., and Bokor, J. (2019c). *Járműirányítás*. Akadémiai Kiadó.

[Németh et al., 2016b] Németh, B., Gáspár, P., and Mihály, A. (2016b). Analysis of interactions between look-ahead control and traffic speed. In *2016 European Control Conference (ECC)*, pages 2459–2464.

[Németh et al., 2016c] Németh, B., Gáspár, P., Mihály, A., and Bokor, J. (2016c). Analysis of look-ahead control on traffic flow. *IFAC-PapersOnLine*, 49(3):261–266. 14th IFAC Symposium on Control in Transportation Systems (CTS).

[Németh et al., 2015b] Németh, B., Gáspár, P., Orjuela, R., and Basset, M. (2015b). LPV-based control design of an adaptive cruise control system for road vehicles. *IFAC-PapersOnLine*, 48(14):62–67. 8th IFAC Symposium on Robust Control Design ROCOND 2015.

[Németh et al., 2015c] Németh, B., Gáspár, P., Orjuela, R., and Basset, M. (2015c). Robust $\mathcal{H}_\infty$ design of an automotive cruise control system. *IFAC-PapersOnLine*, 48(15):341–346. 4th IFAC Workshop on Engine and Powertrain Control, Simulation and Modeling E-COSM 2015.

[Németh et al., 2016d] Németh, B., Gáspár, P., and Péni, T. (2016d). Nonlinear analysis of vehicle control actuations based on controlled invariant sets. *International Journal of Applied Mathematics and Computer Science*, 26(1).

[Németh et al., 2021a] Németh, B., Gáspár, P., and Szabó, Z. (2021a). Guaranteed performances for a learning-based eco-cruise control using robust LPV method. *IFAC-PapersOnLine*, 54(8):83–88. 4th IFAC Workshop on Linear Parameter Varying Systems LPVS 2021.

[Németh et al., 2018b] Németh, B., Gáspár, P., Szőcs, D., and Mihály, A. (2018b). Design of the optimal motions of autonomous vehicles in intersections through neural networks. *IFAC-PapersOnLine*, 51(9):19 – 24. 15th IFAC Symposium on Control in Transportation Systems CTS 2018.

[Németh et al., 2018c] Németh, B., Hegedűs, T., and Gáspár, P. (2018c). Optimal control of overtaking maneuver for intelligent vehicles. *Journal of Advanced Transportation*.

[Németh et al., 2020] Németh, B., Hegedűs, T., and Gáspár, P. (2020). Performance guarantees on machine-learning-based overtaking strategies for autonomous vehicles. In *2020 European Control Conference (ECC)*, pages 136–141.

[Németh et al., 2021b] Németh, B., Hegedűs, T., and Gáspár, P. (2021b). Design framework for achieving guarantees with learning-based observers. *Energies*, 14(8).

[Németh et al., 2021c] Németh, B., Mihály, A., and Gáspár, P. (2021c). Design of fault-tolerant cruise control in a hierarchical framework for connected automated vehicles. In *5th International Conference on Control and Fault-Tolerant Systems*.

[Németh et al., 2015d] Németh, B., Varga, B., and Gáspár, P. (2015d). Hierarchical design of an electro-hydraulic actuator based on robust LPV methods. *International Journal of Control*, 88(8):1429–1440.

[Soumelidis et al., 2018] Soumelidis, A., Gáspár, P., Kisari, A., Bakos, A., Németh, B., Mihály, A., and Hankovszki, Z. (2018). Cloud aided implementation of energy optimal look-ahead speed control. *IFAC-PapersOnLine*, 51(9):361–366. 15th IFAC Symposium on Control in Transportation Systems CTS 2018.

[Szilassy et al., 2019] Szilassy, P., Németh, B., and Gáspár, P. (2019). Design and robustness analysis of autonomous vehicles in intersections. *IFAC-PapersOnLine*, 52(8):321 – 326. 10th IFAC Symposium on Intelligent Autonomous Vehicles IAV 2019.

[Varga et al., 2018] Varga, B., Kulcsár, B., Laine, L., Islam, M., and Németh, B. (2018). Robust tracking controller design for active dolly steering. *Proceedings of the Institution of Mechanical Engineers, Part D: Journal of Automobile Engineering*, 232(5):695–706.

[Varga et al., 2015] Varga, B., Németh, B., and Gáspár, P. (2015). Design of anti-roll bar systems based on hierarchical control. *Strojniski vestnik - Journal of Mechanical Engineering*, 61(6).

BIBLIOGRAPHY

[1] Nonlinear dynamics of vehicle traction. *Vehicle System Dynamics*, 40:377–399, 2003.

[2] B. M. Åkesson and H. T. Toivonen. A neural network model predictive controller. *Journal of Process Control*, 16(9):937–946, 2006.

[3] A. Alam, J. Martensson, and K.H. Johansson. Look-ahead cruise control for heavy duty vehicle platooning. *Proc. 16th IEEE Annual Conference on Intelligent Transportation Systems, The Hague*, 2013.

[4] Francesca Albertini and Eduardo D Sontag. State observability in recurrent neural networks. *Systems & Control Letters*, 22(4):235–244, 1994.

[5] Mohammed Hamad Almannaa, Hao Chen, Hesham A. Rakha, Amara Loulizi, and Ihab El-Shawarby. Field implementation and testing of an automated eco-cooperative adaptive cruise control system in the vicinity of signalized intersections. *Transportation Research Part D: Transport and Environment*, 67:244 – 262, 2019.

[6] William H. U. Anderson, editor. *Technology and Theology*. Vernon Press, 2021.

[7] G.S Aoude, V.R. Desaraju, L.H Stephens, and J.P. How. Driver behavior classification at intersections and validation on large naturalistic data set. *IEEE Transactions on Intelligent Transportation Systems*, 13(2):724–736, 2012.

[8] Szilrd Aradi. Survey of deep reinforcement learning for motion planning of autonomous vehicles. *IEEE Tr. on Int. Transp. Sys.*, pages 1–20, 2020.

[9] W.D. Ashton. *The Theory of Traffic Flow*. Spottiswoode, Ballantyne and Co. Ltd., London, 1966.

[10] E. Awad, S. Dsouza, R. Kim, J. Schulz, J. Henrich, A. Shariff, J-F. Bonnefon, and I. Rahwan. The moral machine experiment. *Nature*, 563:59–64, 2018.

[11] Mozhgan Nasr Azadani and Azzedine Boukerche. Toward driver intention prediction for intelligent vehicles: A deep learning approach. In *2021 IEEE 46th Conference on Local Computer Networks (LCN)*, pages 233–240, 2021.

[12] H. S. Bae, J. Ruy, and J. Gerdes. Road grade and vehicle parameter estimation for longitudinal control using gps. *4th IEEE Conference on Intelligent Transportation Systems*, 2001.

[13] Mate Barany, Botond Bertok, Zoltan Kovacs, Ferenc Friedler, and L.T. Fan. Solving vehicle assignment problems by process-network synthesis to minimize cost and environmental impact of transportation. *Clean Technologies and Environmental Policy*, 13:637–642, 2011.

[14] M. Barth, K. Boriboonsomsin, and G. Wu. The potential role of vehicle automation in reducing traffic-related energy and emissions. *2013 International Conference on Connected Vehicles and Expo (ICCVE)*, pages 604–605, Dec 2013.

[15] N. Bekiaris-Liberis, C. Roncoli, and M. Papageorgiou. Highway traffic state estimation with mixed connected and conventional vehicles. *IEEE Transactions on Intelligent Transportation Systems*, 17(12):3484–3497, 2016.

[16] Pietro Belotti, Leo Liberti, Andrea Lodi, Giacomo Nannicini, and Andrea Tramontani. *Disjunctive Inequalities: Applications And Extensions*. American Cancer Society, 2011.

[17] Youssef Bichiou and Hesham A. Rakha. Real-time optimal intersection control system for automated/cooperative vehicles. *International Journal of Transportation Science and Technology*, 8(1):1 – 12, 2019.

[18] David Bissell, Thomas Birtchnell, Anthony Elliott, and Eric L Hsu. Autonomous automobilities: The social impacts of driverless vehicles. *Current Sociology*, 68(1):116–134, 2020.

[19] Mariusz Bojarski, Davide Del Testa, Daniel Dworakowski, Bernhard Firner, Beat Flepp, Prasoon Goyal, Lawrence D. Jackel, Mathew Monfort, Urs Muller, Jiakai Zhang, Xin Zhang, Jake Zhao, and Karol Zieba. End to end learning for self-driving cars. *CoRR*, abs/1604.07316, 2016.

[20] József Bokor and Gary Balas. Linear parameter varying systems: a geometric theory and applications. *IFAC Proceedings Volumes*, 38(1):12–22, 2005. 16th IFAC World Congress.

[21] Jean-Francois Bonnefon, Azim Shariff, and Iyad Rahwan. The trolley, the bull bar, and why engineers should care about the ethics of autonomous cars [point of view]. *Proceedings of the IEEE*, 107(3):502–504, 2019.

[22] Arnab Bose and Petros Ioannou. Analysis of traffic flow with mixed manual and semi-automated vehicles. *California PATH Research Report*, 1999.

[23] Arnab Bose and Petros Ioannou. Analysis of traffic flow with mixed manual and semi-automated vehicles. *IEEE Transactions on Intelligent Transportation Systems*, 4(4):173–188, 2003.

[24] C. N. Bowman and J. A. Miller. Modeling traffic flow using simulation and big data analytics. In *2016 Winter Simulation Conference (WSC)*, pages 1206–1217, Dec 2016.

[25] S. Boyd, L. El Ghaoui, E. Feron, and V. Balakrishnan. *Linear Matrix Inequalities in System and Control Theory*. Society for Industrial and Applied Mathematics, Philadelphia, 1997.

[26] C. Briat. *Linear Parameter-Varying and Time-Delay Systems*. Advances in Delays and Dynamics. Springer-Verlag Berlin Heidelberg, 2015.

[27] Giacomo Cabri, Manuela Montangero, Filippo Muzzini, and Paolo Valente. Managing human-driven and autonomous vehicles at smart intersections. In *2020 IEEE International Conference on Human-Machine Systems (ICHMS)*, pages 1–4, 2020.

[28] J. Calliess. Online optimisation for online learning and control - from no-regret to generalised error convergence. 18^{th} *European Control Conference (ECC)*, pages 2480–2485, June 2019.

[29] S. Calvert, H. Mahmassani, J-N Meier, P. Varaiya, S. Hamdar, D. Chen, X. Li, A. Talebpour, and S. P. Mattingly. Traffic flow of connected and automated vehicles: Challenges and opportunities. *Road Vehicle Automation 4. Lecture Notes in Mobility. Springer*, pages 235–245, 2018.

[30] S. C. Calvert, W. J. Schakel, and J. W. C. van Lint. Will automated vehicles negatively impact traffic flow? *Journal of Advanced Transportation*, pages 1–17, 2017.

[31] X. Chen, B. Xu, X. Qin, Y. Bian, M. Hu, and N. Sun. Non-signalized intersection network management with connected and automated vehicles. *IEEE Access*, 8:122065–122077, 2020.

[32] H. Chin, H. Okuda, Y. Tazaki, and T. Suzuki. Model predictive cooperative cruise control in mixed traffic. *IECON 2015 - 41st Annual Conference of the IEEE Industrial Electronics Society*, pages 3199–3205, Nov 2015.

[33] S. Chinchali, A. Sharma, J. Harrison, Amine Elhafsi, Daniel Kang, Evgenya Pergament, Eyal Cidon, Sachin Katti, and Marco Pavone. Network offloading policies for cloud robotics: a learning-based approach. *Auton Robot*, 2021.

[34] Lewis M. Clements and Kara M. Kockelman. Economic effects of automated vehicles. *Transportation Research Record*, 2606(1):106–114, 2017.

[35] T.F. Coleman and Y. Li. An interior, trust region approach for nonlinear minimization subject to bounds. *SIAM Journal on Optimization*, 6:418–445, 1996.

[36] A. Csikos, T. Tettamanti, and I. Varga. Nonlinear gating control for urban road traffic network using the network fundamental diagram. *Journal of Advanced Transportation*, 49(5):597–615, 2014.

[37] D. Dang, J. Tanwar, and S. Masood. A smart traffic solution for high priority vehicles. In *2015 1st International Conference on Next Generation Computing Technologies (NGCT)*, pages 466–470, Sept 2015.

[38] Viraj Dawarka and Girish Bekaroo. Building and evaluating cloud robotic systems: A systematic review. *Robotics and Computer-Integrated Manufacturing*, 73:102240, 2022.

[39] T. Defourneau and M. Petreczky. Realization theory of recurrent neural networks and rational systems. In *2019 IEEE 58th Conference on Decision and Control (CDC)*, pages 8048–8053, 2019.

[40] Honghui Dong, Mingchao Wu, Xiaoqing Ding, Lianyu Chu, Limin Jia, Yong Qin, and Xuesong Zhou. Traffic zone division based on big data from mobile phone base stations. *Transportation Research Part C*, 58:278–291, 2015.

[41] György Eigner, Árpád Varga, Miklós Mezei, and Levente Kovács. Lpv-based control of nonlinear compartmental model with input uncertainty. In *2017 IEEE 15th International Symposium on Intelligent Systems and Informatics (SISY)*, pages 000017–000022, 2017.

[42] S. A. Fayazi, A. Vahidi, and A. Luckow. Optimal scheduling of autonomous vehicle arrivals at intelligent intersections via milp. In *2017 American Control Conference (ACC)*, pages 4920–4925, May 2017.

[43] J. F. Fisac, A. K. Akametalu, M. N. Zeilinger, S. Kaynama, J. Gillula, and C. J. Tomlin. A general safety framework for learning-based control in uncertain robotic systems. *IEEE Transactions on Automatic Control*, 64(7):2737–2752, 2019.

[44] J.R.D. Frejo and E.F. Camacho. Global versus local mpc algorithms in freeway traffic control with ramp metering and variable speed limits. *IEEE Transactions on Intelligent Transportation Systems*, 13(4):1556–1565, 2012.

[45] H. Furey and S. Hill. Mit's moral machine project is a psychological roadblock to self-driving cars. *AI and Ethics*, 1:151–155, 2021.

[46] N.H. Gartner and P. Wagner. Analysis of traffic flow characteristics on signalized arterials. *Transportation Research Record*, 1883:94–100, 2008.

[47] P. E. Gill, W. Murray, and M.H. Wright. *Practical Optimization*. Academic Press, London UK, 1981.

[48] D. Gopinath, G. Katz, C. S. Pasareanu, and C. Barrett. Deepsafe: A data-driven approach for assessing robustness of neural networks. In *Automated Technology for Verification and Analysis - 16th International Symposium, ATVA 2018, Los Angeles, CA, USA, October 7-10, 2018, Proceedings*, pages 3–19, 2018.

[49] Jacopo Guanetti and Francesco Borrelli. Stochastic MPC for cloud-aided suspension control. In *IEEE Conf on Dec and Control*, pages 238–243, 2017.

[50] J. Guo, W. Huang, and B. M. Williams. Adaptive kalman filter approach for stochastic short-term traffic flow rate prediction and uncertainty quantification. *Transportation Research Part C: Emerging Technologies*, 43(1):50–64, 2014.

[51] M.T. Hagan, H.B. Demuth, and M.H. Beale. *Neural Network Design*. PWS Publishing, Boston, 1996.

[52] J.O. Hahn, R. Rajamani, S.H. You, and K.I. Lee. Real-time identification of road-bank angle using differential GPS. *IEEE Transactions on Control Systems Technology*, 12:589–599, 2004.

[53] Jihun Han, Ardalan Vahidi, and Antonio Sciarretta. Fundamentals of energy efficient driving for combustion engine and electric vehicles: An optimal control perspective. *Automatica*, 103:558 – 572, 2019.

[54] Zichen He, Jiawei Wang, and Chunwei Song. A review of mobile robot motion planning methods: from classical motion planning workflows to reinforcement learning-based architectures, 2021.

[55] E. Hellström, M. Ivarsson, J. Åslund, and L. Nielsen. Look-ahead control for heavy trucks to minimize trip time and fuel consumption. *Control Engineering Practice*, 17(2):245–254, 2009.

[56] Erik Hellström, Jan Åslund, and Lars Nielsen. Horizon length and fuel equivalents for fuel-optimal look-ahead control. *Advances in Automotive Control*, 2010.

[57] M. Hertneck, J. Köhler, S. Trimpe, and F. Allgöwer. Learning an approximate model predictive controller with guarantees. *IEEE Control Systems Letters*, 2(3):543–548, July 2018.

[58] Lukas Hewing, Kim P. Wabersich, Marcel Menner, and Melanie N. Zeilinger. Learning-based model predictive control: Toward safe learning in control. *Annual Review of Control, Robotics, and Autonomous Systems*, 3(1):269–296, 2020.

[59] X. Huang, M. Kwiatkowska, S. Wang, and M. Wu. Safety verification of deep neural networks. *Proceedings of the International Conference on Computer Aided Verification. CAV 2017.*, 10426:3–29, 2018.

[60] R. Hult, M. Zanon, S. Gros, and P. Falcone. Optimal coordination of automated vehicles at intersections: Theory and experiments. *IEEE Transactions on Control Systems Technology*, 27(6):2510–2525, 2019.

[61] Sándor Imre. Dynamic call admission control for uplink in 3g/4g cdma-based systems. *IEEE Transactions on Vehicular Technology*, 56(5):2617–2629, 2007.

[62] KPMG International. 2020 autonomous vehicles readiness index.

[63] D. Isele, R. Rahimi, A. Cosgun, K. Subramanian, and K. Fujimura. Navigating occluded intersections with autonomous vehicles using deep reinforcement learning. In *2018 IEEE International Conference on Robotics and Automation (ICRA)*, pages 2034–2039, May 2018.

[64] M. Ivarsson, J. Åslund, and L. Nielsen. Look ahead control - consequences of a non-linear fuel map on truck fuel consumption. *Proceedings of the Institution of Mechanical Engineers, Part D, Journal of Automobile Engineering*, 223:1223–1238, 2009.

[65] Z. Jarvis-Wloszek. *Lyapunov Based Analysis and Controller Synthesis for Polynomial Systems using Sum-of-Squares Optimization.* Ph.D. Thesis, University of California, Berkeley, 2003.

[66] Z. Jarvis-Wloszek, R. Feeley, W. Tan, K. Sun, and A. Packard. Some controls applications of sum of squares programming. *42nd IEEE Conference on Decision and Control, Maui, USA*, 5:4676–4681, 2003.

[67] K. Jerath, A. Ray, S. Brennan, and V. V. Gayah. Dynamic prediction of vehicle cluster distribution in mixed traffic: A statistical mechanics-inspired method. *IEEE Transactions on Intelligent Transportation Systems*, 16(5):2424–2434, 2015.

[68] D. Jia, K. Lu, J. Wang, X. Zhang, and X. Shen. A survey on platoon-based vehicular cyber-physical systems. *IEEE Communications Surveys Tutorials*, 18(1):263–284, 2016.

[69] W. D. Jones. Forecasting traffic flow. *IEEE Spectrum*, 38(1):90–91, 2001.

[70] B. Karg and S. Lucia. Learning-based approximation of robust nonlinear predictive control with state estimation applied to a towing kite. 18^{th} *European Control Conference (ECC)*, pages 16–22, June 2019.

[71] G. Károlyi, M. Pattantyús-Ábrahám, T. Krámer, J. Józsa, and T. Tél. Finite-size lyapunov exponents: a new tool for lake dynamics. *Proceedings of the Institution of Civil Engineers - Engineering and Computational Mechanics*, 163(4):251–259, 2010.

[72] Musa Furkan Keskin, Bile Peng, Balazs Kulcsar, and Henk Wymeersch. Altruistic control of connected automated vehicles in mixed-autonomy multi-lane highway traffic. *IFAC-PapersOnLine*, 53(2):14966–14971, 2020. 21th IFAC World Congress.

[73] Femke Kessels. *Traffic Flow Modelling. Introduction to Traffic Flow Theory Through a Genealogy of Models.* Springer Verlag, 2019.

[74] L. Keviczky and Cs. Bányász. *Two-Degree-of-Freedom Control Systems. The Youla Parameterization Approach.* Academic Press, 2015.

[75] K. Kim and P. R. Kumar. An mpc-based approach to provable system-wide safety and liveness of autonomous ground traffic. *IEEE Transactions on Automatic Control*, 59(12):3341–3356, 2014.

[76] T. Koller, F. Berkenkamp, M. Turchetta, and A. Krause. Learning-based model predictive control for safe exploration. In *2018 IEEE Conference on Decision and Control (CDC)*, pages 6059–6066, 2018.

[77] I.V. Kolmanovsky and D.P. Filev. Terrain and traffic optimized vehicle speed control. *IFAC Advances in Automotive Control Conference*, 2010.

[78] M. Korda, D. Henrion, and C. N. Jones. Convex computation of the maximum controlled invariant set for polynomial control systems. *Conference on Decision and Control*, pages 7107 – 7112, 2013.

[79] R. Labayrade, D. Aubert, and J.P. Tarel. Real time obstacle detection in stereovision on non flat road geometry through "v-disparity" representation. *Intelligent Vehicle Symposium IEEE*, 2:646– 651, 2002.

[80] J.C. Lagarias, J. A. Reeds, M. H. Wright, and P. E. Wright. Convergence properties of the nelder-mead simplex method in low dimensions. *SIAM Journal of Optimization*, 9(1):112–147, 1998.

[81] Béla Lantos and Bálint Kiss. Nonlinear model predictive control of robots, cranes and vehicles. *IFAC Proceedings Volumes*, 38(1):397–402, 2005. 16th IFAC World Congress.

[82] J. B. Lasserre. Sum of squares approximation of nonnegative polynomials. *SIAM Journal on Optimization*, 49(4):651–669, 2007.

[83] J. Li, Q. He, H. Zhou, Y. Guan, and W. Dai. Modeling driver behavior near intersections in hidden markov model. *International Journal of Environmental Research and Public Health*, 13(12), 2016.

[84] K. Li and P. Ioannou. Modeling of traffic flow of automated vehicles. *IEEE Trans. Intelligent Transp. Systems*, 5(2):99–113, 2004.

[85] Li Li, Xiaonan Su amd Yanwei Wang, Yuetong Lin, Zhiheng Li, and Yuebiao Li. Robust causal dependence mining in big data network and its application to traffic flow predictions. *Transportation Research Part C*, 58:292–307, 2015.

[86] Zhaojian Li, Ilya Kolmanovsky, Ella Atkins, Jianbo Lu, Dimitar Filev, and John Michelini. Cloud aided safety-based route planning. In *2014 IEEE International Conf. on Systems, Man, and Cybernetics (SMC)*, pages 2495–2500, 2014.

[87] Zhaojian Li, Ilya V. Kolmanovsky, Ella M. Atkins, Jianbo Lu, Dimitar P. Filev, and Yuchen Bai. Road disturbance estimation and cloud-aided comfort-based route planning. *IEEE Tr. on Cybern.*, 47(11):3879–3891, 2017.

[88] Fan Liang, Wei Yu, Xing Liu, David Griffith, and Nada Golmie. Toward edge-based deep learning in industrial internet of things. *IEEE Internet of Things Journal*, 7(5):4329–4341, 2020.

[89] T. P. Lillicrap, J. J. Hunt, A. Pritzel, N. Heess, T. Erez, Y. Tassa, D. Silver, and D. Wierstra. Continuous control with deep reinforcement learning. *International Conference on Learning Representations*, 2016.

[90] Patrick Lin, Keith Abney, and Ryan Jenkins, editors. *Robot Ethics 2.0: From Autonomous Cars to Artificial Intelligence*. Oxford Scholarship Online, 2017.

[91] P. Lingman and B. Schmidtbauer. Road slope and vehicle mass estimation using Kalman filtering. *Vehicle System Dynamics Supplement*, 37:12–23, 2002.

[92] C. Liu, X. Xu, and D. Hu. Multiobjective reinforcement learning: A comprehensive overview. *IEEE Transactions on Systems, Man, and Cybernetics: Systems*, 45(3):385–398, 2015.

[93] Hang Liu, Shiwen Liu, and Kan Zheng. A reinforcement learning-based resource allocation scheme for cloud robotics. *IEEE Access*, 6:17215–17222, 2018.

[94] Hao Liu, Xingan (David) Kan, Steven E. Shladover, Xiao-Yun Lu, and Robert E. Ferlis. Modeling impacts of cooperative adaptive cruise control on mixed traffic flow in multi-lane freeway facilities. *Transportation Research Part C: Emerging Technologies*, 95:261 – 279, 2018.

[95] J. Lofberg. Pre- and post-processing sum-of-squares programs in practice. *IEEE Transactions on Automatic Control*, 54(5):1007–1011, 2009.

[96] J. Logo, V. Potó, N. Krausz, and Á. Barsi. Geometric-topologic description of a complex road junction considering the requirements of highly automated driving. In *WCCM-ECCOMAS2020*, pages 1–10, January 2021.

[97] Hua-pu Lu, Zhi-yuan Sun, and Wen-cong Qu. Big data-driven based real-time traffic flow state identification and prediction. *Discrete Dynamics in Nature and Society*, 2015.

[98] Qiong Lu, Tamás Tettamanti, Dániel Hörcher, and István Varga. The impact of autonomous vehicles on urban traffic network capacity: an experimental analysis by microscopic traffic simulation. *Transportation Letters*, 12(8):540–549, 2020.

[99] Y. Lv, Y. Duan, W. Kang, Z. Li, and F. Y. Wang. Traffic flow prediction with big data: A deep learning approach. *IEEE Transactions on Intelligent Transportation Systems*, 16(2):865–873, 2015.

[100] B. G. Maciel-Pearson, S. Akay, A. Atapour-Abarghouei, C. Holder, and T. P. Breckon. Multi-task regression-based learning for autonomous unmanned aerial vehicle flight control within unstructured outdoor environments. *IEEE Robotics and Automation Letters*, 4(4):4116–4123, 2019.

[101] The MathWorks, Inc. *Reinforcement Learning Toolbox User's Guide*, March 2020.

[102] N. Mattern and G. Wanielik. Camera-based vehicle localization at intersections using detailed digital maps. In *IEEE/ION Position, Location and Navigation Symposium*, pages 1100–1107, May 2010.

[103] Markus Maurer, J. Christian Gerdes, Barbara Lenz, and Hermann Winner, editors. *Autonomous Driving: Technical, Legal and Social Aspects*. Springer, 2016.

[104] C. D. McKinnon and A. P. Schoellig. Learning probabilistic models for safe predictive control in unknown environments. 18^{th} *European Control Conference (ECC)*, pages 2472–2479, June 2019.

[105] A. Messmer and M. Papageorgiou. METANET - a macroscopic simulation program for motorway networks. *Traffic Engineering and Control*, 31:466–470, 1990.

[106] I. Mezgár, Cs. Egresits, and L. Monostori. Design and real-time reconfiguration of robust manufacturing systems by using design of experiments and artificial neural networks. *Computers in Industry*, 33(1):61–70, 1997. Learning in Intellgent Manufacturing Systems.

[107] P Michelberger, József Bokor, Gy Terdik, and P Várlaki. Identification of bilinear models for vibrating systems. *IFAC Proceedings Volumes*, 27(8):883–888, 1994.

[108] András Mihály, Zsófia Farkas, and Péter Gáspár. Multicriteria autonomous vehicle control at non-signalized intersections. *Applied Sciences*, 10(20):7161, Oct 2020.

[109] Sándor Molnár and Márk Molnár. *Approximation of LPV-Systems with Constant-Parametric Switching Systems*, pages 127–154. Springer Singapore, Singapore, 2017.

[110] Fabio Moretti, Stefano Pizzuti, Stefano Panzieri, and Mauro Annunziato. Urban traffic flow forecasting through statistical and neural network bagging ensemble hybrid modeling. *Neurocomputing*, 167(1):3–7, 2015.

[111] Eduardo Rauh Muller, Rodrigo Castelan Carlson, and Werner Kraus Junior. Intersection control for automated vehicles with milp. *IFAC-PapersOnLine*, 49(3):37–42, 2016. 14th IFAC Symposium on Control in Transportation SystemsCTS 2016.

[112] N. Murgovski, G. R. de Campos, and J. Sjberg. Convex modeling of conflict resolution at traffic intersections. In *2015 54th IEEE Conference on Decision and Control (CDC)*, pages 4708–4713, Dec 2015.

[113] K. Nellore and G.P. Hancke. Traffic management for emergency vehicle priority based on visual sensing. *Sensors (Basel, Switzerland)*, 16(11), 2016.

[114] L. Nouveliere, M. Braci, L. Menhour, and H.T. Luu. Fuel consumption optimization for a city bus. *UKACC Control Conference*, 2008.

[115] A. Papachristodoulou and S. Prajna. *Analysis of non-polynomial systems using the sum of squares decomposition. In.: Positive Polynomials in Control*. Springer-Verlag, 2005.

[116] M. Papageorgiou and G. Vigos. Relating time-occupancy measurements to space-occupancy and link vehicle-count. *Transportation Research Part C*, 16(1):1–17, 2008.

[117] P. Parrilo. Semidefinite programming relaxations for semialgebraic problems. *Mathematical Programming Ser. B*, 96(2):293–320, 2003.

[118] B. Passenberg, P. Kock, and O. Stursberg. Combined time and fuel optimal driving of trucks based on a hybrid model. *European Control Conference, Budapest*, 2009.

[119] Manoj Penmetcha and Byung-Cheol Min. A deep reinforcement learning-based dynamic computational offloading method for cloud robotics. *IEEE Access*, 9:60265–60279, 2021.

[120] Zoltan Petres, Peter Baranyi, Peter Gaspar, Peter Varlaki, and Pal Michelberger. Different polytopic decomposition of the model of heavy vehicles by tp model transformation. In *2007 11th International Conference on Intelligent Engineering Systems*, pages 265–270, 2007.

[121] B. Piot, M. Geist, and O. Pietquin. Bridging the gap between imitation learning and inverse reinforcement learning. *IEEE Transactions on Neural Networks and Learning Systems*, 28(8):1814–1826, 2017.

[122] S. Prajna, A. Papachristodoulou, and F. Wu. Nonlinear control synthesis by sum of squares optimization: A lyapunov-based approach. *Proceedings of the 5th IEEE Asian Control Conference*, 1:157–165, 2004.

[123] T. Quack, F. Hesseler, and D. Abel. Infrastructure-based tracking of road users in urban intersections for partially available, variable-delay sensor data. In *2018 26th Mediterranean Conference on Control and Automation (MED)*, pages 1–7, June 2018.

[124] Duy Quang Tran and Sang-Hoon Bae. Proximal policy optimization through a deep reinforcement learning framework for multiple autonomous vehicles at a non-signalized intersection. *Applied Sciences*, 10(16), 2020.

[125] Randall Reed. A.I. in Religion, A.I. for Religion, A.I. and Religion: Towards a Theory of Religious Studies and Artificial Intelligence. *Religions*, 12(6), 2021.

[126] L. Riegger, M. Carlander, N. Lidander, N. Murgovski, and J. Sjberg. Centralized mpc for autonomous intersection crossing. In *2016 IEEE 19th International Conference on Intelligent Transportation Systems (ITSC)*, pages 1372–1377, Nov 2016.

[127] Gábor Rödönyi, Péter Gáspár, József Bokor, and László Palkovics. Experimental verification of robustness in a semi-autonomous heavy vehicle platoon. *Control Engineering Practice*, 28:13–25, 2014.

[128] Claudio Roncoli, Markos Papageorgiou, and Ioannis Papamichail. Traffic flow optimisation in presence of vehicle automation and communication systems - Part II: Optimal control for multi-lane motorways. *Transportation Research Part C*, 57:260–275, 2015.

[129] U. Rosolia and F. Borrelli. Learning model predictive control for iterative tasks. a data-driven control framework. *IEEE Transactions on Automatic Control*, 63(7):1883–1896, July 2018.

[130] M. Ryan. The future of transportation: Ethical, legal, social and economic impacts of self-driving vehicles in the year 2025. *Sci Eng Ethics*, 26:1185–1208, 2020.

[131] B. Saerens, H.A. Rakha, M. Diehl, and E. Van den Bulck. A methodology for assessing eco-cruise control for passenger vehicles. *Transportation Research Part D*, 19:20–27, 2013.

[132] W.J. Schakel, B. Van Arem, and B.D. Netten. Effects of cooperative adaptive cruise control on traffic flow stability. *Intelligent Transportation Systems (ITSC), 2010 13th International IEEE Conference on*, pages 759–764, 2010.

[133] C. Scherer and S. Weiland. *Lecture Notes DISC Course on Linear Matrix Inequalities in Control*. Delft University of Technology, Delft, Netherlands, 2000.

[134] C. W. Scherer and C. W. J. Hol. Matrix sum-of-squares relaxations for robust semi-definite programs. *Math. Program*, 107:189–211, 2006.

[135] F. Schilling, J. Lecoeur, F. Schiano, and D. Floreano. Learning vision-based flight in drone swarms by imitation. *IEEE Robotics and Automation Letters*, 4(4):4523–4530, 2019.

[136] C. Schmid and L.T. Biegler. Quadratic programming methods for reduced hessian SQP. *Computers & Chemical Engineering*, 18(9):817–832, 1994.

[137] Antonio Sciarretta and Ardalan Vahidi. *Energy-Efficient Driving of Road Vehicles*. Springer Verlag, 2019.

[138] O. Sename, P. Gáspár, and J. Bokor. *Robust Control and Linear Parameter Varying Approaches*. Springer Verlag, Berlin, 2013.

[139] B. Sliwa, T. Liebig, T. Vranken, M. Schreckenberg, and C. Wietfeld. System-of-systems modeling, analysis and optimization of hybrid vehicular traffic. In *2019 IEEE International Systems Conference (SysCon)*, pages 1–8, April 2019.

[140] S.L. Smith, M. Pavone, F. Bullo, and E. Frazzoli. Dynamic vehicle routing with priority classes of stochastic demands. *SIAM Journal on Control and Optimization*, 48(5):3224–3245, 2010.

[141] Eduardo D. Sontag. A "universal" construction of Artstein's theorem on nonlinear stabilization. *Systems & Control Letters*, 13:117–123, 1989.

[142] E. Summers, A. Chakraborty, W. Tan, U Topcu, P. Seiler, G. Balas, and A. Packard. Quantitative local l_2-gain and reachability analysis for nonlinear systems. *International Journal of Robust and Nonlinear Control*, 23(10):1115–1135, 2003.

[143] Alireza Talebpour and Hani S Mahmassani. Influence of autonomous and connected vehicles on stability of traffic flow. *Transportation Research Board 94th Annual Meeting, Washington DC, United States*, 2015.

[144] Alireza Talebpour and Hani S. Mahmassani. Influence of connected and autonomous vehicles on traffic flow stability and throughput. *Transportation Research Part C: Emerging Technologies*, 71:143 – 163, 2016.

[145] W. Tan and A. Packard. Stability region analysis using polynomial and composite polynomial lyapunov functions and sum-of-squares programming. *IEEE Transactions on Automatic Control*, 53(2):565–571, 2008.

[146] Jozsef K. Tar, Katalin Lorincz, and Roland Kovacs. Adaptive control of an automatic convoy of vehicles. In *2007 11th International Conference on Intelligent Engineering Systems*, 2007.

[147] T. Tettamanti, T. Luspay, B. Kulcsár, T. Péni, and I. Varga. Robust control for urban road traffic networks. *IEEE Transactions on Intelligent Transportation Systems*, 15(1):385–398, 2014.

[148] Tamás Tettamanti, István Varga, and Zsolt Szalay. Impacts of autonomous cars from a traffic engineering perspective. *Periodica Polytechnica Transportation Engineering*, 44(4):244Ű250, 2016.

[149] S. M. Thornton, S. Pan, S. M. Erlien, and J. C. Gerdes. Incorporating ethical considerations into automated vehicle control. *IEEE Transactions on Intelligent Transportation Systems*, 18(6):1429–1439, June 2017.

[150] U. Topcu and A. Packard. Local robust performance analysis for nonlinear dynamical systems. *Proceedings of the American Control Conference*, pages 784–789, 2009.

[151] Hoang-Dung Tran, Weiming Xiang, and Taylor T. Johnson. Verification approaches for learning-enabled autonomous cyber-physical systems. *IEEE Design Test*, pages 1–1, 2020.

[152] M. Treiber and A. Kesting. *Traffic Flow Dynamics: Data, Models and Simulation.* Springer-Verlag, Berlin,Heidelberg, 2013.

[153] Valerio Turri, Bart Besselink, and Karl H. Johansson. Cooperative look-ahead control for fuel-efficient and safe heavy-duty vehicle platooning. *IEEE Transactions on Control Systems Technology*, 25(1):12–28, 2017.

[154] István Vajk, Jenõ Hetthéssy, and Hassan Charaf. Reduction of modelling error in nonlinear dynamic systems. *IFAC Proceedings Volumes*, 31(17):345–350, 1998.

[155] Bart van Arem, Cornelie J. G. van Driel, and Ruben Visser. The impact of cooperative adaptive cruise control on traffic-flow characteristics. *IEEE Trans. Intelligent Transp. Systems*, 7(4):429–436, 2006.

[156] Michael Wagner and Philip Koopman. *Road Vehicle Automation 2*, chapter A Philosophy for Developing Trust in Self-driving Cars, pages 163–171. Springer, 2015.

[157] Z. Wang, Y. Bian, S. E. Shladover, G. Wu, S. E. Li, and M. J. Barth. A survey on cooperative longitudinal motion control of multiple connected and automated vehicles. *IEEE Intelligent Transportation Systems Magazine*, 12(1):4–24, Spring 2020.

[158] Zhen Wang, Xiangmo Zhao, Zhigang Xu, Xiaopeng Li, and Xiaobo Qu. Modeling and field experiments on autonomous vehicle lane changing with surrounding human-driven vehicles. *Computer-Aided Civil and Infrastructure Engineering*, 36(7):877–889, 2021.

[159] Lijun Wei, Cindy Cappelle, Yassine Ruichek, and Frdrick Zann. Gps and stereovision-based visual odometry: Application to urban scene mapping and intelligent vehicle localization. *International Journal of Vehicular Technology*, pages 1–17, 2011.

[160] F. Wu. Control of linear parameter varying systems. *PhD Thesis, Mechanical Engineering, University of California at Berkeley*, 1995.

[161] F. Wu, X.H. Yang, A. Packard, and G. Becker. Induced L_2 norm controller for LPV systems with bounded parameter variation rates. *Journal of Robust and Nonlinear Control*, 6:983–988, 1996.

[162] G. Wu, F. Ye, P. Hao, D. Esaid, K. Boriboonsomsin, and M.J. Barth. Deep learning-based eco-driving system for battery electric vehicles, 2019.

[163] Min Wu, Matthew Wicker, Wenjie Ruan, Xiaowei Huang, and Marta Kwiatkowska. A game-based approximate verification of deep neural networks with provable guarantees. *Theoretical Computer Science*, 807:298 – 329, 2020. In memory of Maurice Nivat, a founding father of Theoretical Computer Science - Part II.

[164] Tianhao Wu, Mingzhi Jiang, and Lin Zhang. Cooperative multiagent deep deterministic policy gradient (*comaddpg*) for intelligent connected transportation with unsignalized intersection. *Mathematical Problems in Engineering*, 2020.

[165] C. Wuthishuwong and A. Traechtler. Vehicle to infrastructure based safe trajectory planning for autonomous intersection management. In *2013 13th International Conference on ITS Telecommunications (ITST)*, pages 175–180, Nov 2013.

[166] Shuxiang Xu and Ling Chen. A novel approach for determining the optimal number of hidden layer neurons for fnn's and its application in data mining. *5th International Conference on Information Technology and Applications (ICITA 2008)*, pages 683–686, 2008.

[167] D. A. Yudin, A. Skrynnik, A. Krishtopik, I. Belkin, and A. I. Panov. Object detection with deep neural networks for reinforcement learning in the task of autonomous vehicles path planning at the intersection. *Opt. Mem. Neural Networks*, 28:283–295, 2019.

[168] L. Zhai, T. Chai, and S.S. Ge. Stable adaptive neural network control of nonaffine nonlinear discrete-time systems and application. In *2007 IEEE 22nd International Symposium on Intelligent Control*, pages 602–607, Oct 2007.

[169] C. Zhang and A. Vahidi. Predictive cruise control with probabilistic constraints for eco driving. *ASME 2011 Dynamic Systems and Control Conference and Bath/ASME Symposium on Fluid Power and Motion Control*, 2:233–238, 2011.

[170] T. Zhang, G. Kahn, S. Levine, and P. Abbeel. Learning deep control policies for autonomous aerial vehicles with mpc-guided policy search. In *2016 IEEE International Conference on Robotics and Automation (ICRA)*, pages 528–535, May 2016.

[171] D. Zhao, W. Chen, J. Wu, and J. Li. Globally stable adaptive tracking control for uncertain strict-feedback systems based on neural network approximation. *Asian Journal of Control*, 18(2):527–538, March 2016.

[172] Yanggu Zheng, Barys Shyrokau, and Tamas Keviczky. Comfort and time efficiency: A roundabout case study. In *2021 IEEE International Intelligent Transportation Systems Conference (ITSC)*, pages 3877–3883, 2021.

[173] K. Zhou, J.C. Doyle, and K. Glover. *Robust and Optimal Control*. Prentice Hall, 1996.

[174] M. Zhou, Y. Yu, and X. Qu. Development of an efficient driving strategy for connected and automated vehicles at signalized intersections: A reinforcement learning approach. *IEEE Transactions on Intelligent Transportation Systems*, 21(1):433–443, 2020.

APPENDIX

dc_1992_22

A. ILLUSTRATIONS ON ENERGY-OPTIMAL CRUISE CONTROL

A.1 Illustration on the operation of energy-optimal cruise control

Analysis of energy-optimal cruise control in a motorway

The effectiveness of the proposed speed profile selection method on a simulation example of a transportation route with real data is analyzed. The terrain characteristics and geographical information are those of the M1 Hungarian highway between Tatabánya and Budapest in a 56-km-long section. In the simulation a typical F-Class truck travels along the 56 km route. The mass of the 6–gear truck is 2023 kg and its engine power is $300kW$ ($402hp$). The regulated maximal velocity is 130 km/h, but the road section contains other speed limits (e.g., 80 km/h or 100 km/h), and the road section also contains hilly parts. Thus, it is an acceptable route for the analysis of road conditions, i.e., inclinations and speed limits. Publicly accessible up-to-date geographical/navigational databases and visualisation programs, such as Google Earth and Google Maps, are used for the experiment.

Figure A.1(a) shows the altitude of the road along the way. It shows that the chosen motorway contains several uphill and downhill sections. In this example two different controllers are compared. The first is the proposed controller, which considers the road conditions such as inclinations and speed limits and is illustrated by solid line in the figures, while the second controller is a conventional ACC system, which ignores this information and is illustrated by dashed line. Figure A.1(b) shows the velocity of the vehicle with speed limits in both cases. The conventional ACC system tracks the predefined velocity speed limits as accurately as possible and the tracking error is minimal. In the proposed method the velocity of the vehicle is determined by the speed limits and simultaneously it takes the road inclinations into consideration according to the optimal requirement. In the sections of road inclinations the average relative difference between the actual velocity and the speed limit is 8% in the proposed method.

Figure A.1(c) shows the required longitudinal force. The high-precision tracking of the predefined velocities in the conventional ACC system often requires extremely high forces with abrupt changes in the signals. Since the proposed method uses the road inclinations and speed limits in advance in the optimization method, the truck is able to travel along the road with smaller actuation. The actual physical control inputs of the brake cylinder pressure and the throttle are illustrated in Figure A.1(d) and Figure A.1(f), respectively. In the conventional ACC system the engine speed is within smaller bounds than in the proposed controller as Figure A.1(e) shows.

As a result of the road conditions less energy is required during the journey in the proposed control method, see Figures A.1(g) and A.1(h). The proposed method requires

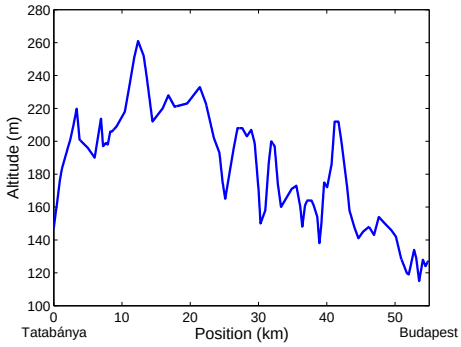

(a) Road altitude

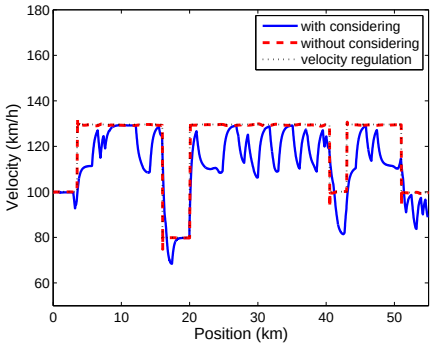

(b) Velocity of vehicle

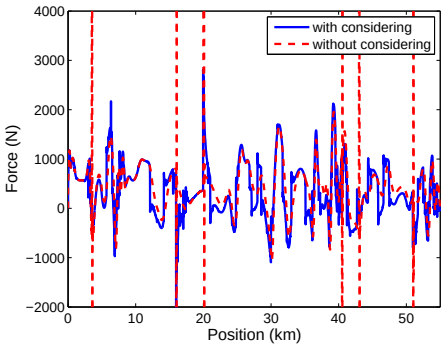

(c) Actuated force of vehicle

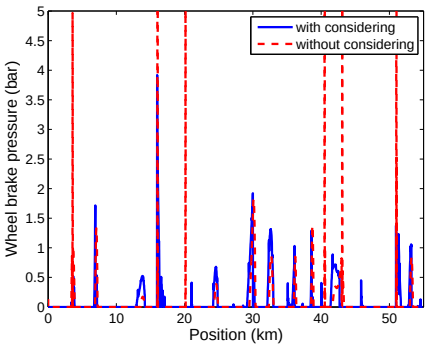

(d) Brake pressure on front wheels

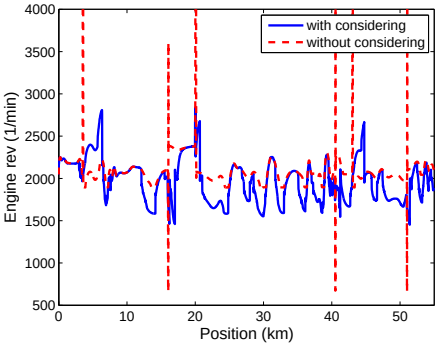

(e) Engine rev

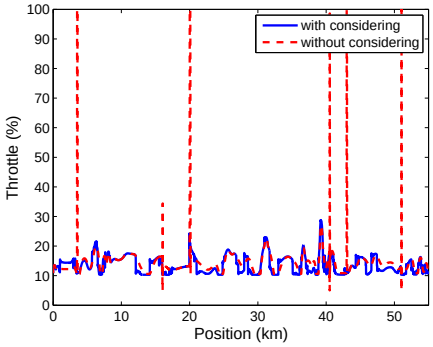

(f) Throttle

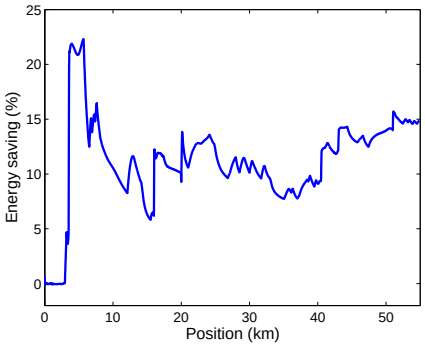

(g) Energy saving

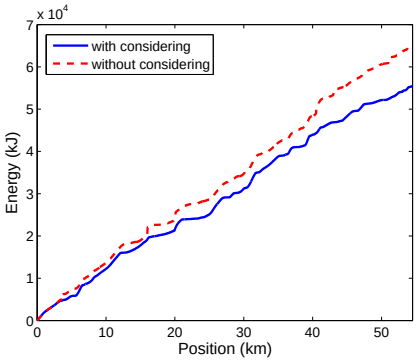

(h) Total energy

Fig. A.1: Real data motorway simulation

smaller energy (47.2 MJ) than the conventional method (55.6 MJ), and the energy saving is 8.4 MJ, which is 15.1%. Approximately half of this value is realized by the driveline system (51.4%). The fuel consumption can also be calculated by using the following equation: $V = (F_{l1}\dot{\xi}_0)/(\eta L_h \rho_{fuel})$ where $\eta = 0.25$ is the efficiency of the driveline system, $L_h = 47.3\ MJ/kg$ is the heat of combustion and $\rho_{fuel} = 730 kg/m^3$ is the density of petrol. The fuel consumption of the conventional system is 6.44 l while that of the proposed method is 5.47 l, which results in 0.97 l reduction in fuel consumption in the analyzed 56 km length section. But, the difference in the duration is only 2 minutes.

Comparison of the method with dynamic programming

The results of the proposed predictive cruise control is compared with the result of a dynamic programming method through a simulation scenario. In the example the vehicle must be driven on a 10 km long segment of the Hungarian M1 highway between Budapest and Tatabánya, see Figure A.2. In case of the dynamic programming algorithm the following criteria must be guaranteed

- The speed limitation is 130 km/h on the highway, and the maximum reduction of the vehicle speed is 20%, which results in 105 km/h minimum speed.
- The maximum speed of the vehicle allowed to be maximum 1.5% higher, which results in 132 km/h.
- The vehicle must reach the maximum speed limit at the end of the highway section.

During the computation of the optimum speed profile the 10 km long section is divided into 200 equidistant sections with 50 m lengths. The goal of the optimization is to guarantee the minimization of the longitudinal control forces $F_{l,i}$ for the sum of the segments i

$$\min_{F_{l,1}\dots F_{l,200}} \sum_{i=1}^{200} |F_{l,i}|, \tag{A.1}$$

such that the previous criteria and the longitudinal dynamics of the vehicle (see Section 3.1) are guaranteed.

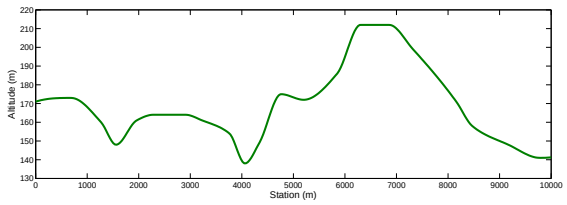

Fig. A.2: Altitude of the highway segment

The results of the dynamic programming, such as the speed profile and the control force are presented in Figure A.3.It can be seen that the resulted speed profile and force characteristics fits to the uphill/downhill sections of the highway (see Figure A.2), by

which the acceleration and deceleration effects of the highway are utilized. The speed profile in Figure A.3(a) shows that in the section 3000 . . . 7000 km the speed profile is significantly influenced by the terrain characteristics. For example at 4000 m there is valley, which results in the local minimum of the speed. Moreover, the longitudinal force is continuously reduced before the section point 4000 m, while the increased speed is advantageous for the uphill section of the exit of the valley.

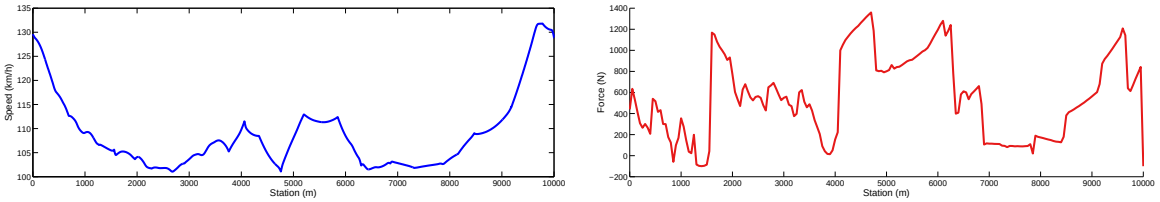

(a) Speed of the vehicle (b) Longitudinal control force

Fig. A.3: Results of the dynamic programming

Figure A.4 illustrates the result of the proposed predictive cruise control with different look-ahead horizon length L. Due to the long highway section the horizon significantly influences the speed profile of the vehicle. Although the optimization task of the dynamic programming (A.1) with its constraints slightly differs from the proposed predictive cruise control strategy, it provides a good benchmark for the evaluation of the method. In case of short horizon (500 . . . 2000 m) the speed of the vehicles often reaches the speed limit 130 km/h, while at long horizon scenarios (5000 . . . 10000 m) the variation of the terrain characteristics has higher impact on the speed profile. Moreover, with increasing horizons the speed profiles approximate the result of the dynamic programming. In case of the control forces the similar tendency can be found, see Figure A.4. Thus, the proposed predictive cruise control method provides an appropriate approximation of the dynamic programming.

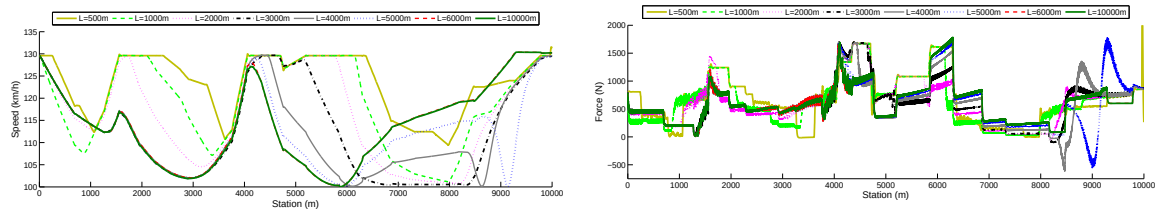

(a) Speed of the vehicle (b) Longitudinal control force

Fig. A.4: Results of the proposed predictive cruise control

The energy consumption values in the various methods are illustrated in Figure A.5. It shows that the energy consumption at the predictive cruise control is approximately unchangeable at $L > 3000$ m. Thus, it is enough to consider information from 3000 . . . 4000 m ahead of the vehicle. Moreover, the comparison of the global optimal dynamic programming and the predictive cruise control demonstrates that the proposed method provides a good approximation in the results of the energy consumption. The predictive cruise

control results in only 7% energy increase during the simulation at $L = 3000$ m. However, the huge advantage of the predictive cruise control is the reduction of the computation effort, regarding to the dynamic programming.

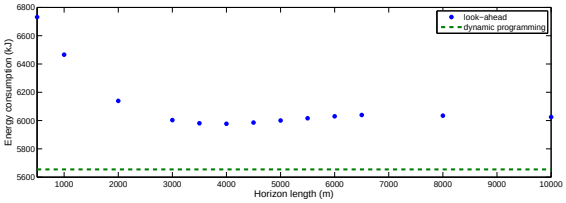

Fig. A.5: Energy consumption depending on the horizon length

A.2 Simulation examples on the operation of enhanced cruise control

Overtaking scenario with degradation in the communication

This simulation example presents a lane change scenario, in which the automated vehicle in the inner lane of a two-lane road overtakes a slower vehicle. There is also a preceding vehicle in the inner lane, which has higher speed, compared to the automated vehicle. In this situation the automated vehicle cannot change lane due to the overtaken vehicle, which is in the outer lane. Moreover, the vehicles in the inner lane also cannot be forced to reduce their speed, which means that the automated vehicle must be accelerated. The goal of the cruise control is to minimize the control force of the automated vehicle, while the safe distance between the vehicles is guaranteed.

In the example three scenarios are illustrated. In all scenarios the automated vehicle has information about the longitudinal acceleration, speed and position of the preceding vehicle through V2V communication, which is used in the predicted cruise control system to compute R. In $Scenario_A$ the time delay in the communication is $0.05s$, which is considered to be the nominal time delay value, while in $Scenario_B$ and in $Scenario_C$ the V2V communication has a degradation in the time delay, which is increased to $0.5s$. In $Scenario_A$ and in $Scenario_B$ the automated vehicle uses the presented predictive cruise control ($u \equiv u_P$), while in $Scenario_C$ the enhanced cruise control structure is in the loop, which also uses on-board distance measurement about the distance between the vehicles. The purpose of the simulation examples is to illustrate that the proposed enhanced cruise control method is able to guarantee the safe distance, even if the V2V communication delay is degraded.

Figure A.6(a) shows vehicle speed and Figure A.6(b) illustrates the distance between the vehicles in each scenarios. In $Scenario_A$ the predictive cruise control is able to guarantee the safe distance $20m$, which is resulted by the increase of its speed to $100km/h$. The increase of the speed is resulted by the reduction of R (Figure A.6(c)), which is computed based on the reduction of the predicted distances, see e.g. section $0 \ldots 200m$ of $Scenario_A$ in Figure A.6(d). It induces sharp increase in u_P, see Figure A.6(e). Thus, the predicted cruise control is able to guarantee the safe distance, if the signals in the communication have low time delay value.

If time delay is increased, the predictions of the distances in $Scenario_B$ significantly differ from the predictions in $Scenario_A$, see Figure A.6(d). Due to the increased time delay the preceding vehicle is predicted to have significantly smaller acceleration, which means that the automated vehicle focuses on the minimization of the control force. The increased R (Figure A.6(c)) leads to reduced u_P (Figure A.6(e)), which results in reduced speed profile (Figure A.6(a)). Consequently, the safe distance between the vehicles is not kept (Figure A.6(b)), which can force the preceding vehicle to unwanted braking intervention.

The resulted speed profile in $Scenario_C$ is illustrated in Figure A.6(a). Since the supervisor uses the onboard measurement about the distance between the vehicles, the reduction in $\xi_0 - \eta_0$ is perceived. It leads to the reduction of ρ_P and Δ_P, with which the tracking of $v_{ref,0}$ is highlighted. The resulted control signal u of $Scenario_C$ (Figure A.6(f)) is close to the u_P of $Scenario_A$, which results in keeping safe distance (Figure A.6(b)). Thus, the energy-optimal cruise control system is able to guarantee safe distance, even if the time delay in the communication is significantly increased.

Impact of computational issues on performances

In this simulation example the impact of the computational issues on the performance of keeping speed in a predefined range is illustrated. In the predicted cruise control a filtering on λ through a first-order filter $\frac{1}{s/T_f+1}$ is used, where T_f is the time constant, which is modified in different scenarios. In $Scenario_A$ the filter smooths λ with $T_f = 1.5s$, which results in slight variation of the vehicle speed and reduced $\ddot{\xi}_0$. In $Scenario_B$ and $Scenario_C$ the filter has lower smoothing impact with $T_f = 0.27s$, which can result in the sharp variation of $\ddot{\xi}_0$. Since $\ddot{\xi}_0$ is measured for the computation of λ (3.9), the acceleration signal is in feedback loop of the predictive cruise control. Therefore, the smoothing of λ has a high impact on the resulted control input u_P, as it has been analyzed in [Németh and Gáspár, 2015b]. Sharp λ can result oscillation in u_P, which can lead to significantly reduced performance in keeping speed in the limited range. In $Scenario_A$ and in $Scenario_B$ the automated vehicle uses the predictive cruise control ($u \equiv u_P$), while in $Scenario_C$ the enhanced cruise control structure is in the loop.

Figure A.7(a) illustrates the altitude of the road, which is a short section of the highway $M1$. In the example the prediction horizon is $1000m$ long. The value of $v_{ref,0}$ is $130km/h$ and the bounds of the range are $v_{min,0} = 100km/h$, $v_{max,0} = 135km/h$. Due to the uphill and downhill sections the speed of the vehicle is varied to achieve minimum control intervention. The speeds of the vehicle in the three scenarios are shown in Figure A.7(b). In case of $Scenario_A$ the predictive cruise control is able to guarantee the primary performance (4.2), the control intervention u_P is shown in Figure A.7(c). In contrast, in $Scenario_B$ u_P has significant oscillation, which leads to the violation of the primary performance, see Figure A.7(b),(d). Using the enhanced cruise control ($Scenario_C$), the violation of the performance can be avoided, even if $T_f = 0.27s$, see Figure A.7(b). The u control signal is presented in Figure A.7(e), which is significantly smoother than u_P in $Scenario_B$. The reduction of the oscillation is achieved by ρ_P, Δ_P, see the signals in Figure A.7(f),(g). Thus, the proposed enhanced cruise control system is able to guarantee keeping speed in the predefined range, even if the predicted cruise control has performance

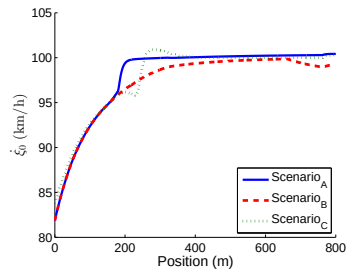

(a) Vehicle speed

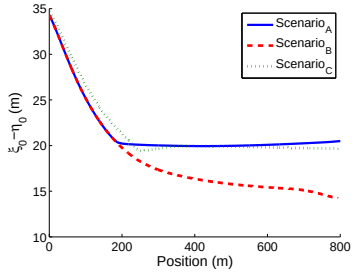

(b) Distance between the vehicles

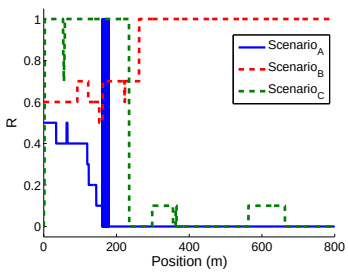

(c) Value of R

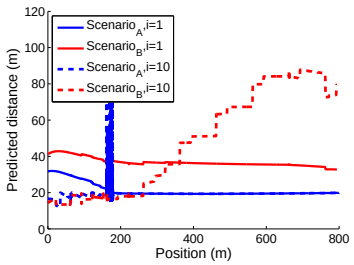

(d) Predicted distances in $Scenario_A$, $Scenario_B$

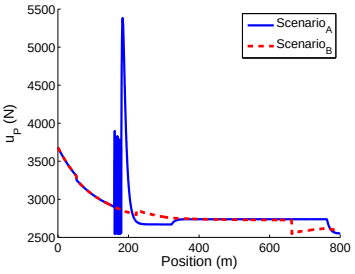

(e) Control signal u_P in $Scenario_A$, $Scenario_B$

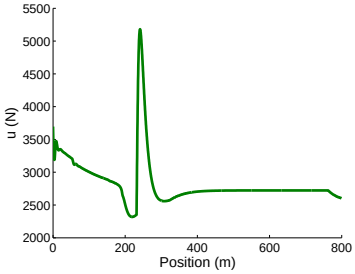

(f) Control signal u in $Scenario_C$

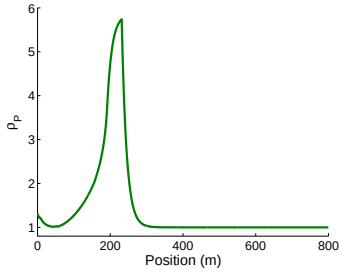

(g) Scheduling variable ρ_P

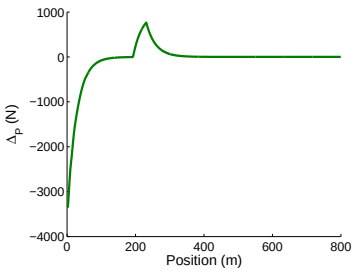

(h) Uncertainty Δ_P

Fig. A.6: Simulations in overtaking scenario

loss due to computational problems.

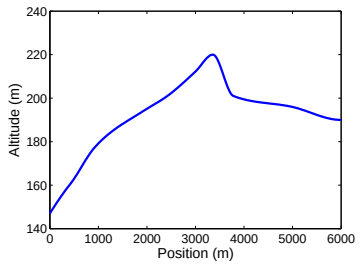

(a) Altitude of the road section

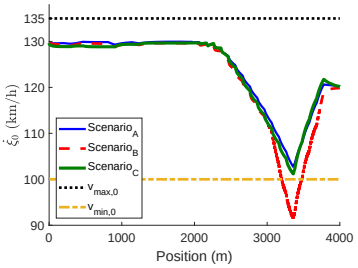

(b) Vehicle speed

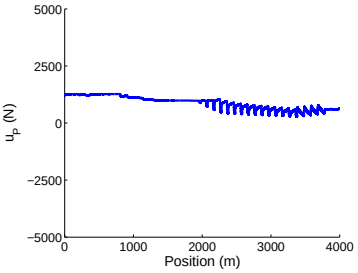

(c) Control signal u_P in $Scenario_A$

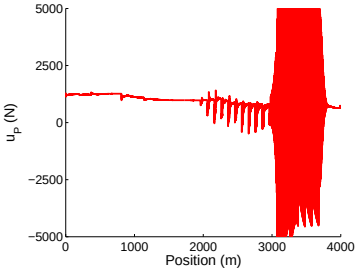

(d) Control signal u_P in $Scenario_B$

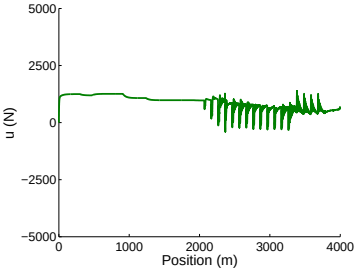

(e) Control signal u in $Scenario_C$

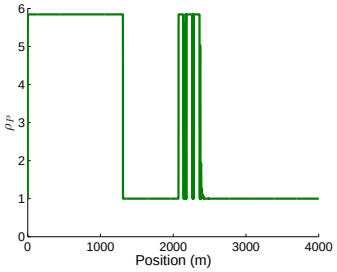

(f) Scheduling variable ρ_P

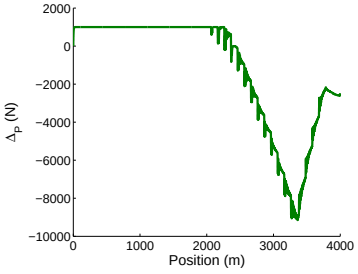

(g) Uncertainty Δ_P

Fig. A.7: Simulation analysis on the impact of computational issues

B. ILLUSTRATIONS ON INTERACTIONS OF MULTIPLE AUTOMATED VEHICLES

B.1 Illustration on the interaction of human-driven and autonomous vehicles

Example on the formulation of quasi-kinetic energy function

As an example regarding to Section 5.2, in case of three automated vehicles the following constraints for the formulation of quasi-kinetic energy are determined:

- $j = 1$: For a selected value of $R_{1,1}$ the vectors $\Xi_1, \Delta T_i$ are computed, which results in t_1 using the measurement e_1, see (5.12). Moreover, (5.8) results in $\xi_2(t_1), \xi_3(t_1)$ through the computation of $\Delta T_2, \Delta T_3, \Xi_2, \Xi_3$. The constraints are $e_2 - \xi_2(t_1) > s_{safety}$ and $e_3 - \xi_3(t_1) > s_{safety}$.
- $j = 2$: Similarly, in case of a given $R_{1,2}$ the value of t_2 is computed. It results in the constraints $e_1 - \xi_1(t_2) > s_{safety}$ and $e_3 - \xi_3(t_2) > s_{safety}$.
- $j = 3$: Finally $R_{1,3}$ leads to the computation of t_3, which results in the constraints $e_1 - \xi_1(t_3) > s_{safety}$ and $e_2 - \xi_2(t_3) > s_{safety}$.

Thus, the optimization problem in this example is formed as

$$\max_{R_{1,i}(t)\in[0;R_{1,max}]} \sum_{i=1}^{3} E_i(t) R_{1,i}(t), \tag{B.1}$$

such that

$$\begin{aligned} &e_2 - \xi_2(t_1) > s_{safety}, e_3 - \xi_3(t_1) > s_{safety}, \\ &e_1 - \xi_1(t_2) > s_{safety}, e_3 - \xi_3(t_2) > s_{safety}, \\ &e_1 - \xi_1(t_3) > s_{safety}, e_2 - \xi_2(t_3) > s_{safety}. \end{aligned}$$

Simulation example on the interactions of vehicles

The simulation scenario contains two vehicles, in which three simulation cases are performed by the CarSim vehicle dynamic software. The different cases are distinguished through the initial position of the automated vehicle. In these simulations the human-driven vehicle is on the primary route, while the automated vehicle with predictive cruise control in on the non-primary route. Note that in case of pure automated vehicles it is insufficient to define hierarchy among the routes, but in case of mixed traffic scenarios the presence of human driver requests the rules. Moreover, the safety distance is increased to

$s_{safety} = 20$ m to create the confidence for the human participant. It is visualized by the cone in front of the automated vehicle.

In all simulation cases the conventional vehicle has the same initial speed and position. Thus, $t_{int} = 8.5$ s in all simulations. The difference between the three cases is the initial position of the controlled vehicle. In Case 1 the automated vehicle is initially 90 m from the intersection, while in Case 2 the distance is 110 m, at Case 3 it increased to 150 m. Figure B.1 shows the time moment t_{int}, when the conventional vehicle reaches the intersection. In Case 1 the cooperation between the vehicles is possible, which means that the automated vehicle reaches the intersection first, see Figure B.1(a). Figure B.1(b) illustrates Case 2, when the cooperation is impossible and the speed of the automated vehicles must significantly be reduced. However, it can be seen that the conflict in the intersection is avoided and the safety cruising is guaranteed. Case 3 demonstrates the result, when criterion the maximum set of the cooperation incorporates in also both vehicles. Although, the human-driven vehicle reaches the intersection first, and the automated vehicle secondly, as illustrated in Figure B.1(c).

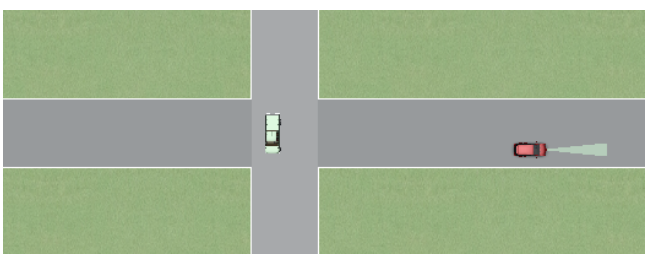

(a) Scenario *Veh1*

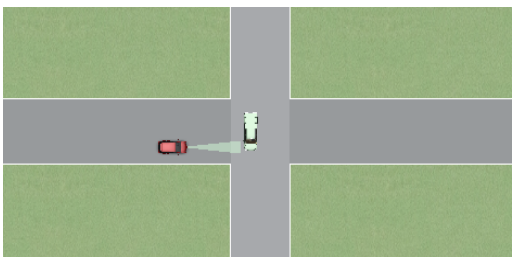

(b) Scenario *Veh2*

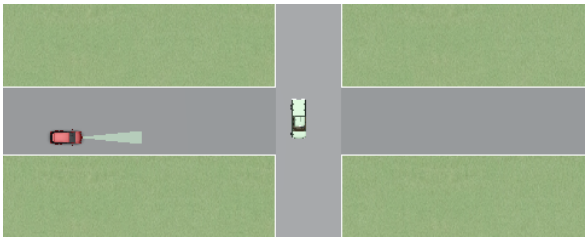

(c) Scenario *Veh3*

Fig. B.1: Vehicles in the intersection (automated vehicle: red, human-driven vehicle: green)

The numerical results of the simulation cases are presented in Figure B.2. The speed of the vehicles can be seen in Figure B.2(a). Speed of controlled vehicle in Case 1 is increased to reach the intersection rapidly, while in Case 3 the speed is slightly reduced. Their reasons are the different selection of R_1 weights, which is illustrated in Figure B.2(b). R_1 of Case 3 is continuously on the maximum $R_{1,max} = 1$, while R_1 in Case 1 is slightly reduced. In both cases the motion of the vehicles can be considered as energy-optimal through the coordination, but in Case 3 the energy consumption is reduced.

In Case 2 the situation in the intersection differs from the previous cases. Until the station point $-70m$ the maximum set of coordination contains both vehicles. It is predicted that the automated vehicle is able to reach the intersection first, which results in the significant reduction of R_1 and the vehicle speed is increased, see Figure B.2(a)-

(b). However, after $-70m$ the prediction is modified, which means that the coordination cannot be guaranteed. This change is induced by the speed increase of the human-driven vehicle, which is predicted in all computation steps, see Figure B.2(d). Thus, after the point $-70m$ the W is activated, as depicted in Figure B.2(c).

B.2 Examples on learning-based control design for safety-critical interactions

In the next simulation examples it is illustrated that the proposed algorithm provides safe motion for the automated vehicle in various scenarios. The intersection scenario is illustrated in Figure B.3, where vehicle 1 represents the automated vehicle and the further vehicles are the surrounding vehicles. In the next four simulations the initial positions and velocity values of the vehicles are varied, and thus, varying ordering in the intersection is yielded. In all of the simulations vehicle 1 has conflicts with the surrounding vehicles because of their route crossing. The goal of the simulations are to show that the automated vehicle is able to adapt to various traffic scenarios and the proposed optimization (6.12) together with the reinforcement learning is efficient. The initial position and velocity values of the scenarios are listed in Table B.1.

initial condition	scenario 3a	scenario 3b	scenario 3c	scenario 3d
$s_1(0)$	-8 m	-25 m	-26 m	-30 m
$s_2(0)$	-20 m	-10 m	-20 m	-10 m
$s_3(0)$	-30 m	-30 m	-8 m	-25 m
$s_4(0)$	-25 m	-8 m	-25 m	-8 m
$s_5(0)$	-35 m	-35 m	-45 m	-30 m
$v_1(0)$	50 km/h	50 km/h	40 km/h	35 km/h
$v_2(0)$	50 km/h	50 km/h	50 km/h	50 km/h
$v_3(0)$	35 km/h	35 km/h	50 km/h	50 km/h
$v_4(0)$	50 km/h	50 km/h	50 km/h	50 km/h
$v_5(0)$	45 km/h	45 km/h	40 km/h	45 km/h

Tab. B.1: Initial conditions for scenario 3

Figure B.4 shows the results of each scenarios in the third simulation setup, related to Figure B.3. Figure B.4(a) illustrates the trajectories of scenario 3a, where vehicle 1 can go through the intersections first. Thus, the velocity of vehicle 1 is set to the constant maximum 50 km/h, with which the avoidance of the collision is guaranteed, see Figure B.4(b) and the related control inputs in Figure B.4(c). In scenario 3b the automated vehicle is further from the intersection at the beginning of the simulation, see Table B.1. Thus, it is not possible to go through the intersection first and therefore, vehicle 1 is the third in the ordering, see the trajectories in Figure B.4(d). v_1 is slightly reduced before 2 s to guarantee the safe distance. Figure B.4(f) shows that u is close to u_L during the entire simulation, which means that the learning process and the optimization (6.12) are efficient. In scenario 3c the vehicle has reduced velocity related to the surrounding vehicles and thus, it has fourth ordering in the intersection (see Figure B.4(g)). Guaranteeing

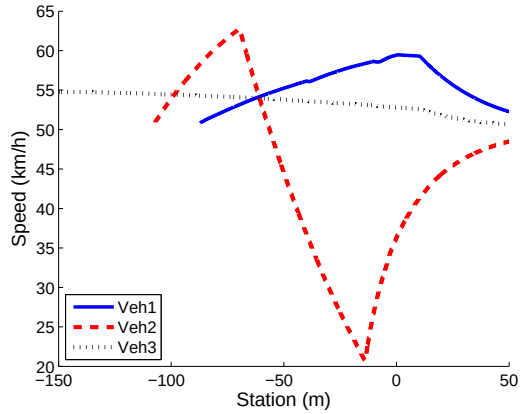

(a) Speed of automated vehicle

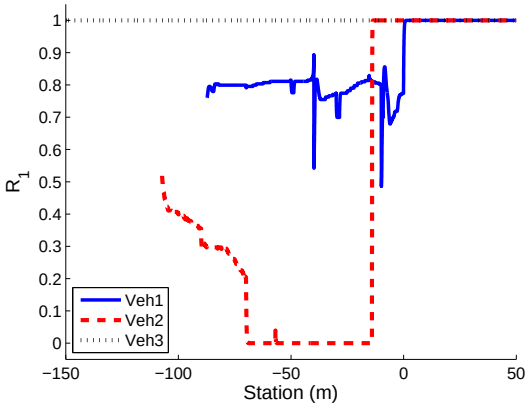

(b) R_1 weight

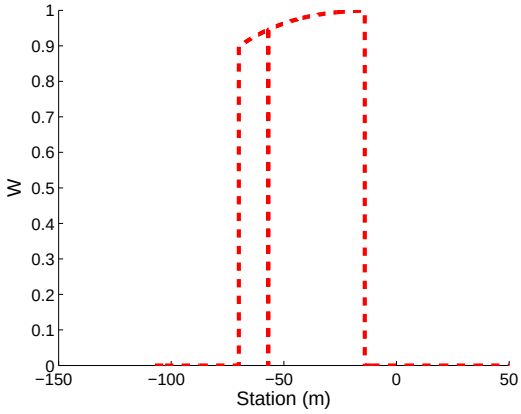

(c) W weight

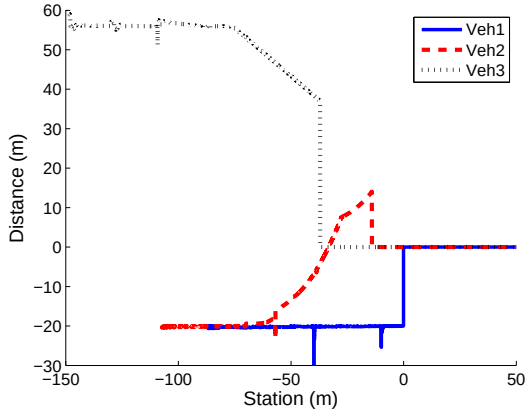

(d) Predicted distance from the intersection at $t_{TrL,2}$

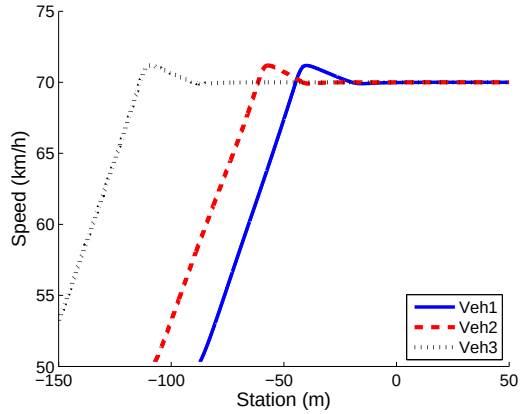

(e) Speed of conventional vehicle

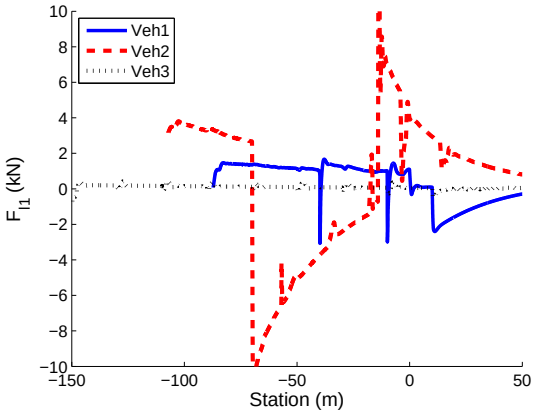

(f) Control force of the vehicle

Fig. B.2: Simulation results with two vehicles in a mixed traffic

safety distance the velocity is reduced and at 5 s the the maximum velocity is achieved, see Figure B.4(h). Although u is close to u_L, it is necessary to modify it to avoid the

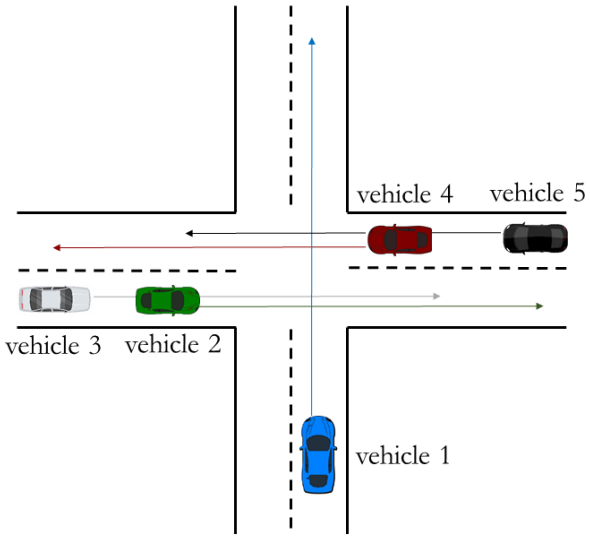

Fig. B.3: Illustration on the intersection scenario with 5 vehicles

collision, e.g., between $1.5s \dots 3.8s$ (Figure B.4(i)). Figure B.4(j) shows the trajectories of scenario 3d, where vehicle 1 is the last in the ordering. Its reason is that the initial velocity is smaller than in scenario 3c, see Figure B.4(k). Since for vehicle 5 the priority must be guaranteed, vehicle 1 must accelerate with a reduced value between $2s \dots 6s$, see the velocity profile in Figure B.4(k) and the acceleration command in Figure B.4(l). Nevertheless, u can be selected to be close to u_L, which can provide improved level on the economy performance, while the safety performance are simultaneously guaranteed.

Finally, the operation of the designed automated vehicle control system in a complex simulation scenario in urban context is analyzed. In the example 7 vehicles take part, i.e., the automated vehicle and 6 further surrounding human-driven vehicles. The illustration of the fourth scenario is found in Figure B.5. In this scenario the automated ego vehicle is illustrated as vehicle 1. In the example all of the further vehicles are in conflict with vehicle 1, which means that the signals of vehicle 2 ... vehicle 7 are used during the design of the control input a. The initial positions and velocity values are as follows: $s_1 = -34$ m, $s_2 = -25$ m, $s_3 = -4$ m, $s_4 = -30$ m, $s_5 = -75$ m, $s_6 = -102$ m, $s_7 = -128$ m and $v_1 = 50$ km/h, $v_2 = 50$ km/h, $v_3 = 40$ km/h, $v_4 = 50$ km/h, $v_5 = 50$ km/h, $v_6 = 40$ km/h, $v_7 = 50$ km/h. In the scenario $n_s = 3$ number of surrounding vehicles during the solution of the optimization problem are considered.

Some scenes on scenario 4 can be found in Figure B.6. Figure B.6(a) shows that vehicle 2 and vehicle 3 have already left the intersection and vehicle 4 is in the intersection for performing left turn. Since vehicle 2...vehicle 4 are closer to the intersection than vehicle 1, the ego vehicle must reduce its velocity to give way, see Figure B.7(b). It is yielded by the actuation, see the acceleration command u in Figure B.7(c). Moreover, after vehicle 4 leaves the intersection, vehicle 5 arrives at 50 km/h velocity, see Figure B.6(b). Due to the reduced velocity of vehicle 1 it is not possible to go through between vehicle 4 and vehicle 5 and thus, vehicle 1 is stopped. Figure B.6(c) shows when vehicle 5 leaves the intersection, the velocity of vehicle 1 is increased to go through the intersection before

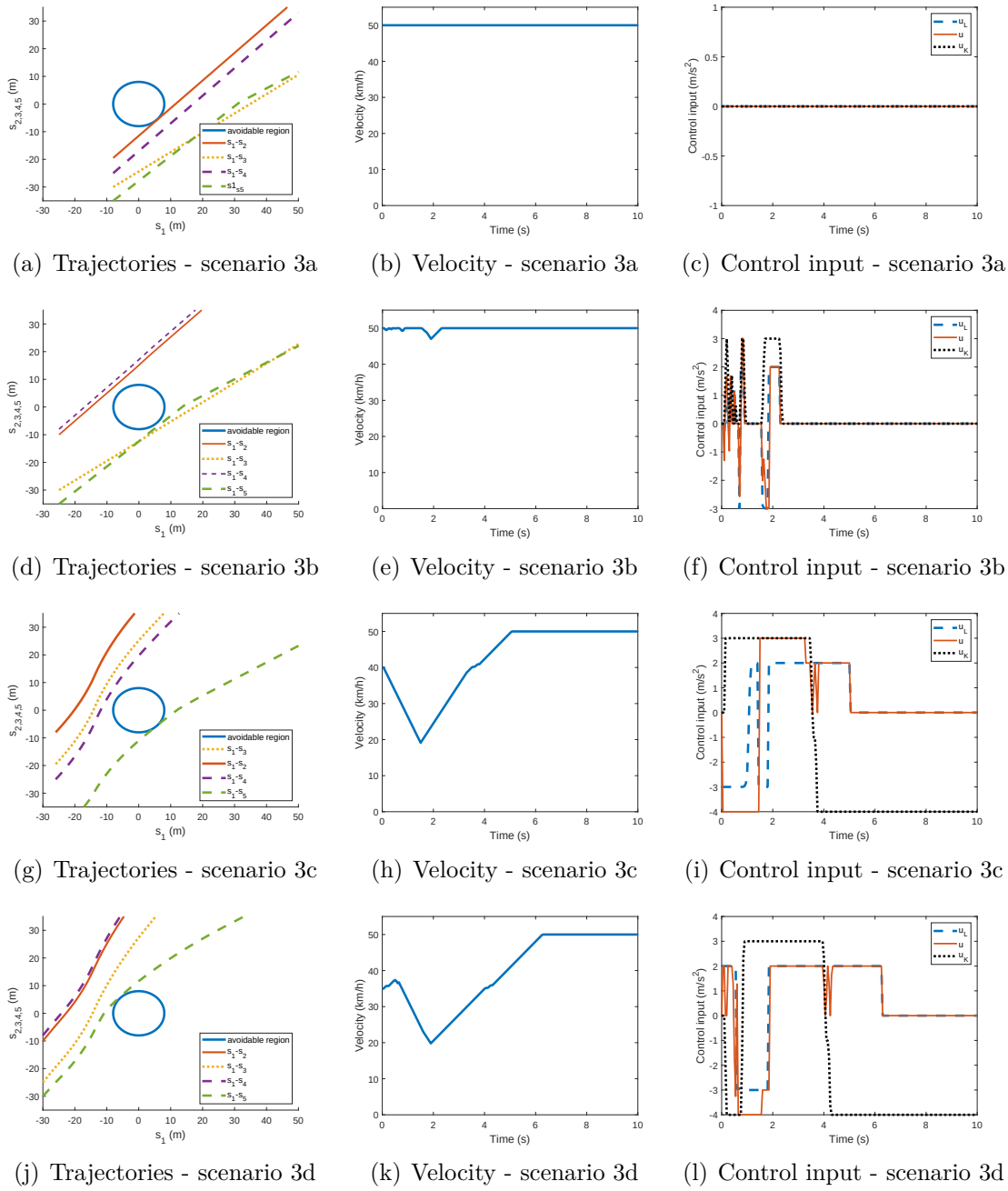

(a) Trajectories - scenario 3a (b) Velocity - scenario 3a (c) Control input - scenario 3a

(d) Trajectories - scenario 3b (e) Velocity - scenario 3b (f) Control input - scenario 3b

(g) Trajectories - scenario 3c (h) Velocity - scenario 3c (i) Control input - scenario 3c

(j) Trajectories - scenario 3d (k) Velocity - scenario 3d (l) Control input - scenario 3d

Fig. B.4: Signals of third scenarios

vehicle 6 and vehicle 7 arrive (Figure B.6(d)).

Figure B.7 shows an insight into the operation of the control system. Figure B.7(a) illustrates the trajectories of the vehicles and the avoidable region. The illustration shows that all of the trajectories are outside of the avoidable region and thus, the safety constraint on the motion of the automated vehicle can be guaranteed. Figure B.7(b) shows the distances between vehicle 1 and the closest $n_s = 3$ vehicles, where d_1 is related to the distance between vehicle 1 and the closest vehicle and d_3 is related to the distance

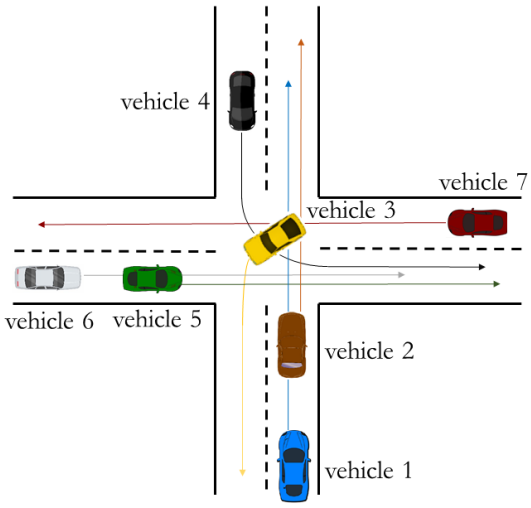

Fig. B.5: Illustration on the complex intersection scenario

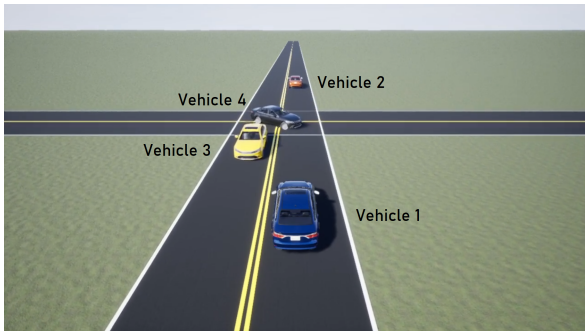

(a) Vehicle 4 turns left

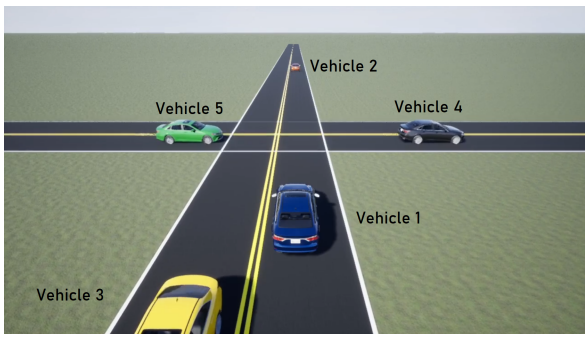

(b) Vehicle 5 enters into the intersection

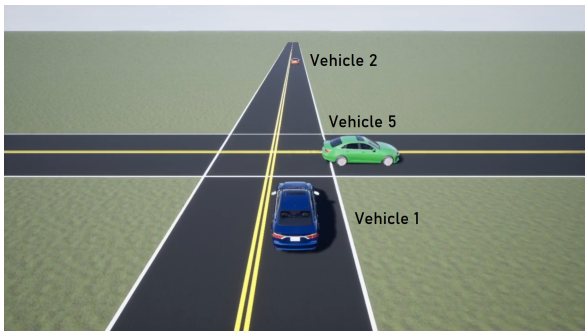

(c) Vehicle 1 starts to enter into the intersection

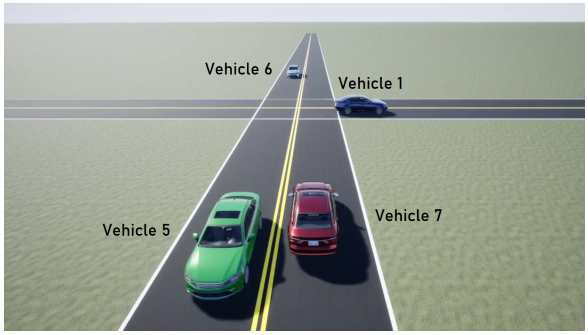

(d) Vehicle 1 leaves the intersection

Fig. B.6: Illustration of the complex fourth scenario

between vehicle 1 and the third closest vehicle. Note that the vehicles in n_s vary during the simulation, e.g., directly before $t = 4\ s$ distance d_1 is related to s_1 - s_4, d_2 is related s_1 - s_5 and d_3 is related to s_1 - s_6, while directly after $t = 4\ s$ d_1 is related to s_1 - s_5, d_2 is related s_1 - s_6 and d_3 is related to s_1 - s_7. If there are less than three closest vehicles, virtual vehicles with constant 100 m position are defined, see e.g., d_3 after 5.5 s. Figure B.7(b) shows that all of the distances are above $s_{safe} = 8\ m$ during the entire simulation,

independently from the selection of the closest vehicle. It is yielded by the control input u, which is illustrated in Figure B.7(d). Figure B.7(d) also shows the further inputs, such as u_K and u_L. Since the role of u_K is to provide velocity tracking, its value is 3 m/s^2 constantly, because $v_1 < 50$ km/h during the entire simulation, except the initial velocity. The role of u_L is to provide a vehicle motion, with which the reward function is maximized, such as energy consumption is minimized and the traveled distance of the vehicle is maximized. However, none of the control inputs u_K and u_L are acceptable, because the safety constraints are not guaranteed. Thus, u_K is modified through Δ, which results in the control input signal u. The maximum deceleration of the vehicle before $5.5s$ guarantees the avoidance of collision with vehicle 2...vehicle 5 and the maximum acceleration between $5.5s \ldots 8s$ guarantees the avoidance of the collision with vehicle 6 and vehicle 7. After $8s$ the conflict between the vehicles ceases and thus, vehicle 1 can move with $u = u_L$ to minimize the objective in (6.12) to zero. As a result the velocity of vehicle 1 is slightly increased after $8s$, see Figure B.7(c). Moreover, Figure B.7(c) presents that the difference between v_{ref} and v_1 is very small, which illustrates the effectiveness of the designed robust cruise control.

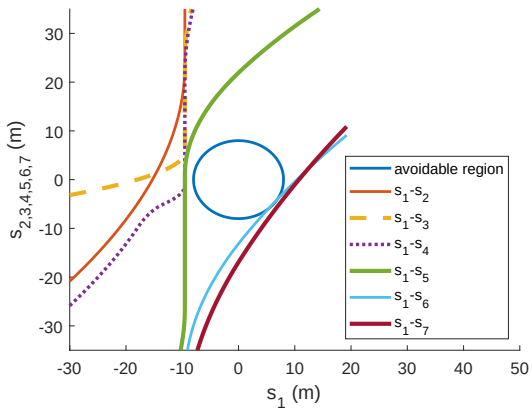

(a) Trajectories of the vehicles

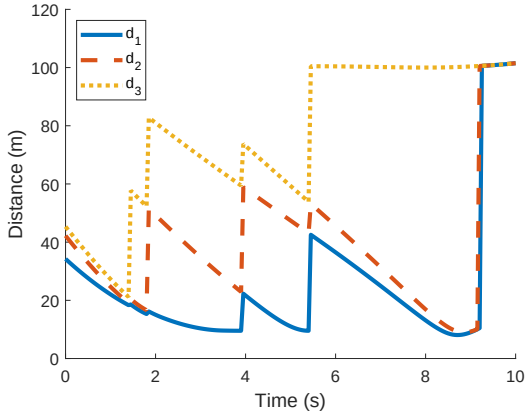

(b) Distances between vehicle 1 and the closest further vehicles

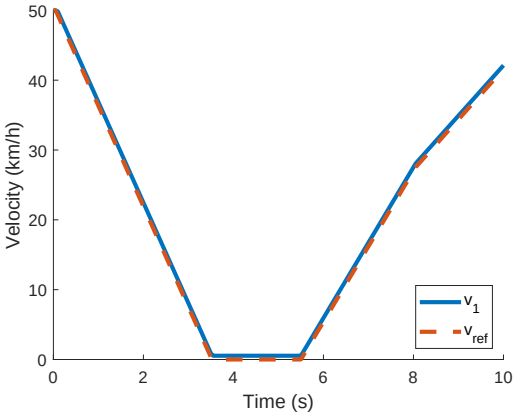

(c) Velocity of the automated vehicle

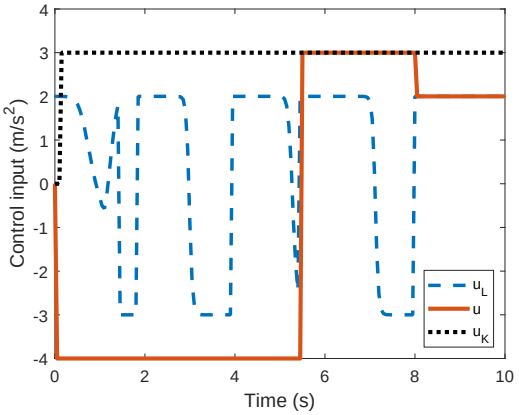

(d) Control input of the automated vehicle

Fig. B.7: Signals of the complex fourth scenario

The simulation examples have shown that the proposed control algorithm is able to guarantee the safe motion of the automated vehicle, i.e., the collisions in the intersection are avoided. The contribution of the complex scenario is that the automated vehicle is able to handle the presence of increased number of vehicles in the intersection.

C. ILLUSTRATIONS ON AUTOMATED VEHICLES IN TRAFFIC

C.1 Fundamentals for set-based analysis

The following definitions and theorems are some essential fundamentals for SOS programming [66]. Let $\mathbb{R}$ denote the real numbers and $\mathbb{Z}_+^n$ denote the set of nonnegative integers. The basic elements of the method are polynomials and SOS as defined below:

Definition 2: *A **Polynomial** f in n variables is a finite linear combination of the functions $m_\alpha(x) := x^\alpha = x_1^{\alpha_1} x_2^{\alpha_2} \cdots x_n^{\alpha_n}$ for $\alpha \in \mathbb{Z}_+^n$, $\deg m_\alpha = \sum_{i=1}^n \alpha_i$:*

$$f := \sum_\alpha c_\alpha m_\alpha = \sum_\alpha c_\alpha x^\alpha \tag{C.1}$$

with $c_\alpha \in \mathbb{R}$. Define $\mathcal{R}_n$ to be the set of all polynomials in n variables. The degree of f is defined as $f := \max_\alpha \deg m_\alpha$.

Definition 3: *The **set of SOS** polynomials in n variables is defined as:*

$$\Sigma_n := \left\{ p \in \mathcal{R}_n \,\middle|\, p = \sum_{i=1}^t f_i^2,\ f_i \in \mathcal{R}_n,\ i = 1, \ldots, t \right\} \tag{C.2}$$

for some $t < \infty$.

A central theorem of SOS programming is Positivstellensatz. By the application of this theorem the set emptiness constraints of an optimization task can be transformed into SOS feasibility problems.

Theorem 1: **Positivstellensatz** *Given polynomials $\{f_1, \ldots, f_r\}$, $\{g_1, \ldots, g_t\}$ and $\{h_1, \ldots, h_u\}$ in $\mathcal{R}_n$, the following are equivalent:*

1. *The set*

$$\left\{ x \in \mathbb{R}^n \,\middle|\, \begin{array}{c} f_1(x) \geq 0, \ldots, f_r(x) \geq 0 \\ g_1(x) \neq 0, \ldots, g_t(x) \neq 0 \\ h_1(x) = 0, \ldots, h_u(x) = 0 \end{array} \right\} \tag{C.3}$$

   is empty.

2. *There exists polynomials $f \in \mathcal{P}(f_1, \ldots, f_r)$ ($\mathcal{P}$ is multiplicative convex cone), $g \in \mathcal{M}(g_1, \ldots, g_t)$ ($\mathcal{M}$ is multiplicative monoid), $h \in \mathcal{I}(h_1, \ldots, h_u)$ ($\mathcal{I}$ is ideal) such that*

$$f + g^2 + h = 0. \tag{C.4}$$

The multiplicative monoid and the cone are defined as follows.

Definition 4: **Multiplicative monoid** *Given $g_1, \ldots, g_t \in \mathcal{R}_n$, the Multiplicative Monoid generated by g_j is the set of all finite products of g_j, including the empty product, defined to be* 1. *It is denoted as $\mathcal{M}(g_1, \ldots, g_t)$. For completeness define $\mathcal{M}(\phi) = 1$.*

Definition 5: **Cone** *Given $\{f_1, \ldots, f_s\} \in \mathcal{R}$, the cone is generated by f_i is*

$$\mathcal{P}(f_1, \ldots, f_s) = \left\{ s_0 + \sum s_i b_i | s_i \in \sum_n, b_i \in \mathcal{M}(f_1, \ldots, f_s) \right\}.$$

For completeness note that $\phi = \sum_n$.

In the practical application of the Positivstellensatz some assumptions are considered. For example, $g = p_0 \in \mathcal{M}(p_0)$ and $f = -qp_0 - \sum_{i=1}^{n} s_i p_0 p_i$, $q \in \sum_n$, $p_i \in \mathcal{R}_n$, $h = 0$ are defined. Since q and s_i are SOS, $f \in \mathcal{P}(p_1, \ldots, p_m, -p_0)$. Therefore

$$f + g^2 + h = -qp_0 - \sum_{i=1}^{n} s_i p_0 p_i + p_0^2 = -\left(p_0 - \sum_{i=1}^{m} s_i p_i \right) p_0 - \sum_{i=1}^{n} s_i p_0 p_i + p_0^2 = 0 \quad \text{(C.5)}$$

It leads to the generalized S-Procedure, which is formed as follows, see [65].

Theorem 2: **Generalized S-procedure** *Given symmetric matrices $\{p_i\}_{i=0}^{m} \in \mathcal{R}_n$. If there exist nonnegative scalars $\{s_i\}_{i=1}^{m} \in \Sigma_n$ such that*

$$p_0 - \sum_{i=1}^{m} s_i p_i \succeq q \quad \text{(C.6)}$$

with $q \in \Sigma_n$, then

$$\bigcap_{i=1}^{m} \{x \in \mathbb{R}^n \,|\, p_i(x) \geq 0\} \subseteq \{x \in \mathbb{R}^n \,|\, p_0(x) \geq 0\}. \quad \text{(C.7)}$$

The related set emptiness question asks if

$$W := \{x \in \mathbb{R}^n \,|\, p_1(x) \geq 0, \ldots, p_m(x) \geq 0, -p_0(x) \geq 0, p_0(x) \neq 0\} \quad \text{(C.8)}$$

is empty.

Moreover, there is an important connection between SOS programming and LMI problems, which was proved by [117].

Theorem 3: **LMI feasibility problem** *Given a finite set*

$$\{p_i\}_{i=0}^{m} \in \mathcal{R}_n,$$

the existence of $\{a_i\}_{i=0}^{m} \in \mathbb{R}_n$ such that

$$p_0 + \sum_{i=1}^{m} a_i p_i \in \Sigma_n \quad \text{(C.9)}$$

is an LMI feasibility problem.

C.2 Illustration on the predictive coordination strategy

In this simulation example a $20km$ long section of the highway $M1$ between Budapest and Vienna is also demonstrated. The highway section is divided into 5 segments, and it contains two controlled on-ramps and one off-ramp, see Figure C.1. During the simulation it is necessary to minimize the lengths of the queues on the on-ramps, while the traffic flow and the energy-saving of the vehicles are maximized.

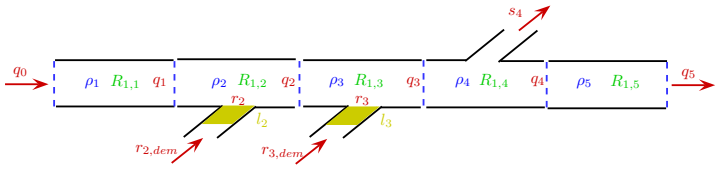

Fig. C.1: Simulation scenario in the second example

The simulation parameter is $T = 30$ sec sampling time in the prediction with $n = 12$ points, which leads to a total of 6 min prediction horizon. However, $T = 30$ sec is too small sampling time for the intervention in the traffic control system, thus $T = 120$ sec is selected with $n = 3$ points for the control horizon [44]. Since the control input is computed as a flow value, it is transformed into green time with a 120 sec cycle. Moreover, in the simulation $\kappa = 10\%$ and $\kappa = 30\%$ values along the highway are considered. During the simulation the signals in $w(k)$ are considered.

The results of the simulation in case of low rate of look-ahead vehicles $\kappa = 10\%$ are shown in Figure C.2. The simulation shows a scenario between two rush traffic peaks, whose maximum is approximately at 1.7 $hours$, see the density and the flow values at Figures C.2(a)-(b). Due to the reduction of the inflows q_0 and $r_{2,dem}, r_{3,dem}, s_4$, the controller is able to increase the controlled inflow r_i, while the stability of the system is preserved, see Figure C.2(c)-(d). Since r_2, r_3 values are increased, the length of the queues in the controlled gates can be reduced and the look-ahead parameter is increased, see Figure C.2(e)-(f).

Another simulation scenario for $\kappa = 30\%$ is presented in Figure C.3. The results show the efficiency of the control strategy, because the intervention of r_2, r_3 and $R_{1,i}$ are able to adapt to the change of the vehicle rate. The stability constraint of the system is formed as $u_{max}(R_{1,i}(k), \kappa(k)) = 2023 - 492\kappa(k)R_{1,i}(k)$, which means that κ and $R_{1,i}$ cannot be increased simultaneously to avoid the limitation of flow. The impact of the increase in κ is shown around the time $2h$, where $R_{1,3}$ cannot be increased to the maximum value in $\kappa = 30\%$ scenario, while in $\kappa = 10\%$ scenario $R_{1,3} = 1$. Thus, the queue length is higher at $\kappa = 30\%$, as shown in Figure C.3(f).

Summarizing, the simulation examples show that the control strategy is able to guarantee the stability of the traffic flow and the control of the energy-efficient look-ahead vehicles. In the strategy the inflow of the traffic system and the look-ahead parameter of the individual vehicles are coordinated. The control strategy is able to adapt to the variation in the traffic signals, such as the inflow disturbances and the ratio of the energy-efficient vehicles.

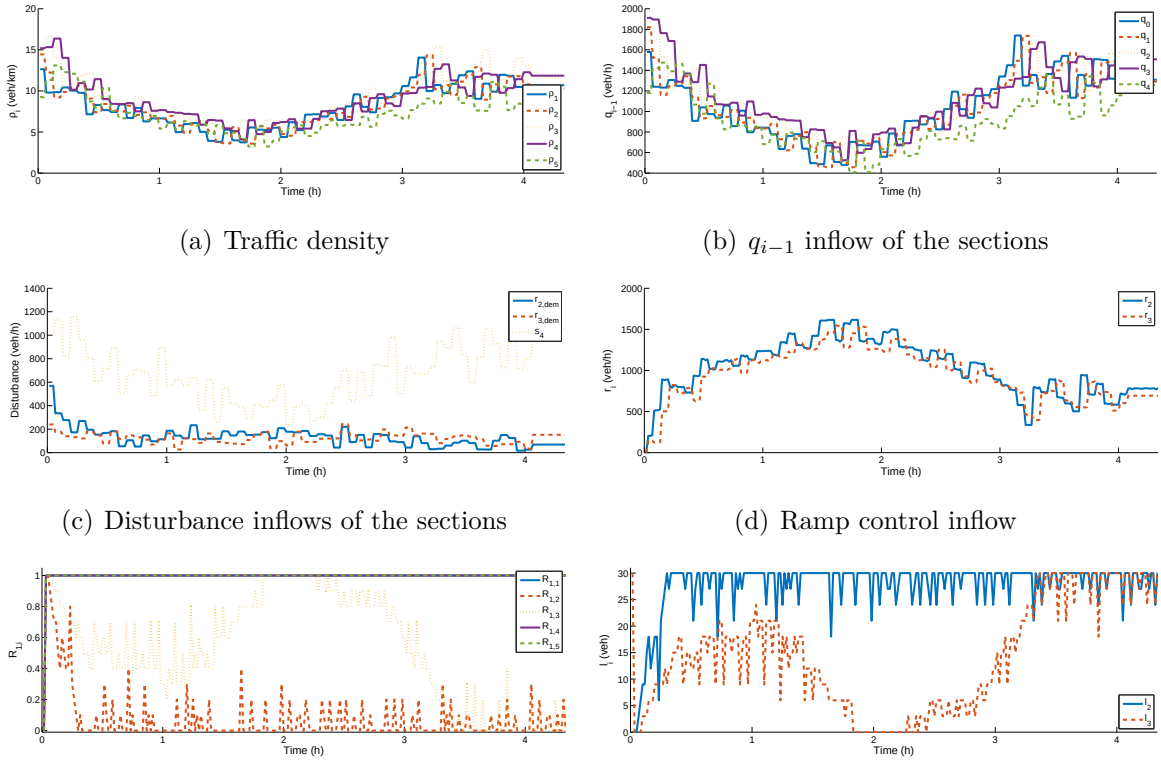

(a) Traffic density

(b) q_{i-1} inflow of the sections

(c) Disturbance inflows of the sections

(d) Ramp control inflow

(e) Look-ahead parameter $R_{1,i}$

(f) Queue length on the controlled gates

Fig. C.2: Results of the VISSIM simulation at $\kappa = 10\%$

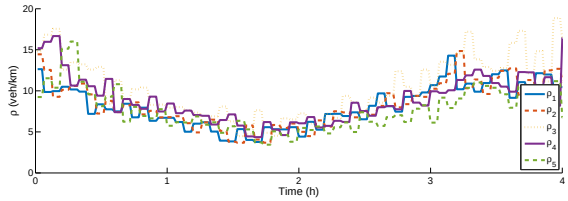

(a) Traffic density

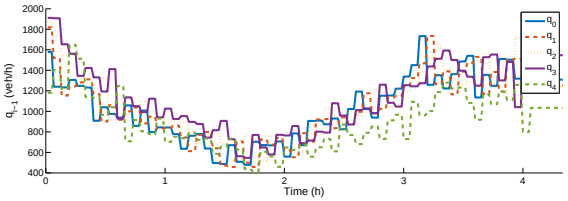

(b) q_{i-1} inflow of the sections

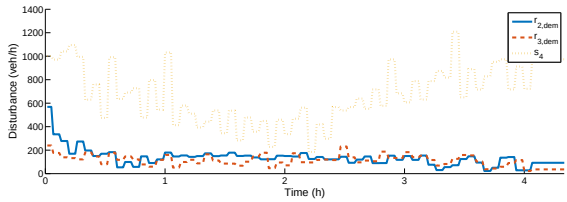

(c) Disturbance inflows of the sections

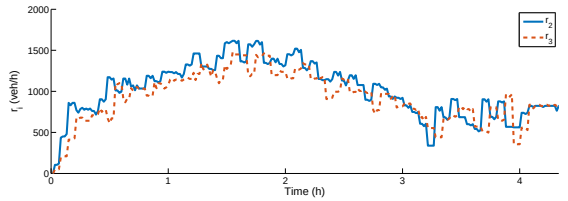

(d) Ramp control inflow

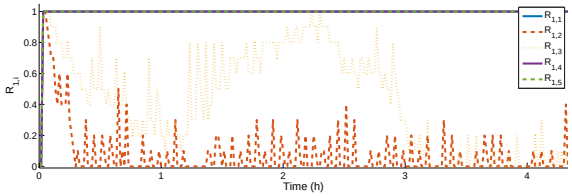

(e) Look-ahead parameter $R_{1,i}$

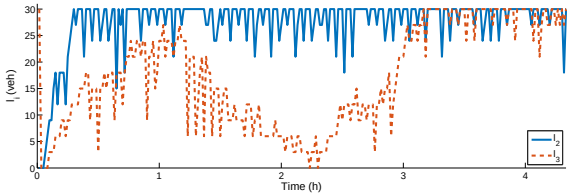

(f) Queue length on the controlled gates

Fig. C.3: Results of the VISSIM simulation at $\kappa = 30\%$

LIST OF FIGURES

LIST OF TABLES

LIST OF ACRONYMS

ACC	Adaptive Cruise Control
CPU	Central Processing Unit
ECU	Electronic Control Unit
I2V	Infrastructure to Vehicle
LiDAR	Light Detection and Ranging
LPV	Linear Parameter-Varying
MPC	Model Predictive Control
RL	Reinforcement Learning
SOS	Sum-of-Squares
V2V	Vehicle to Vehicle